Development of Fluorescent nanoparticles “Quantum Dots” for biomedical application

Sanjay Taribagil MBBS, MS, FRCS(Ed), FRCS (Gen)

A thesis submitted for an MD Research degree

Division of Surgery & Interventional Science

University College London

Royal Free Campus

2013

DOCTOR OF MEDICINE

I, **Sanjay Taribagil**

Of University Department of Surgery, University College Medical School, Royal Free Campus, Pond Street, London NW3 2QG

Solemnly and sincerely declare, in relation to the thesis entitled:

Development of Fluorescent nanoparticles “Quantum Dots” for biomedical application

that the work presented in this thesis is my own. Where information has been derived from other sources, I confirm that this has been indicated in the thesis. The material has not previously been accepted in whole, or in part, for any other degree or diploma.

Signature: Date:

Acknowledgements

The experimental work was carried out in the tissue culture laboratory and animal laboratory at the University Department of Surgery at Royal Free Campus (Hospital), University College London. I am grateful to my supervisors Prof. Alexander Seifalian, Prof. Marc Winslet, Dr. Shiyu Yang and Dr.Bala Ramesh for their constant encouragement, supervision, help and guidance during my study.

I would like to thank the Department of Surgery staff Dr. Kevin Sales and Mr. Geoffrey Punshon, for their help during the course of my work in the Department

I would also like to thank Elnaz Yaghini and Dr Sandy MacRobert of University College London for the spectrophotometer work and Mr. Innes Clatworthy, of Royal Free NHS Hospital Trust, Electron Microscopy Department for the help with Transmission Electron Microscopy (TEM) and X-ray microanalysis work.

Abstract

Background: Quantum dots (QDs) have emerged as one of the most exciting fluorescent nanoparticles with a potential for diagnostic and therapeutic application in the field of nanomedicine. The aim of this study was to synthesize water soluble QDs; bio-conjugating these QDs with RGD peptides prior to linking the QD-conjugated peptide to cancer cells with the aim to study cytotoxicity and assess its feasibility for in vivo studies.

Methods: Water soluble Cadmium Telluride (CdTe) QDs were synthesized by the reaction of cadmium chloride with sodium tellurite in the presence of buffer solution of Mercaptosuccinic acid (MSA) as a capping ligand. Water soluble red emitting QDs thus obtained were characterized using spectrophotometric analysis. These QDs revealed a wide absorption spectrum with an excitonic absorption peak of 380nm and a narrow symmetrical emission spectrum of 630nm. The size and pattern of these QDs were studied using Transmission Electron Microscopy (TEM). These nanocrystals revealed their configuration in the form of isolated crystals or clusters measuring from 5-10nm in diameter. X-ray microanalysis combined with TEM permitted analysis of the elemental configuration of these QDs. These CdTe QDs were subsequently bound to HT 29 colon cancer cells to study the interaction of QDs in vitro. As colon cancer cells over-express integrins, QDs were conjugated with RGD (Lysine) and RGD (Cysteine) peptides for the purpose of active binding with HT29 colon cancer cells. The conjugated QDs were applied to colorectal cancer cells to assess their affinity to cellular adhesion molecules. The toxicity of naked and conjugated QDs was also assessed by analyzing cell survival and cell death after exposure to C2C12 mouse skeletal muscle cells. *In vivo* experiment using Sprague

Dawley (SD) rat established feasibility of biodistribution studies with a small dose of 10µg/ml.

Results: These water soluble fluorescent CdTe nanocrystals were synthesized using relatively stable precursors. It was possible to demonstrate binding of these red emitting QDs to the HT29 colon cancer cells *in vitro*. Significant and stable binding was noted after QDs were conjugated with RGD peptides. Toxicity assay evaluation studies suggested that both nonconjugated and conjugated QDs were nontoxic to C2C12 mouse skeletal muscle cells at a concentration of 50 µg /ml indicating that they are less toxic to normal cells, and are safe to be applied to *in vivo* models. Further *in vivo* experimentation in SD rats established feasibility for imaging sentinel lymph nodes following interdigital web space injection of QDs.

Conclusions: RGD-conjugated QDs can selectively target HT29 colorectal cancer cells with low toxicity to normal muscle cells offering a potential novel detection strategy for colorectal cancer. This property can be explored for early diagnostic and therapeutic purpose by selectively targeting cancer cells. Further studies are required in an *in vivo* model to analyze systemic biodistribution and toxicity studies.

Dedication

I would like to express my sincere gratitude to all the staff in the University Department of Surgery at Royal Free Hospital that helped me during my research period.

I would like to thank my wife Savita and my daughters Priyal and Anushka for their continued support during the period of my research.

Hypothesis

1. Novel CdTe quantum dots can bind / be taken up by cancer cells therefore demonstrating potential for clinical application.

2. Nonconjugated and RGD conjugated CdTe quantum dots are less toxic to normal cells than to cancer cells.

Table of Contents:

List of abbreviations

Au	Gold
BRET	Bioluminescence resonance energy transfer
CAM	Cell adhesion molecules
$CdCL_2$	Cadmium chloride
$CdMe_2$	Dimethyl cadmium
CdSe	Cadmium selenide
CdTe	Cadmium telluride
c(RGDfC	Cyclo(Arg-Gly-Asp-D-Phe-Cys)
c(RGDfK)	Cyclo(Arg-Gly-Asp-D-Phe-Lys)
c(RADfV)	Cyclo(Arg-Ala-Asp-D-Phe-Val)
CuInSe2	Copper indium diselenide
DHLA	Dihydrolipoic acid
DMEM	Dulbecco's modified eagle medium
ECIS	Electric cell substrate impedance
ECM	Extracellular matrix
FRET	Fluorescence resonance energy transfer
FWHM	Full width at half maximum
GaAs	Gallium arsenate
GaN	Gallium nitride
H_2O_2	Hydrogen peroxide
HEK	Human epidermal keratinocyte
ICAM-1	Intercellular adhesion molecule-1
InAs	Indium arsenate

InP	Indium phosphate
IR	Infrared
mAbs	Monoclonal antibodies
MoSe	Molybdenum diselenide
MPA	Mercaptopropionic acid
MSA	Mercaptosuccinic acid
MVD	Microvessel density
$NaBH_4$	Sodium tetrahydridoborate
Na_2TeO_3	Sodium tellurite
NIR	Near infra-red
PDT	Photodynamic therapy
PEG	Polyethylene glycol
PKC	Protein kinase C
PL	Photoluminescence
POSS	Polyhedral oligomeric silsesquioxane
QD	Quantum dot
QY	Quantum yield
RGD	Arginine-glycine-aspartic acid
ROS	Reactive oxygen species
RPM	Revolutions per minute
SD	Sprague Dawley
TBP	Tributylphosphine
TEM	Transmission electron microscopy
TGA	Thioglycolic acid

$(TMS)_2S$	Hexamethyldisilathiane
TOP	Trioctylphosphine
TOPO	Trioctylphosphine oxide
UV	Ultraviolet
VCAM-1	Vascular cellular adhesion molecule
VEGF	Vascular endothelial growth factor
VWF	Von Willibrand factor
$ZnEt_2$	Diethylzinc
ZnS	Zinc Sulfide
ZnSe	Zinc-selenium

List of figures

List of Tables

Chapter 1

Introduction

1.1 INTRODUCTION

Nanotechnology has been at the forefront of research in the last two decades. This deals with design, synthesis & fabrication of structures at the molecular scale. The ever expanding field of bionanotechnology aims at revolutionizing biomedical research and clinical practice and has the potential of being incorporated into modern medicine with the aid of exciting physical and chemical properties of nanoparticles aiming at early and precise diagnosis of various life threatening diseases and selective targeting of drugs as well as minimizing the systemic side effects responsible for the morbidity.

Nanotechnology is a multidisciplinary field that involves design and engineering of objects less than 100nm in size. At this size the particles acquire unique physical, chemical, biological, structural and functional properties not presented by their discrete molecules or bulk materials.

Tumors result from genetic alterations of cells, which may involve over or under expression of normal genes, or mutations generating abnormal gene products. This may affect any of the molecules within the cell, the cell membrane or the cancer-cell milieu. In addition, stromal and vascular endothelial cells are important for the exponential growth and spread of the tumour by providing appropriate microenvironment[1].

Cancer nanotechnology is a rapidly expanding field of diagnostic medicine and its allied fields and is expected to rapidly conquest the advances in early diagnosis and effective curative treatments alongside providing in depth knowledge of cancer biology in order to treat aggressive and lethal cancer phenotypes[2,3,4].

Quantum Dots (QDs) are semiconductor nanoparticles in the order of 2-10 nanometers containing approximately 200-10,000 atoms. These nanosized particles have structural and functional properties that are not available from discrete molecules or bulk materials. Structurally, these nanoparticles encompass large surface areas for the attachment of multiple diagnostic (optical, magnetic or radio isotopic) and therapeutic agents. When conjugated with biomolecular affinity ligands such as antibodies, peptides or small molecules, these nanoparticles can be used to target malignant tumors with high affinity and specificity.

In general, QDs are produced using atoms from group II and VI of the periodic table e.g. Cadmium–Selenide (CdSe),Cadmium Tellurium (CdTe), Zinc-selenium (ZnSe), group III-V elements e.g. Indium phosphate (InP), Indium arsenate (InAs),Gallium arsenate (GaAs) Gallium nitride (GaN) or group IV-VI elements e.g. Lead-selenium (PbSe).

Most commonly used QDs are CdSe or CdTe with a passivation shell made of ZnS which protect the core from oxidation and increases the photoluminescence quantum yield. The surface of the QD is further coated with solubilization ligand making them water soluble for their use in cell biology.

As illustrated in fig. 1.1 The QD core determines optical properties of the probe and provides structural scaffolding for engineering of nanodevices.

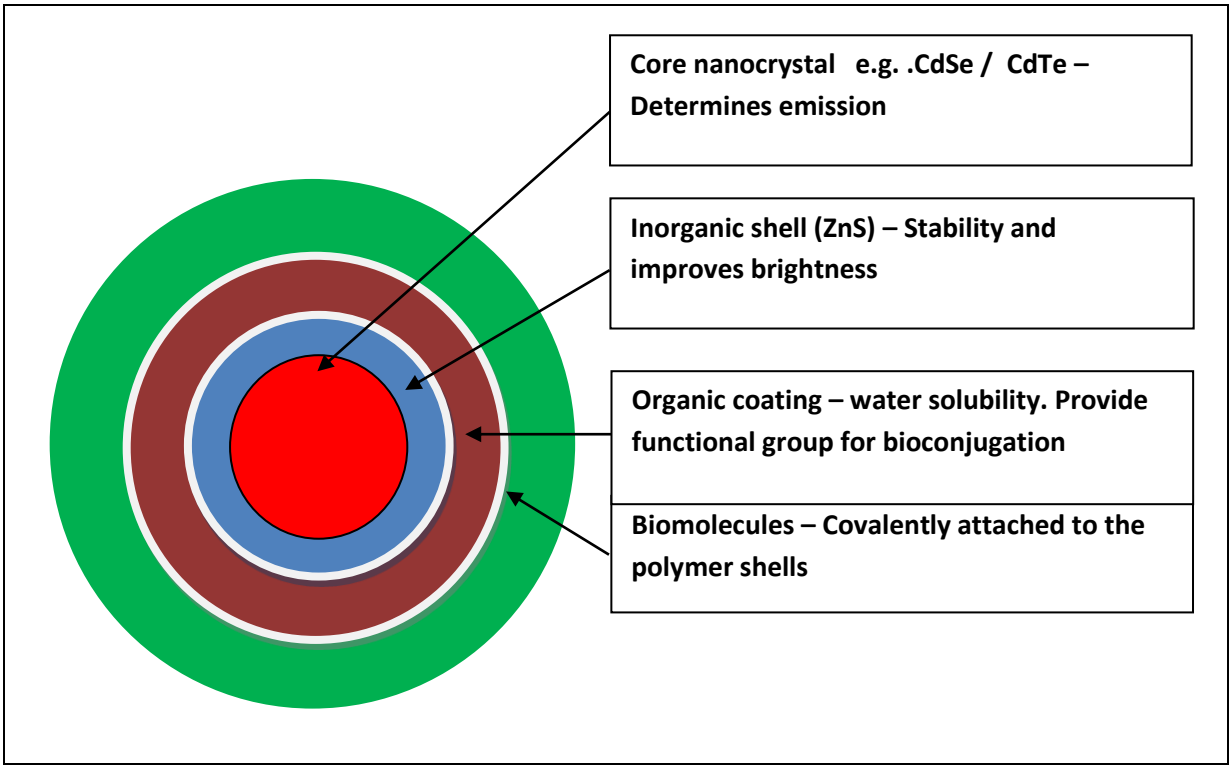

Fig. 1.1 Structure of quantum dot

Quantum dots have emerged as one of the most exciting nanoparticles with a potential for diagnostic and therapeutic application in the field of nanomedicine. The current fluorophores such as organic dyes, fluorescent proteins and lanthanide chelates suffer the problems of instability, photobleaching and sensitivity to environmental conditions such as pH variations. The unique optical and spectroscopic properties of QDs offer a compelling alternative to traditional fluorophores due to their high quantum yield, high molar extinction coefficient (~600,000 M-1 cm-1, roughly an order of magnitude higher than even the strongly absorbing Rhodamine 6G), exceptional resistance to photobleaching as well as to photo and chemical degradation[5,6]. In addition, the intensity of fluorescence produced by the quantum dots is 10-20 times brighter than the organic dyes. Conventional dyes suffer from narrow excitation spectra. This requires excitation by light of specific wavelength, which varies between particular dyes. In addition, they

have broad emission spectra. This means, the spectra of different dyes may overlap to a large extent limiting the number of fluorescent probes that may be used to tag different biological molecules.

Bulk semiconductor materials have a fully populated valence band and an empty conduction band separated by a relatively small band gap (less than 4 eV) between valence and conduction bands, thus behaving like insulators at ambient conditions and exhibiting electrical conductivity only under external stimulation. When an energy exceeding the band gap is supplied, valence-band electrons acquire sufficient energy to populate conduction band and enable electric current flow. In nanoparticles, valence and conduction bands split into discrete energy levels, with the energy gap between closest possible valence and conduction levels increasing with decreasing particle size (and increasing degree of confinement of charge carriers as illustrated in fig. 1.2).

Quantum dots are semiconductors whose excitons are confined in the three spatial dimensions. When a photon enters the semiconductor, an electron is released. This electron possesses enough energy to cross the band gap by migrating from the valence band to populate the higher energy conducting band. When this occurs, a hole which is of opposite charge to the electron is created into the valence band. The radiative recombination of the charge carriers (hole and pair) results in fluorescent emission when the electron falls back into the valence band giving rise to the exciton. This relaxation of an electron results in the release of bandgap energy in the form of light (fluorescence)[7,8,9].

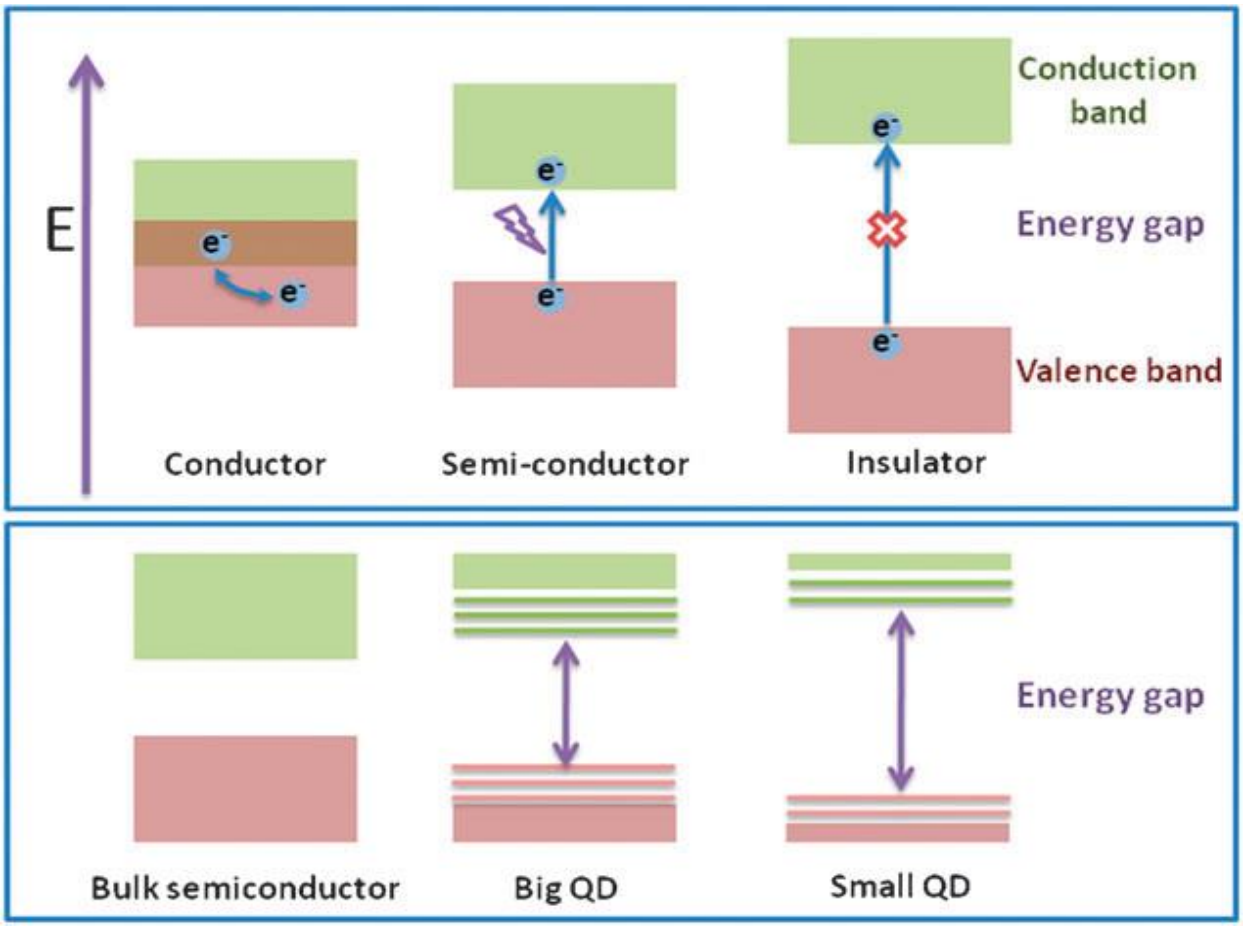

Fig. 1.2 Electronic structure of bulk conductor, semiconductor, and insulator materials (top panel) and semiconductor nanoparticles (bottom panel)[10].

Besides retaining bulk property of the material from which these QDs are derived, they also acquire novel properties in view of their nanosize. These include large absorption spectra, narrow and symmetric emission spectra (full width at half maximum of 25-35nm) with a light spectrum ranging between Ultraviolet (UV) to Near- Infrared (NIR) (400-1350nm) and the stokes shifts that can be greater than 200nm. As the QDs have broad absorption spectra, excitation by a wide range of wavelengths is feasible. This property can be exploited to simultaneously excite different coloured QDs using a single wavelength. QDs have narrow emission spectra. This can be controlled in a simple manner by producing variations in the size, composition and surface coating.

Besides possessing the ability to produce a very high quantum yield of up to 90% (ratio of emitted to absorbed photons), they also have large absorption cross sections and long fluorescence lifetimes (> 10 ns) As a result these quantum dots have emerged as a new class of fluorescent bio-probes. Other properties of QDs include large absorption cross section (extinction coefficient), good quantum yield and large saturation intensity. These properties render the quantum dots brighter than any available fluorescent dyes.

Physical size smaller than the exciton Bohr radius results in a 3-dimensional quantum confinement of charge carriers within the QD and limits the number of possible energy states that an electron can occupy, thus giving nanoparticles novel properties not achievable in bulk materials. Additionally, relatively small size comparable to that of large biomolecules (e.g. antibodies) aids in engineering of biologically functional materials. The inorganic nanoparticle core provides a rigid foundation for the development of QD probes. Manipulation of the core chemical composition, size, and structure controls the photo-physical properties of the probe.

Quantum Dots offer tunable photoluminescence (PL) due to quantum confinement effects related to the size and composition of these nanocrystals. The inherent benefits of narrow emission bands, large stokes shifts and long half-lives is that the mixture of QDs can be used to concurrently track different targets in multiplexed analysis and imaging. Manipulation of QD size & composition permits tuning of PL emission in NIR region within the optical windows of 700-1100nm. This allows for effective deep tissue imaging uninterrupted by optical interference from biological components. The size, shape and composition of QDs determine the PL emission range which can vary between Ultraviolet and infrared region of electromagnetic spectrum[11].

Fluorescence lifetime is the measure of decay of fluorescence emission after excitation. Autofluorescence of cells lasts 2 nanoseconds. The fluorescence lifetime of organic fluorophore lasts between 1-4ns however that of QDs is between 20-30ns. Autofluorescence of cells provide background fluorescence reducing detection sensitivity. This can be easily overcome by the prolonged fluorescence lifetime of the QDs which continue to emit photons long enough benefiting fluorescent cellular imaging of biological samples[12].

1.2 BACKGROUND

To date, QDs have been synthesized by different methods including organic and aqueous synthesis. Bare QDs are not routinely employed for biological application as a result of structural imperfections associated with blinking, predisposition to photochemical degradation and toxicity. Passivation with high band gap inorganic shell result in the synthesis of more stable QDs with superior photoluminescent properties. High temperature synthesis involving pyrolysis of organometallic precursors has been the most frequently used method for synthesis of high quality QDs in organic solvents. Often the precursors used in this synthetic process are highly toxic and unstable. By using alternative cheaper and safer Cadmium precursor materials, QDs with reasonable photoluminescence can be synthesized in the organic solvents. However being water insoluble, these surfactant coated QDs need surface modification either in the form of encapsulation in phospholipid micelle or amphiphilic polymers. Alternatively, ligand exchange method can be applied to switch hydrophobic surface ligands with hydrophilic ones in order to be safely utilized in the biological environment. Aqueous synthesis although result in fabrication of

QDs with poor size distribution and low fluorescence efficiency, it carries the advantage of being simple, less toxic and reproducible.

Ying et al[24] published a simpler one pot approach to synthesize water soluble CdTe QDs using Sodium Tellurite as a Te source totally eliminating the need for highly toxic H_2Te (Tellurane) or highly unstable NaHTe as a Tellurium precursor. Using Thiol stabilizer Mercaptosuccinic acid (MSA) as a capping ligand, they could improve the QY from < 20 % to 83% at pH 5 and in excess of 70% at pH 6-8. The authors highlighted the influence of pH, molar ratio and the reaction temperature in the synthesis of high quality water soluble CdTe QDs. This technique forms the basis of present study.

1.3 AIM OF THE THESIS

This study aimed at designing and synthesizing water soluble CdTe QDs from the stable precursors cadmium chloride and sodium tellurite in the presence of mercaptosuccinic acid as a capping ligand. The QDs thus synthesized were intended to be studied for following features-

a) To assess the stability of these QDs.
b) Spectrophotometric analysis to identify excitation and emission spectrum.
c) To measure the size of these QDs at TEM studies.
d) Analysis of chemical composition at X-ray microanalysis.
e) To evaluate cytotoxicity assay of nonconjugated and conjugated QDs.
f) To study interaction of these QDs with HT-29 colon cancer cells *in vitro* and
g) To explore the feasibility of application of these QDs in the animal experiment *in vivo.*

DESCRIPTION OF CHAPTERS

Chapter 1 This chapter gives a brief introduction of structure and physico-chemical properties of quantum dots in general and mentions the aims of this thesis.

Chapter 2 This chapter critically reviews of development of QDs and their biomedical application.

Chapter 3 This chapter elaborates the method of synthesis of water soluble CdTe QDs and describes characterization of these QDs.

Chapter 4 This chapter describes materials and methods used in the cell culture experiments, transmission electron microscopic studies and cytotoxicity assay.

Chapter 5 This chapter explains cytotoxicity assay of nonconjugated and conjugated CdTe QDs.

Chapter 6 This chapter mentions about the outcome of QD interaction with cancer cells *in vitro*.

Chapter 7 This chapter enumerates the feasibility of quantum dots for *in vivo* application.

Chapter 8 This chapter summarizes the results of these various studies and gives an insight into the future direction of these novel fluorescent nanoparticles for diagnosis and treatment of various cancers.

Chapter 2.

Development of quantum dots and their biomedical application – a review

2.1 QUANTUM DOT SYNTHESIS

The QD core defines the optical properties of the probe and exemplifies a structural scaffold for engineering of various nanodevices. The QD core has to be stable and compact with precisely controlled size distribution, chemical composition, geometry and surface chemistry. QD synthesis was first described by Efros and Ekimov in 1982 when they grew nanocrystals and microcrystals of semiconductors in glass matrices. Subsequently researchers prepared QDs in different media such as aqueous solution, high temperature organic solvents and solid substrates. QDs synthesized in aqueous media resulted in poor size distribution and low fluorescence efficiency.

Bare core QDs have their own disadvantages. The crystalline structure of these nanoparticles impart themselves to imperfections resulting in emission irregularities particularly blinking in which single QDs switch between fluorescent and nonfluorescent states despite continuous illumination. Also, in view of their large surface area: volume ratio they are prone to photochemical degradation. Core-shell QDs has several advantages over core only QDs in the form of higher physical, chemical stability and photoluminescence, quantum efficiencies when shelled by higher band-gap semiconductors and polymers. The photostability results from hole confinement in the core. Electronic accessibility results from electron spreading into the shell. In addition, the shell provides a platform for conjugation of various biologically active molecules for diagnostic and therapeutic purpose without interfering with the optical properties of the core compound. The surfaces of these nanocrystals are made up of atoms that are not fully coordinated and hence they act as defects unless passivated. Overcoating these nanocrystallites such as CdSe with

higher bandgap, inorganic materials such as ZnS have been shown to improve the photoluminescence quality yield by passivating surface nonradiative recombination sites. These passivated quantum dots with inorganic shell structures provide a robust crystal lattice in building up complex bioconjugated chemical agents. The core, shell and the coating characteristics affect the photochemical properties of the QDs. So the synthesis of the QDs can be tailored accordingly using precise growth techniques involving high annealing temperatures.

Advances in synthetic procedures and surface chemistry have enabled production of water soluble QDs with high quantum yield (40-50%) and relatively narrow size distribution. High temperature synthesis is the most commonly used method of Quantum Dot production. Bawendi et al in 1993 first reported synthesis of high quality monodisperse QDs from Cadmium Sulfide (CdS), Cadmium Selenide (CdSe) and Cadmium Telluride (CdTe) through high temperature organometallic procedure[13]. In this procedure pyrolysis of organometallic precursors at high temperature yielded nucleation and growth of nanocrystals, while coordination of trioctyl phosphine/trioctyl phosphine oxide (TOP/TOPO) base with unsaturated metal atoms on the QD surface prevented the formation of bulk semiconductor. But utilization of a highly toxic, volatile, explosive, pyrophoric and expensive Cadmium precursor (dimethyl cadmium) had their own disadvantage of imposing restrictions on the equipment with limited flexibility in the QD core design. During the synthesis of QDs using organometallic procedure, precise kinetic control can be achieved over growth of the nanocrystals. So QD population with a narrow size distribution can be easily achieved. Relatively simple reaction conditions along with slower nucleation and growth rates offer extensive flexibility in engineering of QD chemical composition, geometry, and photo-physical properties. As the difference in energy

between the discrete ground and excited states increases with increasing degree of confinement (i.e. decreasing particle size), the size of the band gap and, consequently, the colour of emitted light can be fine-tuned by adjusting the QD size.

Qu et al. used alternative cheaper and greener Cadmium precursor materials such as Cadmium oxide and Cadmium acetate[14-16].

Gaponik et al in 2002 synthesized biocompatible CdTe QDs capped with thioglycolic acid (TGA) by the reaction between an aqueous solution of cadmium perchlorate hexahydrate (2.35 mmol, 125 mL) and H2Te gas in the presence of TGA (5.7 mmol) at 100 °C and ~11.5 pH; H2Te gas was prepared by adding aluminum telluride (0.46 mmol) into a dilute sulfuric acid solution (30 mL, 0.5M) under N2 atmosphere. The advantage of aqueous synthesis over organometallic synthesis was simplicity and high reproducibility at a significantly lower cost. The authors however did agree that the nanocrystals synthesized by aqueous approach do not possess the degree of crystallinity of the organometallically prepared QDs produced at high annealing temperature (200-360ºC) by so called hot injection technique resulting in very effective separation of nucleation and growth stages. However it was possible to synthesize smaller CdTe and CdSe QDs using size selective precipitation procedure which was more reproducible[14;17].

Dabbousi et al in 1997 synthesized CdSe /ZnS QDs via the pyrolysis of the organometallic precursors, dimethylcadmium and trioctylphosphine selenide in a co-coordinating solvent Trioctylphosphine oxide (TOPO). They prepared a solvent mixture (10:1 weight: weight) composed of TOPO and TOP by heating TOPO at 190 °C under vacuum, cooling to 60 °C and adding TOP. Also, a CdSe QD (0.4 mmol) suspension was prepared in hexane, transferred into the solvent mixture, and hexane was distilled out. A solution of Diethylzinc ($ZnEt_2$) and hexamethyldisilathiane

($(TMS)_2S$) in TOP was added drop-wise into the CdSe suspension kept at 140– 220 °C, and ZnS shells were grown at this temperature. When required thickness for ZnS shells was attained, judged from the absorption spectrum, the reaction was stopped by adding 1-butanol.The reaction mixture was cooled to room temperature, and the core/shell QDs were separated by precipitation from a mixture of 1-butanol and methanol[14;18].

There are two major approaches to synthesizing QDs. One of these is the 'bottom-up' approach, more familiar to the chemists. This process utilizes molecular or ionic precursors of QDs that are allowed to react together in solution to produce the nanocrystals as colloids. The other approach, more familiar to engineers, is the 'top-down' approach where feature sizes on the 1–10-nm scale are carved out lithographically or electrochemically from a semiconductor substrate. More recently, a third class known as the hybrid route has been proposed as an alternative for QDs synthesis. Researchers make molecular precursors for the QDs, which then react in the gas phase and are deposited as thin films on substrates. So far, the colloidal route has become the most popular process for QDs synthesis. In fact, QDs used in bioapplications are exclusively colloidal nanocrystals. They are commonly synthesized through the introduction of semiconductor precursors under mild and simple reaction conditions that thermodynamically favor slower nucleation and crystal growth, in the presence of semiconductor-binding agents, which function to kinetically limit particle growth and maintain their size within the 'quantum confinement' size regime. The size-dependent optical properties of QDs can only be achieved if the semiconductor nanocrystals are prepared within narrow size distributions[19]. As the difference in energy between discrete ground and excited states increases with increasing degree of confinement (decreasing particle size),

size of the band gap and consequently the colour of emitted light can be fine-tuned by adjusting the QD size. By varying the chemical composition of the nanocrystals and application of band gap engineering, it is possible to produce QDs emitting light from UV, throughout the visible spectra into the infrared spectra. (400-4000nm).

QDs have a huge surface area: volume ratio which makes them extremely unstable in solution causing them to agglomerate forming clusters because of the high surface energy. Hence, any route one chooses to synthesize QDs should consider stabilizing the just formed nanocrystals by minimizing surface energy via 'capping' and avoiding further structure growth. The QDs thus produced by organometallic procedure have low quantum yield. Moreover TOPO coated QDs are unstable with respect to photo-oxidation resulting in degradation of nanocrystals and potential toxicity due to release of free Cadmium ions. As the radius of the spherical particle decreases, the ratio of its surface area to volume rapidly increases exposing larger number of atoms on its surface. These surface atoms lack their neighbors to form chemical bonds. As a result, unoccupied electron orbitals commonly known as dangling bonds or surface trap sites can trap charge carriers to either prevent or delay electron-hole recombination with subsequent photon emission reducing the fluorescence quantum yield. In addition, these sites might exhibit enhanced chemical reactivity and compromise chemical stability of the nanoparticles. In order to prevent these adverse effects, these surface trap sites can be saturated by organic and inorganic capping layers.

Several groups have utilized high band gap energy inorganic shells made up of several atomic layers thick CdS or Zns to effectively passivate the photoactive core of QDs. The wider bandgap of these shells effectively confine the exciton to the QD core reducing the nonradiative relaxation pathways and increasing the quantum

yield. Although thin shells made up of 1-2 monolayers produce highest fluorescence yield, thicker shells consisting of 4-6 monolayers provide more core protection from photo-oxidation and degradation. Peng et al synthesized CdSe/CdS core/shell QDs by adding 15 mL anhydrous pyridine to TOPO capped CdSe nanocrystals (2–13 mg) and by refluxing the mixture overnight under an argon atmosphere. Temperature of the CdSe solution was set at 100 °C, and a precursor solution was added for CdS consisting of hexamethyldisilathiane and CdMe2 dissolved in tributylphosphine (TBP). The shell growth was carried out at 100 °C, and the reaction was stopped by removing heat when desired shell-thickness was obtained. The CdSe/CdS QDs were separated from the reaction mixture by adding dodecylamine. Shelling CdSe QDs with CdS resulted in considerable red-shifts in the absorption and photoluminescence bands of QDs[20]. They observed confinement of the hole created during excitation within the CdSe core by a higher band-gap CdS shell. As a result of this confinement the hole dependent photo-oxidative processes causing QD degradation resulting in loss of fluorescence are impeded. They also suggested that thicker shell might reduce QD blinking associated with charge trapping and un-trapping at surface defect of the nanomaterial.

Alternative approaches to improve fluorescence efficiency by optimizing surface structure of the nanocrystals and minimizing the number of surface trap sites have proven to be successful. These include improving surface coating with multiple organic ligands by use of alkylamine surfactants such as (hexa/octa/do) decylamine along with TOPO to achieve QY of up to 40-50%.

Advances in synthesis and surface passivation technologies have opened a new platform for these QDs to be used as biological probes with advantages of enhanced

photostability, improved brightness, tunable fluorescence and single source multicolor excitation.

QDs are synthesized in nonpolar organic solvents such as toluene, hexane or chloroform in presence of surfactants at a high temperature. These surfactant coated QDs have hydrophobic chains protruding from the surface of inorganic QD core. Due to the presence of a hydrophobic surface layer, they are not soluble in aqueous media. In order to be useful for biological applications QDs must be made water soluble. Water solubilization procedure should render these nanocrystals soluble and stable in biological buffer solutions preserving the original photophysical properties without alteration in their size and providing reactive groups for subsequent conjugation to biomolecules.

To achieve this either the surfactant layer can be shielded with an additional layer introducing hydrophilic moieties such as polymer or the surface hydrophobic ligands can be exchanged with the amphiphilic ones.

The surface shielding in the form of encapsulation in phospholipid micelles or coating with amphiphilic polymers can retain the original hydrophobic surface ligands preserving the original QD photophysical properties and minimally affecting the fluorescence quantum yield. During this process the original native TOPO coating is retained and the hydrophobic QDs are encapsulated with amphiphilic molecules such as polymers or phospholipids. The hydrophobic portion of this molecule intercalates with alkyl-chain-terminated surface ligands and the hydrophilic portion protrudes outwards interacting with the aqueous solvent and rendering the particle water soluble. The water soluble QDs thus synthesized are exceptionally stable with preserved optical properties. However the disadvantage of this process is the increase in the resultant diameter of the quantum dot which is three –four times the

original size. As a result, difficulties may be encountered during experiments in live cells and in vivo applications. The increased thickness of the polymer coating might preclude utilization of QDs in Forster resonance energy transfer (FRET) based applications.

In contrast, the original hydrophobic surface ligands can be replaced with hydrophilic ones by means of ligand exchange. This can be accomplished by substitution of native TOPO coating with bifunctional ligands, which present both, a surface anchoring thiol group and a hydrophilic end group such as carboxyl or hydroxyl group. Examples include deployment of negatively charged carboxy-terminated thiols such as Mercaptoacetic acid (MAA) and Mercaptopropionic acid (MPA) and thiol-containing Zwitterionic molecules such as cysteine. These QDs provide various reactive groups such as amine (-NH3), carboxyl (-COOH) or mercapto (-SH) for conjugation to various biomolecules. The ligand exchange method involves mixing the solution containing excess of heterobifunctional ligand to the suspension of TOPO coated QDs to displace hydrophobic TOPO ligands to be replaced by adsorption of bifunctional ligands. The example of this method includes coating of CdSe –ZnS QDs with mercaptoacetic acid in order to bind the basic thiol groups to the surface of QDs yielding QDs displaying carboxylic acids. By this method, it is possible to synthesize water soluble QDs with ultra-small hydrodynamic diameter (below 6 nm) providing amine and carboxylic acid groups for cross-linking to proteins, peptides and nucleic acids. The disadvantages of QD synthesis by this method include detachment of ligands from QD surface leaving behind surface trap sites resulting in nanoparticle aggregation and decreasing fluorescence efficiency, photochemical stability as well as decrease in the shelf life of the probes.

Another ligand exchange approach is available involving the formation of polymerized silanol shells on the surface of QDs using 3-(mercaptopropyl) trimethoxysilane (MPS) to displace the native TOPO molecules have been described. These polymerized siloxane coated nanoparticles are highly stable against flocculation however residual silanol groups on the surface of the QDs often leads to precipitation and gel formation at neutral pH.

Polyethylene Glycol (PEG) is one of the most widely used molecules for the purpose of QD solubilization in the amphiphilic organic surface layer. Addition of PEG (pegylation) prolongs the half-life of these QDs possibly from decreased opsonisation and delays recognition and clearance by reticuloendothelial system. Other advantages of pegylation include improved aqueous solubility and reduction in the nonspecific adhesion to the biological cells of the QDs.

Yin et al in 1999 prepared Zinc Sulfide (ZnS) QDs using γ-Irradiation. Tsuji et al in 2005 synthesized gold (Au) QDs using microwave assisted synthesis. The authors observed that microwave irradiation resulted in stabilization of water soluble surfactant at the surfaces on the gold metal and accelerated precipitation as well as nucleation processes leading to synthesis of uniform QDs. Besides the preparation of Au QDs, microwave heating has also been used to synthesize cadmium sulfide (CdS), cadmium selenide (CdSe), lead sulfide (PbS), copper indium diselenide (CuInSe2), and molybdenum diselenide (MoSe2) QDs. The advantages of using microwave radiation in the synthesis of QDs include absence of a convection processes while heating giving a homogeneous vessel temperature for uniform nucleation and growth, as well as shorter crystallization time.

Utilization of Langmuir- Blodgett surfactant films using stearate and *n*-octadecylacetoacetate as a matrix has also been used for synthesis of ZnS, PbS,

and a PbS–CdS combination of QDs in order to provide restricting environments giving specific size, shape, and orientation to the QD[9].

Since then significant advances have been made in the synthesis of fluorescent QDs with particular focus on Cadmium Selenide (CdSe) QDs with their vast biological applications. QD production is now a molecular engineering process. Most commonly available QDs are CdSe-ZnS core shell complexes containing Cadmium Selenide (CdSe) core synthesized in a nonpolar solvent coated with Zinc Sulfide (ZnS) shell subsequently encapsulated with an amphiphilic polymer capable of cross linking to various biomolecules to specifically target molecular agents[21].

In designing the Quantum dot probes, the QD core composition is determined by a desired wavelength of emission.eg CdSe QDs to emit in the range of 450-650nm or CdTe QDs to emit in the range of 500-750nm. InAs or PbSe which can emit above 800nm[22].QDs are then synthesized by adding the precursors in presence of a co-coordinating ligand under inert conditions grown to the appropriate wavelength-dependent size.

In a typical synthesis of CdSe QDs, selenium precursor trioctylphosphine –selenide or tributyl phosphine –selenide at room temperature is injected into a hot mixture of cadmium precursor dimethylcadmium or cadmium oleate and a co-coordinating ligand trioctylphosphine oxide or hexadecylamine at an approximate temperature of 300°c under inert conditions (nitrogen or argon atmosphere) to form the nuclei of CdSe nanocrystals. The remaining cadmium and selenium precursors grow on these existing nuclei at lower temperature of 240-270°c and a slower rate. Once the QDs reach the desired size and wavelength, the reaction mixture is cooled to room temperature to arrest the growth of these crystals. To enhance the photoluminescence efficiency and to reduce the rate of oxidative photobleaching, the

CdSe cores are coated with ZnS shell. Zn^{2+}atoms on the surface of QDs bind more strongly to ligands such as phosphines and alkyl amines as well as they increase the colloidal stability of the nanoparticles[23].

Ying et al [24] in 2008 published a simpler approach to prepare luminescent cysteine–coated CdTe nanocrystals with QY of 10% using Sodium Tellurite as the Te source. This eliminated the need for highly toxic H_2Te or highly unstable NaHTe as a Tellurium precursor for the aqueous synthesis of Thiol-capped CdTe nanocrystals in the inert atmospheric conditions. As the QYs of CdTe nanocrystals synthesized in the aqueous phase is < 20%, the authors used thiol stabilizer Mercaptosuccinic acid (MSA) as a capping ligand. They demonstrated that by optimizing the growth conditions, such as pH of solution and the concentration of precursor solutions, the QY can be dramatically improved up to 83% at pH 5 without any post-treatment and up to in excess of 70% at pH 6-8.

The predominant chemicals used during the synthesis of CdTe nanocrystals by this method included Cadmium chloride ($CdCL_2$), Sodium Tellurite (Na_2TeO_3), Mercaptosuccinic acid (MSA) and Sodium tetrahydridoborate ($NaBH_4$) in the presence of buffer solution consisting of Borax ($Na_2B_4O_2$)and citric acid. The presence of buffer solution is crucial for successful synthesis of highly luminescent CdTe QDs.

The following chemical reaction takes place during the synthetic process-

$$TeO_3^{2-} + BH_4^- \rightarrow Te^{2-} + B(OH)_3 + H_2O \quad (1)$$

$$CdL + Te^2 \rightarrow CdTe + L \text{ , Where L = MSA} \quad (2)$$

During this reaction, $NaBH_4$ reduces TeO_3^{2-} to Te^{2-} . Cd^{2+} reacts with this fresh Te^{2-} to generate CdTe. The citrate is added to this mixture to avoid deposition of Cadmium Tellurite ($CdTeO_3$).

Te^{2-} is very sensitive to the oxygen. During the above process, initially formed Te^{2-} may possibly be reoxidized to higher valence of Tellurium by the oxygen dissolved in the water but is instantly reduced back to Te^{2-} by an excess of $NaBH_4$. Thus $NaBH_4$ not only acts as a strong reductant but produces an inert atmosphere to avoid reoxidizing Te^{2-}.

An excess of $NaBH_4$ is either hydrolyzed or oxidized by the oxygen diffused from air through one of the following reactions-

$$BH^-_4 + H_2O \rightarrow B(OH)_3 + OH^- + H_2$$

$$BH^-_4 + O_2 \rightarrow B(OH)_3 + H_2O$$

During this method of CdTe synthesis, air-stable sodium tellurite was used as a source of Te. MSA proved to be protective even at lower pH aqueous solution (pH <8). The CdTe Quantum dots thus produced continued to retain bright photoluminescence over a few months when stored in the refrigerator at 4 º C.

Bao et al [25] in 2006 synthesized cysteine- capped CdTe nanocrystals by this technique. They observed absorption and photoluminescence spectrum serially during time gated QD growth stages as shown in fig. 2.1.

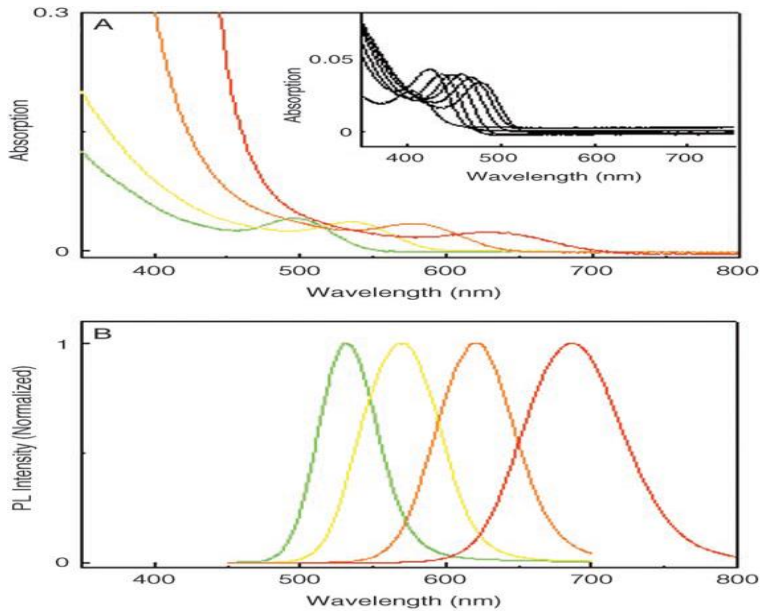

Fig. 2.1 *Absorption (A) and photoluminescence (PL) (B) spectra of L-cysteine-capped CdTe nanocrystals recorded after particle growth for 45 min Green),75 min (yellow), 180 min (orange; λ_{ex}=400 nm), and 12 hr. (red; λ_{ex}=450nm*[25]

Ying et al[24] from the same institute synthesized highly luminescent Mercaptosuccinic acid coated CdTe using similar technique[24] Their observation of photoluminescence spectrum published in 2008 remains as shown in fig. 2.2.

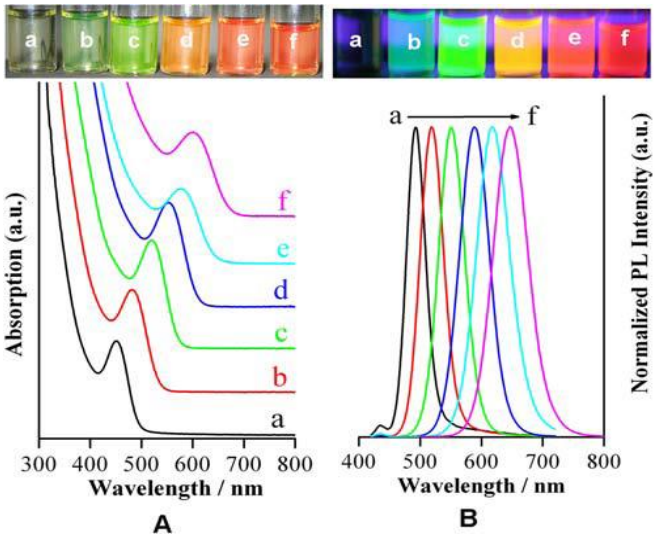

Fig. 2.2, The image of MSA-coated CdTe QDs with different sizes and the corresponding absorption spectra (bottom); photoluminescence were at a) 493 nm, b) 519 nm, c) 551 nm, d) 589 nm, e) 617 nm, f) 647 nm.

2.2 BIOCONJUGATION & INTRACELLULAR DELIVERY OF QUANTUM DOTS

The QDs thus synthesized are inert nanoparticles. In order for these to be utilized for biological applications, the surface of these QDs needs alteration in order to allow conjugation of biomolecules without altering the biological activity of the conjugated form. This can be achieved by conjugating them with proteins, peptides, nucleic acids or other biomolecules. One of the simplest and most popular bioconjugation methods involves covalent bond formation between reactive functional groups such as primary amines, carboxylic acid, hydroxyls and thiols. An example includes linking of proteins to carboxylic acid containing QDs through naturally existing amine groups via carbodiimide- mediated amide formation. This reaction does not require additional chemical modification of proteins thereby preserving their natural structure. However no precise control can be achieved over molecular orientation of the attached proteins. This may result in partial or complete loss of biological functionality of the ligand.

Another covalent bonding procedure involves active ester maleimide- mediated amine and sulfhydryl coupling. However during this procedure, ligands such as antibodies may require additional treatments in the form of reduction with dithiothreitol in order for the free sulfhydryl groups to be made available. This procedure may yield stable QD-ligand complexes but the chemical treatment might alter the biological activity of the ligand reducing the sensitivity and specificity of the biological probe.

Covalent binding provides simple, effective and more stable bioconjugation to achieve specific targeting abilities using biomolecules such as oligonucleotides,

antibodies[26] or small molecule ligands, streptavidin, avidin, biotin, Immunoglobulin G, transferrin peptides, nucleic acids, adenine, serotonin, adenine monophosphate or wheat germ agglutinin in order to specifically target the cellular organelle of interest.

Silanized Quantum Dots are one of the most popular bioconjugated nanocrystals. Coating with polymerized silica increases the stability of the QDs in buffer solutions under physiological conditions. The optical properties of the QD are still retained. The silica coating allows easy introduction of biological functional groups and the toxicity of inorganic nanocrystals is diminished too[22,27] During synthesis silica, silane derivatives, or other coatings can include functional groups capable of direct conjugation. Such cross-linking strategies exploit the functional groups present on both the quantum dot surface and the biomolecule. For example: carbodiimide compounds are commonly used to link amino-functionality with carboxyl-groups. Another very commonly applied conjugation scheme involves the biotin–streptavidin linkage, which requires coupling of the quantum dot to streptavidin. Quantum dot–streptavidin conjugates are useful because a wide range of proteins and other biomolecules can be biotinylated. These conjugates have applications in staining and labeling, live tracking, and drug screening. For the large majority of applications QDs entities act simply as nonfunctional probes and have minimal impact on the experiment, the binding event or the surroundings. Nonspecific attachment to unintended molecules and aggregation of quantum dot-conjugates is possible and may negatively impact on the results of an experiment. Some strategies have been developed seeking to minimize or even eliminating possible nonspecific binding. Example of which include coating QDs with an inert hydrophilic polymer, such as polyethylene glycol (PEG).

Fluorescence microscopy is a widely used optical imaging modality for the evaluation of healthy cell phenotypes, and for the detection of the molecular signatures of disease. Histological techniques such as fluorescence in situ hybridization (FISH) and immunohistochemistry (IHC) are used to detect nucleic acids and protein biomarkers within cells and tissue specimens with a very high degree of sensitivity and spatial resolution. As labeling biomarkers; organic fluorophores have been widely utilized. However due to quick photobleaching, spectral overlap between probes and the need to excite fluorophores at unique wavelengths their application for multiplexed imaging and for quantitative analysis for molecular profiling is limited. However QD probes are able to overcome these shortcomings of organic fluorophores.

Lidke et al successfully demonstrated the use of red light emitting CdSe –ZnS QDs coupled with epidermal growth factor to bind to cultured human cancer cells expressing erb/HER membrane receptor to which they had specific affinity. They could continuously track the protein diffusion and internalization of these fluorescent quantum dots within these cancer cells successfully. Wu et al demonstrated utility of QD-streptavidin and QD-antibody bioconjugates for simultaneous labeling of membrane –associated HeR2 receptor and of a nuclear antigen in breast cancer cells as shown in fig. 2.3. Since then QDs were used to monitor binding to various plasma membrane proteins such as integrins, tyrosine kinases and G-protein coupled receptors. The procedure of receptor labeling and receptor dynamics has also been described recently. QDs have been successfully used for in vitro bioassay, fixed cell labeling, imaging of tissue specimens and imaging of membrane proteins on living cells.

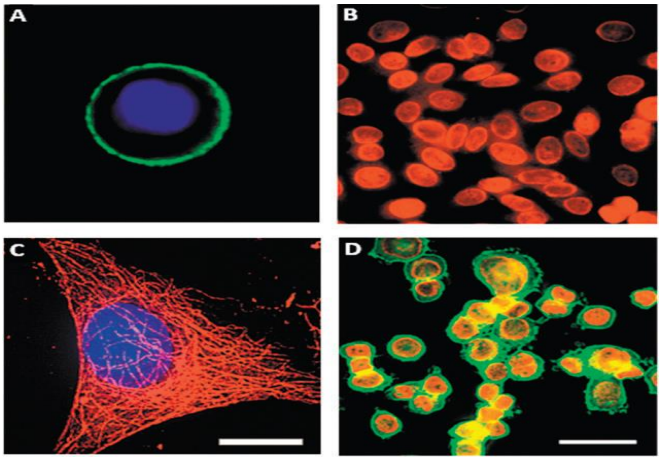

Fig. 2.3 labeling of surface and intracellular targets with QD probes. In single-color examples membrane-associated Her2 receptors are detected with primary antibodies and QD-labeled secondary IgG (A, green), while intracellular nuclear antigens (B, red) and microtubules (C, red) are visualized with primary IgG/secondary IgG-biotin/ QD-Streptavidin cascade. Both labeling routes can be applied simultaneously for a two-color staining (D). The nuclei are counterstained with Hoechst 33 342 (blue) in A and C[28].

The process of staining fixed cells and tissue specimens provides valuable information regarding expression of biomarkers and their distribution within the cells. However real-time imaging of live cells enables the study of physiological, dynamic processes occurring at the molecular level. The relatively large sized QD probe often tends to target biomarkers expressed on the surface of the cell membrane. During live cell imaging, QDs tend to aggregate inside the cells trapped in the endocytotic vesicles as endosomes and lysosomes. Quantum dots can be internalized into a variety of cells using various techniques. The cells take up particles from the extracellular space through endocytosis. This type of passive uptake is diffuse, slow and nonspecific. Some small diameter QDs can even enter the nuclei. However, labeled QDs with antibodies, targeting peptides or receptor ligands can be selectively targeted to intracellular organelle or plasma membranes. This process of quantum dot uptake can be facilitated by coupling the QDs to membrane receptors

which results in the rapid uptake and isolation of QDs in the vesicles within the cells. Though selective targeting of intracellular organelles is not possible by this method, cells can be labeled with QDs very effectively. Chemically mediated delivery involves translocation of the plasma membrane using cationic lipids or peptides. Mechanical delivery methods include microinjection of QDs into individual cells or electroporation using pulsed electric fields to improve membrane permeability in order to deliver QDs within the cells Despite of difficulties encountered in organelle led intracellular target imaging several reports have been published in their success. In 2004 Derfus et al demonstrated that QDs conjugated to organelle targeting peptides, when microinjected into fibroblast cytoplasm, could selectively stain mitochondria or cellular nuclei[29]. Chen and Gerion used electroporation to overcome the plasma membrane barrier to target peptide –QD conjugates to cellular nuclei[30]. Strategy of QD cell loading using osmotic lysis has been explores widely to encourage efficient uptake by the cells. This involves inducing pinocytosis by incubation of cells in a hypertonic solution followed by osmotic lysis of the vesicle and cytoplasmic release of QD. This process enables uniform loading of all cells within a population by intact single QD probes. Courty et al demonstrated that it was possible to image individual kinesin motors in HeLa cells using QDs which were delivered into the cytoplasm via osmotic lysis of pinocytotic vesicle[31]. However during this process of external triggering of osmotic lysis can interfere with QD loading of fragile cells and requires extensive optimization of procedure.

An alternative approach using engineering of on-demand endosome disrupting capacity within the QD probes. Kim et al employed 100 nm external biodegradable delivery vesicles made of poly (D, L-lactide-co-glycolide) (PLGA). These vesicles were further bioconjugated with antibodies for specific interaction with the cell

surface markers. Once taken up within the cells, PLGA charge reversal within low pH endosomal environment results in membrane destabilization and endosomal escape. Upon entering the cytosol, the polymer nanosphere undergoes hydrolysis, thus releasing the QD bioconjugates. This approach facilitates multiplexed labeling of subcellular structures inside live cells[32]. Duan and Nie reported a new generation of QDs based on the use of multivalent and endosome-disrupting surface coating. They coated QDs with hyperbranched copolymer ligand such as PEG grafted polyethylenimine (PEI) to encapsulate and solubilize luminescent QDs through ligand exchange reactions. Due to the positive charges and 'Proton sponge effect' associated with multivalent amine groups, these ligand exchanged QDs were found to penetrate the cell membranes and to disrupt the endosomal organelles in living cells. Polyethylenimine has been known to be cytotoxic. The grafted highly hydrophilic PEG segment was found to significantly reduce the toxicity, improve overall nanoparticle stability and biocompatibility. In addition, these QDs were smaller in size with a HD of 15-22nm and exceedingly stable in acidic environment. As a result when incubated with live HeLa cells, these QDs were internalized escaped from the endosomes and became distributed throughout the cytosol. However ligand exchange method and direct interaction of PEI with the QD surface did result in undesirable drop in the fluorescence QY and detection sensitivity.

Lovric et al reported that size of the QDs contribute to their subcellular distribution. They observed in murine microglial N9 cell lines that red cationic QDs (5.2nm) were distributed throughout the cytoplasm however similarly charged smaller green QDs (2.2nm) were found in the nucleus of the cells following cellular uptake through passive endocytosis.[33] Nabiev et al proposed that nonfunctionalized QDs exploit the cell's active transport machineries for delivery to the specific intranuclear destination.

In live human macrophages they observed rapid uptake and accumulation of QDs in distinct cellular compartments depending upon the QD size and charge. They also concluded that smallest QDs (2-3nm) specifically target histones in the cell nuclei and nucleoli by combination of endocytosis, active cytoplasmic transport finally entering the nucleus via nuclear pore complexes. The authors also proposed that the' proton sponge effect' was responsible for endosomal escape of the QDs due to protonation at acidic pH resulting in increase in intra-endosomal pH and a charge gradient provoking water influx, endosomal swelling and their disintegration[34].

2.3 *IN VIVO* IMAGING

Various imaging modalities are currently being for examination of internal structures, molecular targets and metabolic processes such as MRI, CT , PET and SPECT. Out of these MRI and CT scans provide structural information with poor sensitivity. PET and SPECT scans which are based on detection of radioactive labels suffer from poor spatial resolution. QD based fluorescence imaging can provide high resolution multiplexed cellular and vascular imaging, real time cell tracking and intraoperative image guidance such as sentinel lymph node mapping.

In vivo imaging of QDs involves injection of QDs intravenously into the blood stream of the animal to be imaged. Upon intravenous administration the QDs are distributed to the various organs and peripheral tissues within the body. In the intravascular compartment, these particles encounter blood cells, platelets, coagulation factors and plasma proteins. Depending upon the size, composition and charge, they may undergo adsorption or opsonization by serum proteins. This alters the effective size of the QDs and results in a particle diameter referred to as the *in vivo* hydrodynamic diameter (HD) which is considerably larger than the *in vitro* diameter. This

hydrodynamic diameter in turn affects the blood clearance and the half-life of these nanoparticles. The vascular endothelial monolayer offers a pore size of approximately 5 nm for the transport of fluid and macromolecules between intravascular and extravascular extracellular space. QDs with a HD of less than 5 nm achieve rapid equilibrium with the extravascular extracellular space. However larger particles experience prolonged circulation time. Lymphatic vessel endothelial cell layer is slightly more permeable allowing particles with a HD of up to 6 nm in diameter.

Hepatobiliary system is the primary route of excretion of QDs that do not undergo renal clearance. QDs after intravenous injection are non-specifically taken up by reticulo-endothelial cells including liver, spleen and lymphatic system. Ballou et al demonstrated that CdSe-ZnS QDs were rapidly removed from the bloodstream into the reticulo-endothelial system where they remained fluorescent for 4 months. Electron microscopy didn't reveal any sign of breakdown of these QDs. They concluded that the stability to the QDs was a result of appropriate coating which preserved the fluorescence and prevented degradation of the QDs[35]. Fischer et al's work on biodistribution of QDs with different coatings revealed that albumin coated QDs were rapidly removed from the circulation and sequestered in the liver, predominantly within the kupffer cells at the edges of liver sinusoids. They were also localized in the red pulp of the spleen, subcapsular sinus in the lymph nodes and in the vascular sinus periphery within the bone marrow[36].

Kidneys are capable of rapidly clearing the QDs from the vascular compartment unaltered from their original form. As no intracellular enzymatic modification occurs during this process, there remains reduced possibility of retention and cytotoxicity. The functional or physiologic pore size within the glomerular capillary wall is 4.5-5

nm in diameter. Therefore, molecules with a HD of less than 6nm are typically filtered and ones with a HD of more than 8nm in diameter are not capable of glomerular filtration.

Choi et al examined renal clearance of QDs and defined the relationship between HD, renal clearance and total body retention of QDs of different sizes. They observed that QDs with hydrodynamic diameter less than 5.5nm resulted in rapid and complete elimination of quantum dots via urinary excretion. Serum half-life of particles ranging from 4.36 to 8.65 nm was shown to positively correlate with size, to range from 48 min. to 20 hours. They also demonstrated that the charge affected renal clearance of the QDs. Due to charge related adsorption by serum proteins, purely cationic or anionic charge increased the HD to more than 15 nm in diameter, thereby shifting the route of excretion from kidneys to the liver. Zwitterionic coating prevented serum protein adsorption and improved renal filtration. The authors concluded that hydrodynamic diameter of QDs and renal filtration threshold need consideration for designing and development of QDs to be utilized for biomedical applications[37].

Biodistribution studies have confirmed that quantum dots have significantly long half-life ranging from weeks to months. This obviously increases the potential of QDs to inflict toxic adverse effects to the surrounding tissues. Zhang et al used PEG coated QD 621 containing Cadmium selenide core surrounded by Cadmium Sulfide shell with a hydrodynamic diameter of 39 ± 1mm to demonstrate their capability of penetrating only the uppermost layers of stratum corneum of porcine skin 24 hours after exposure and localizing in the outer root sheath of the hair follicle as well as within the intercellular spaces of this outermost stratum corneum layer as a result of penetration of intercellular bilipid layer. They also demonstrated cytotoxic and

inflammatory potential of QD 621 in Human epidermal keratinocyte (HEK) cells with dose and time dependent decrease in viability from 1.25nm to 10nm dose[38].

Schipper et al evaluated quantitative biodistribution of commercially available CdSe quantum dots in mice. They radiolabeled larger 800-nm emission wavelength 21nm diameter QDs and smaller 525-nm emission wavelength 12 nm diameter QDs with ^{64}Cu with or without 2000 MW (molecular weight) polyethylene glycol (PEG). These were injected intravenously into the tail vein of mice and were studied using conventional well counting or by serial micro PET and region-of interest analysis. Both methods demonstrated rapid uptake by liver and spleen. Pegylated QDs demonstrated slower uptake into liver and spleen (6vs 2 min) and showed additional low level bone uptake. Size of the particles had no influence on biodistribution[39].

Yang et al studied tissue deposition and pharmacokinetics of commercially available QD 705 in mice after single intravenous injection of 40 pmol for a period of 28 days after injection to observe increasingly continued deposition of QDs in the spleen, liver and kidney without any fecal or urinary excretion over these 28 days indicating a very long half-life potentially weeks or even months[40].

Near Infrared Imaging- Unlike *in vitro* imaging where monolayer of cells or thin tissue sections are used for imaging, *in vivo* imaging is encountered with technical difficulties as a result of thickness of the tissues limiting the penetration depth and attenuation of the signals used for optical imaging resulting from high absorption and autofluorescence of the biological tissues across most of the electromagnetic spectrum.

Near-infrared (NIR) Fluorescence imaging provides sensitive, specific and real time imaging of surgical anatomy with high spatial resolution. In the near-infrared region

(700-1000 nm), the absorbance spectra for most biomolecules is at the minimum e.g. oxy-and deoxyhaemoglobin (λ_{max} < 600 nm) and water (λ_{max} > 1150 nm). This 'spectral imaging window' provides a real opportunity for in vivo optical imaging. As a result NIR light penetrates deeper into and out of the tissue than does the traditional UV light as haemoglobin, muscle and fat are least absorbent in this light range. Also the endogenous cellular components produce very little autofluorescence diminishing background interference, enhancing signal-to-noise ratios and provide very low detection limit with NIR fluorescence.

In comparison to Type I QDs, Type II QDs consist of materials for which both valence and conduction bands in the core are lower (or higher) than in the shell. As a result, one carrier is mostly confined to the core and the other is confined to the shell. This property is known as *spatial separation of carriers*. Fluorescence emission results from the radiative recombination of the electron- hole pair across the core-shell interface. So the energy of emission depends on the band offsets of the two materials producing the core and the shell. Hence the type- II QDs can emit at energies that are smaller than the band gap of either material, which allow access to higher wavelengths that would otherwise not be available with a single material[41].

Kim et al first produced CdTe/CdSe and CdSe /ZnTe core-shell type-II colloidal QDs and coated these with polydentate phosphine to allow solubility and serum stability in mouse and pig models . They injected 400 pm concentration of quantum dots intradermally for sentinel node imaging. This method of sentinel node lymphography was then shown to be equivalent to the traditional 'blue dye' method, demonstrating nodes up to 1 cm deep, along with the lymphatic vessels[42].

Hama et al. have shown the ability of fluorescence lymphangiography using two NIR quantum dots with different emission spectra to visualize two separate lymphatic

flows that drain into a common nodal basin. Two quantum dots with emission peaks of 705 and 800 nm were injected simultaneously into the mouse mammary fat pad and the middle phalanx of the upper extremity, respectively. The lymphatics were successfully imaged as they drained into the axillary lymph nodes as shown in fig. 2.4[43].

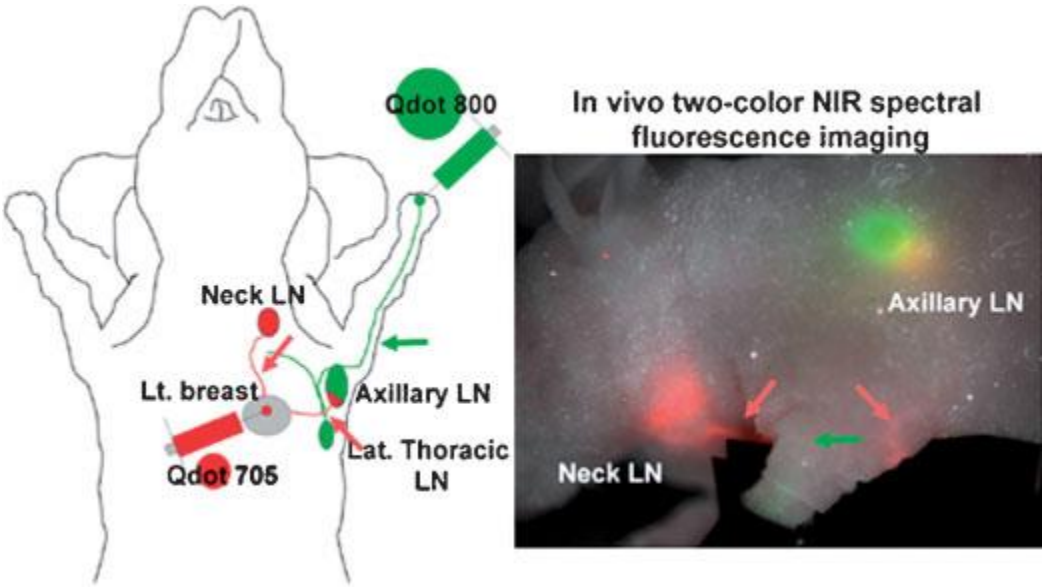

Fig. 2.4 A two-color optical lymphatic image of lymphatic drainages from the breast tissue (red) and the upper extremity (green) obtained using 2 NIR QDs (QD 705 and QD 800) and a spectral fluorescence imaging technique is shown together with a schematic illustration[43].

Successful sentinel node real time imaging by several researchers have opened a new horizon in the field of cancer diagnosis and successful detection of sentinel lymph nodes on research settings.[44,45,46,47,48] Current methods of identifying sentinel lymph nodes such as computerized tomography (CT), positron emission tomography (PET) or endoscopic ultrasonography (EUS) are 60-80% accurate. Sentinel lymph node mapping with blue dye or radioactive tracer has its own limitations. Intra-operative sentinel lymph node mapping in thorax with blue dye only can successfully identify the sentinel node in less than 50% of cases due to poor tissue penetration and anthracotic mediastinal lymph nodes. Even hand held gamma camera can miss

the sentinel node in approximately similar number of cases. Near-infrared fluorescent type II quantum dot has been used to label the sentinel nodes for mapping and imaging. The near-infrared QDs are able to detect and image objects that are not detectable by QDs that emit in the visible range by virtue of the increased depth of penetration into the living tissues. This type of QD technology provides the surgeon with an image of the lymph node, allows real-time visualization of organ during surgery, and can be used for confirmation that the operation has been complete by observing the loss of concentrated QD fluorescence in the lymph node area.[45,49] In the treatment of oesophageal cancer, though extensive lymphadenectomy can improve survival, it is not without associated morbidity or mortality. Selective removal of sentinel lymph node can provide accurate staging and local control, minimizing unnecessary extensive lymphadenectomy. Parungo and coworkers used Type II core/shell QDs containing inorganic core of cadmium telluride, inorganic shell of cadmium selenide and outer organic coating of solubilizing oligomeric phosphines. They were engineered to fluoresce in the NIR, with peak emission at 840 nm. After submucosal injection of QD into the oesophageal wall their migration to a single sentinel node was observed in real time within 5 minutes. These NIR fluorescent lymph tracers continued to demonstrate the fluorescence for up to 4 hours providing great flexibility in administration as shown in fig.2.5[45].

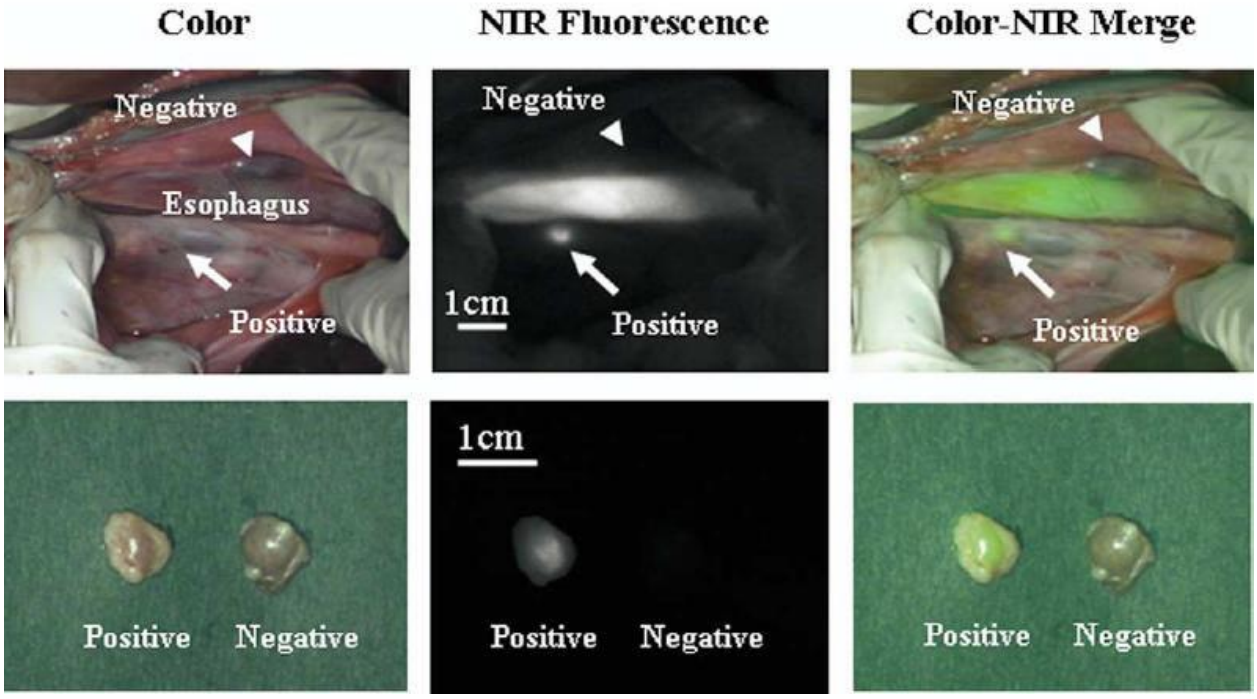

Fig. 2.5. QDs migrate from esophagus to specific lymph nodes of pig. Top row shows in vivo esophagus of pig visualized with color video (left column), NIR fluorescence middle column), and color- NIR merge images (right column). Lymph nodes shown are positive (arrows) and negative (arrowheads) for QD uptake. Bottom row shows same lymph nodes after resection.[45]

The presence of lymph node metastasis is an important prognostic marker in the patients with non-small cell lung cancer. In order to develop an optimal noninvasive tool for intra-operative sentinel lymph node mapping for real time image guided localization and resection Soltesz et al successfully synthesized Type II NIR fluorescent QDs with hydrodynamic diameter of 15-20 nm , fluorescent emission of 840-860 nm with a stable oligomeric phosphine coating and demonstrated successful real time imaging of pulmonary sentinel lymph nodes in animal studies as demonstrated in fig.2.6 [46].

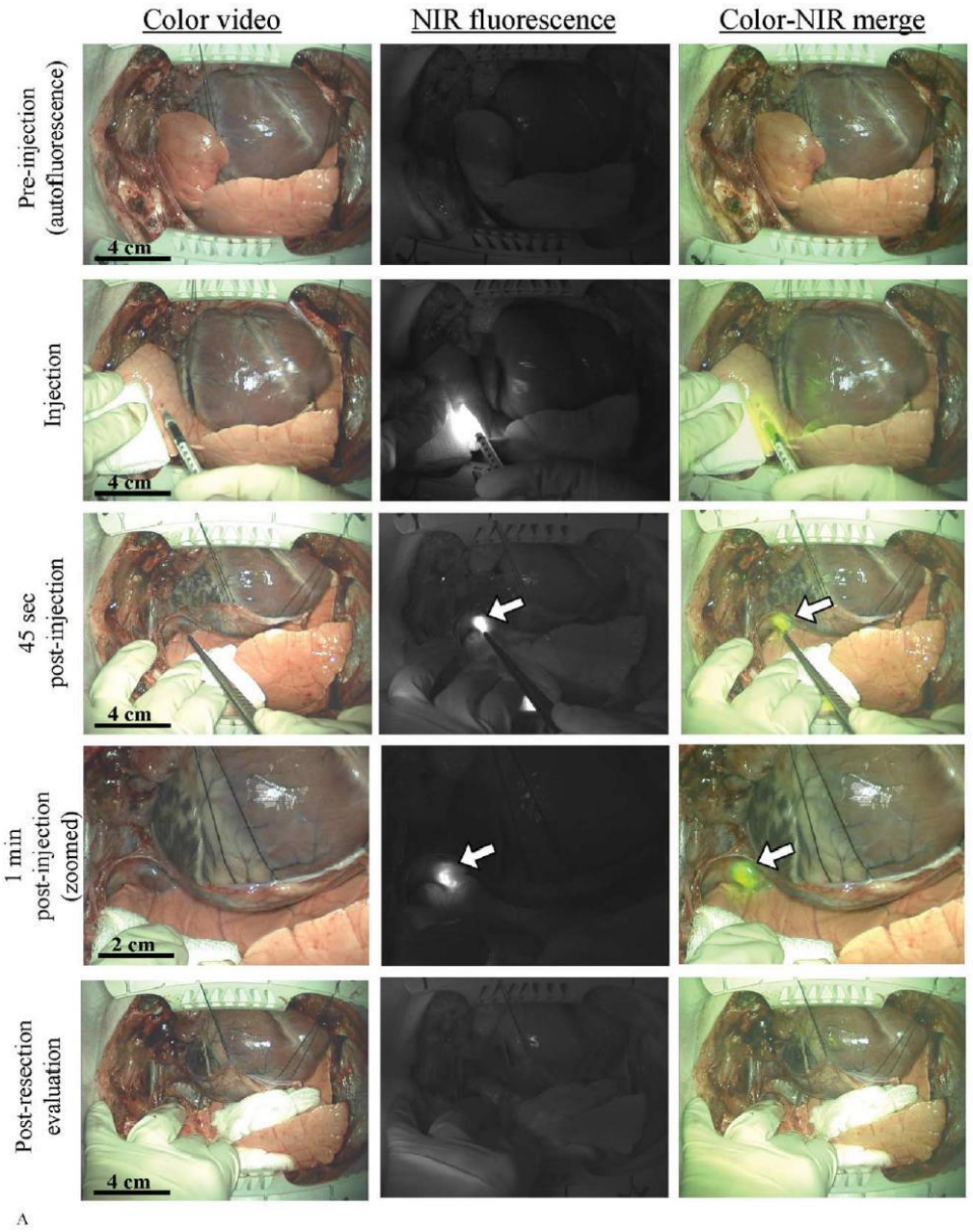

Fig.2.6 *NIR fluorescence images of the surgical field before QD injection (autofluorescence), during QD injection, 45 seconds after injection (lung retracted), 1 minute after injection, and after SLN resection. For each time point, color video (left), NIR fluorescence (middle), and color-NIR merge (right) images are presented. Fluorescence images exhibit identical exposure times and normalization. QDs rapidly localize to the SLN (white arrow). Lack of fluorescence in the nodal basin after resection confirms complete removal of the sentinel nodal tissue*[46].

***IN VIVO* VASCULAR IMAGING** Larson et al used QDs to image capillaries within the adipose tissue and skin of living mouse following intravenous injection of water soluble QDs[50]. Smith et al, using intravitally injected QDs imaged chorioallantoic membrane (CAM) vessels and capillaries superiorly as compared to routinely used FITC –dextrans. QDs exhibited more uniform illumination across the vessel lumens , had longer residence times, had low background interference with improved depth of imaging and could be used at much lower concentrations[50].

2.4 DIAGNOSTIC AND THERAPEUTIC APPLICATIONS IN CANCER–

As compared to normal cells, cancer cells are unique in that they have abnormal growth and abnormal differentiation. Once solid tumors grow approximately beyond 2 mm in size they stimulate their own blood supply to deliver the oxygen and nutrients to sustain their growth. This is achieved through production of angiogenic factors such as VEGF resulting in increased microvascular density within the tumor. These vasculatures tend to be highly permeable due to leaky capillaries resulting in increased interstitial pressure which makes macroparticle drug delivery less efficient.

Wu et al successfully demonstrated the expression of Her2 on the surface of human Sk-BR-3 breast cancer cells, fixed & live SK-BR-3 cells and fixed mouse mammary tumor tissue sections by labeling with QDs bound to humanized anti- Her2 antibody[28].

A QD-based assay for the detection of the ovarian cancer marker CA125 in various specimen types (fixed cells, tissue sections, and xenograft tissues) was successfully developed by Wang et al[51].

Monitoring of tumor progression and bone/bone marrow metastases after injecting MDA-MB-231 breast cancer cells was demonstrated by Henriquez et al[52].

Kaul et al. used QD immunoconjugates to show that mortalin could be a reliable marker for distinguishing between normal and cancer cells[53].

Angiogenesis is a prime feature of most tumours. Formation of new vessels is extremely essential for tumor growth and progression. A cell adhesion molecule Integrin $\alpha_v\beta_3$ is upregulated in most tumour cells and tumour vasculature. RGD, a potent antagonist of Integrin $\alpha_v\beta_3$ can be used to target tumor vasculature using peptide conjugated QDs. Cai et al successfully demonstrated use of RGD containing peptide bound to QD 705 to selectively target Integrin $\alpha_v\beta_3$ on the tumour vasculature in *ex vivo* and *in vivo* studies[54].

For early detection of cancer to improve survival, it is essential that multiple biomarkers can be detected with high sensitivity and specificity. It is possible to achieve this aim with quantum dot protein microarray. Combination of QDs with protein microarray allows detection of ultra-low levels of tumor markers in biological specimen (serum, plasma etc.). Due to outstanding optical properties of QDs, multiplexed microarray is possible. Zajac and coworkers were able to detect six different cytokines in a protein solution such as TNF-α, IL-8, IL-6, MIP-1β, IL-13 and IL-1β down to picomolar concentration[55].

Traditionally immunohistochemistry has been used for diagnostic and prognostic classification of human tumours for identification of tumour oncoproteins. Molecular profiling technologies enable us to read the molecular signature of individual patient's tumour in order to predict the clinical outcome of personalized therapy. There are a few limitations of immunohistochemistry methods in the form of inability to perform multiplexed molecular profiling, significant inter -observer variations and need for destructive preparation of cells or tissues into homogenous solution leading to loss of 3D cellular and tissue molecular architecture. Yezhelyev et al successfully exhibited the use of QDs for multiplexed detection of five breast cancer biomarkers such as ER, PR, mTOR, EGFR and HER2. They also demonstrated close correlation of quantification of ER,PR and HER2 receptors with traditional methods such as Immunohistochemistry, western blotting and FISH (fluorescence in situ hybridization) indicating successful use of QD based technology for molecular profiling of tumour biomarkers *in vitro*[56].

The property of tunable and narrow emission can successfully be applied to customize the emission between QD donors and fluorescent dye acceptors in Fluorescence resonance energy transfer (FRET) assay thereby QDs behaving as a new class of sensors. The theory of resonance energy transfer was first derived by Forster. This process involves transfer of fluorescence energy from the donor particle to an acceptor particle when the distance between the donor and acceptor particle is smaller than the critical Forster radius. This result in decrease in the donor's excited state lifetime and an increase in the acceptor's emission intensity. FRET is a distance dependent radiationless transmission of energy from donor to acceptor molecule. Due to its sensitivity to the distance, FRET has been used to investigate molecular interactions. The interacting pair of molecules involved in the

process of FRET is often referred to as donor/acceptor pair. For an efficient energy transfer, the donor and acceptor molecules must be in close proximity to one another. FRET can occur when the emission spectrum of a donor fluorophore significantly overlaps (>30%) the absorption spectrum of an acceptor, provided that the donor and acceptor fluorophores dipoles are in favorable mutual orientation.

FRET can be observed by monitoring quenching of donor fluorescence and by observing acceptor enhancement. Fluorescence Resonance Energy transfer was successfully demonstrated between CdSe−ZnS core−shell quantum dots energy donors and engineered maltose binding protein (MBP) appended with an oligohistidine tail labeled with an acceptor dye (Cy3) by Clapp et al[57]. Several recent studies have confirmed that CdSe and CdTe QDs are able to participate in the resonance energy transfer process due to their unique spectroscopic properties with potential application in the design of assays of ligand receptor binding, antibody-antigen binding, DNA hybridization and enzyme-substrate interaction. QDs prepared in a single synthetic batch can vary in their structural and spectral characteristics due to variations and defects in either the core, shell or the organic layers during the complex process of their synthesis and the large number of atoms the QDs is made of. This would result in heterogeneity of the Forster radius R_0 which may affect the precision of single molecule FRET measurement unless each individual QDs spectrum can be measured.

Though quantum dots have exceptional potential for molecular imaging *in vivo*, their utility is limited because of need for excitation from external illumination source to fluoresce. Also, this results in strong autofluorescence and scarcity of excitation light at deeper locations. This drawback was overcome by bioluminescence resonance energy transfer (BRET) studies. In this, the QDs can emit fluorescence without an

external source of excitation when conjugated to enzymes (e.g., luciferase) that catalyze bioluminescent reactions[8]. The authors, in this study, coupled carboxylate-presenting QDs to a mutant of bioluminescent protein *Renilla reniformis* luciferase to reveal that the conjugates emit long-wavelength (from red to near-infrared) in the cells even in deep tissues. Moreover, compared to fluorescence imaging, bioluminescence has extremely high sensitivity for *in vivo* imaging purposes associated with the fact that the energy comes from a chemical reaction catalyzed by the donor enzyme (BRET) rather than absorption of excitation photons (FRET).

Table 1 provides a comprehensive summary of scientific studies of QD utilization using different cancer cells within the in vitro studies. Table 2 outlines a brief overview of recently published in vivo studies demonstrating successful use of QDs for cancer studies . These studies give a broad perspective of the future potential of these QDs for early diagnosis of cancer at molecular level.

Table 1. Comprehensive summary indicating scientific studies using Quantum Dots for the diagnosis of cancer – (*in vitro* studies)

REFERENCE	**QD**	**BIOCONJUGATION**	**CELL LINES**	**OUTCOME**
Wu [28]	ZnS capped CdSe	Antimouse IgG + monoclonal anti-Her2 antibody	Human Sk-BR-3 breast cancer cells	Her2 labeling
		Streptavidin +humanized anti-	Fixed + live SK-BR-3	Her2 labeling

		Her2 antibody and biotinylated goat anti-human IgG Streptavidin + biotinylated goat anti-rabbit IgG + antiserum reacting with cytoplasmic domain of Her2	cells Her2 positive mouse mammary tumor tissue sections	Labeling of tumor cells
Nida[58]	ZnS capped CdSe	Streptavidin + Biotinylated anti-EGFR monoclonal antibody	SiHa cervical cancer cells	Illumination of cervical cancer cells due to EGFR over-expression
Kaul[53]	ZnS capped CdSe	Streptavidin + anti-mortalin antibodies	Normal human fetal fibroblasts (WI-38) and osteogenic sarcoma (U2OS)	Mortalin staining in normal and transformed cells.
Qian[59]	CdSe/ CdS/ ZnS (QDs)	Lysine coating. Transferrin and anti-Claudin-4 (pancreatic cancer specific monoclonal antibody) as targeting ligands	Live human pancreatic cancer cells	Labeling of pancreatic cancer cells
Yang[60]	CdSe QDs	Mercaptoacetic acid +	HeLa cells	Detection of CEA (carcino-

		Nhydroxy-succinimide as a cross linker + rabbit anti-CEA8 as a primary antibody + goat anti-rabbit IgG as a secondary antibody		embryonic antigen on the membranes of HeLa cells Direct and indirect immunolabeling of HeLa cells
Li[61]	CdTe	Biotin and polyethylene glycol	Human tongue cancer cells Tca8113	Immuno-fluorescent labeling of cancer cells with water-soluble QDs
Wang[62]	QD 525	Streptavidin Anti EGFR antibodies	SKMG-3, U87 Human glioma tumor cell lines with elevated EGFR expression + Brain tumor tissue specimen	Recognition and imaging of glioma cells
Hu[63]	CdTe	3-mercapto-propionic acid + Thiolated PEG+ Anti CEA monoclonal antibody	CEA positive human colon carcinoma LS 180 cell lines	Successful detection of CEA

Table 2. Comprehensive summary indicating scientific studies using Quantum Dots for the diagnosis of cancer – (*in vivo* studies)

REFERENCE	QD	BIOCONJUGATION	CELL LINES	OUTCOME
Akerman[64]	ZnS capped CdSe	Mercaptoacetic acid + homing peptide coating	Lung endothelial cells, Brain endothelial cells, Human breast carcinoma MDA-MB-435 cells	Selective targeting of peptide coated QDs to the vasculature of normal lungs and tumors,
Knapp[65]	NIR CdTe (CdSe) core (shell) type II QDs	Oligomeric phosphine	Naturally occurring invasive transitional cell carcinoma of the urinary bladder	Real time imaging of sentinel lymph node
Wang[51]	ZnS capped CdSe	Streptavidin + Biotin labeled Monoclonal anti-CA125 antibody	Human ovarian carcinoma HO8910 cells in fixed	Detection of tumor marker CA125

			cells, tissue sections, and xenograft piece	
Yu[66]	ZnS capped CdSe	Mouse anti-human monoclonal alpha-fetoprotein (AFP) antibody	Hepato-carcinoma cell line HCCLM6	Immuno-fluorescent detection of hepatoma
Gao[67]	ZnS capped CdSe	Tri-*n*-octylphosphine oxide (TOPO) capped QDs + Amphiphilic triblock polymer +PSMA monoclonal antibody	PSMA-positive human prostate cancer cells	Imaging of cancer cells in vivo
Estrada[68]	ZnS capped CdSe	-	TCCSUP and 253JBV bladder cancer cell lines-transitional cell carcinoma of the bladder	Behavioral profiling of human TCC cells + Response to intravesical chemotherapy
Diagaradjane[69]	ZnS capped CdSeTe (NIR) QD	Human recombinant EGF (Epidermal Growth Factor) using thiol-maleimide conjugation	HCT116 and DiFi colorectal cancer cell lines with EGFR over-	EGFR imaging nanoprobe characterization

			expression	
Tada[70]	QD 800	Polyethylene glycol (PEG) Trastuzumab	Human breast cancer cell line KPL-4, which over-expresses HER2	Real time tracking of single particle QD labeled with the monoclonal anti-HER2 antibody in HER2- over-expressing breast cancer
Ballou[71]	ZnS capped CdSe ZnS-CdSe-CdTe	Amphiphilic polymer coating Polyethylene Glycol (PEG)	M21 Human Melanoma tumour model, MH15 Mouse terato-carcinoma model	Successful and rapid visualization of sentinel node.
Cai[25]	QD 705	Polyethylene Glycol (PEG) + RGD (arginine-glycine-aspartic acid)	U87MG human glio-blastoma And MCF-7 human breast cancer cell	Tumor vasculature targeted imaging

NANOTECHNOLOGY BASED DRUG DELIVERY SYSTEM- In order to effectively treat diseases in the human being it is imperative that highly efficient therapeutic compounds are efficiently delivered at the diseased sites. Conventional therapeutic agents tend to undergo nonspecific bio-distribution and active metabolism of free drug radicals prior to reaching their targeted sites resulting in their high dosage requirement. Using nanotechnology tools, drug delivery system can be developed using an array of nanoscaled polymeric, liposomal and inorganic materials. These nano drug delivery systems offer easier tissue penetration through biological and physiological barriers that are normally impermeable for larger particulate structures, due to their small size. In addition to this, they carry multifunctional capabilities of simultaneous imaging and therapeutic applications. Also their surfaces can be easily modified using conventional chemical techniques in order to alter and tune the pharmacokinetic or pharmacodynamic properties. e.g. Linkage with Polyethelene Glycol on the surface of these nanocrystals prolongs their circulation time within the body and reduces nonspecific uptake and destruction by the reticuloendothelial system. Surface modification enables conjugation of biological agents such as antibodies, peptides to their surfaces in order to target disease specific sites. By this methodology, significantly higher doses of drugs can be selectively targeted to the cancer specific sites with minimal adverse reactions, enhanced patient compliance and superior therapeutic efficacy[10,72,73].

However there are concerns about potential hazards of these nanodrug delivery systems. Limited data is available regarding pharmacokinetics & toxicological studies to assess the risk associated with this novel technology. Pharmaceutical sciences are exploiting the possibility of use of QDs for diagnosis and treatment of cancers minimizing the inherent risk of toxic Cadmium to human beings and the environment.

PHOTODYNAMIC THERAPY (PDT)- One such property of quantum dots is being explored for their potential use as photosensitizers in photodynamic therapy (PDT) for cancers. Photosensitizers are photosensitive molecules that can transfer the light energy to the surrounding molecular oxygen to generate reactive oxygen species (ROS) such as singlet oxygen($^1O_2$), hydroxyl radicals ($^{\cdot}OH$) , super oxide anions ($^{\cdot}O_2$) and hydrogen peroxide (H_2O_2) through a series of energy and electron transfer reactions initiated between photosensitizers and dissolved oxygen ($^3O_2$). These reactive oxygen intermediates immediately react with and damage vital biomolecules in cell organelles leading to cell death. When photons are absorbed by these photosensitizers, they achieve excited triplet state from the ground state. Quantum dots can generate ROS and free radicals following long term optical irradiation. These ROS are able to induce tumor cell death through direct photo damage. These photosensitizers not only induce microvascular collapse from severe tumor tissue hypoxia but also cause immune response activation through IL-10 and IL-6 upregulation following ROS exposure. The main advantages of fluorescence imaging over other biomedical imaging techniques such as X-rays, CT and PET are that the fluorescence imaging is non-ionizing and less hazardous.

Porphyrins, phthalocyanines and chlorine derivatives are the standard photosensitizer drugs used for the purpose of PDT. With the synthesis of new generation of photosensitizer drugs, targeted drug delivery, tunable and fiber-optic laser light source and image –guided PDT, skin cancers, Barrett's oesophagus, bronchial cancers, head and neck cancers, lung cancer, prostate cancer and bladder cancers are being treated with superior results.

The efficacy of photodynamic therapy is entirely determined by the ability of photosensitizers to generate ROS. The quantity of singlet oxygen generated using a

typical CdSe quantum dot is much lower in comparison to traditionally used photosensitizers. However, as the QDs are stable against photobleaching, prolonged irradiation with UV / visible light can potentially maintain similar level of steady state singlet oxygen generation.

Alternatively, classic photosensitizers can be attached to the surface of functionalized QDs. Besides specifically targeting the disease specific sites, at closed proximity quantum dots can be used as energy donors and classical photosensitizers as energy acceptors to enhance the effectiveness of photodynamic therapy by Forster Resonance Energy Transfer (FRET) [73,74].

There are several advantages of Quantum Dots- Photosensitizer conjugates over conventional photosensitizer drugs. Indirect photoactivation of photosensitizer drugs by photostable QDs permits prolonged imaging and PDT without photobleaching. In addition, larger surface area allows abundant space for conjugating multiple photosensitizers on the surface of the QDs and cancer markers for targeted cancer imaging and PDT[74].

2.5 CELL ADHESION MOLECULES-

Adhesion to extracellular matrix (ECM) is necessary for the survival of epithelial cells. Inadequate or inappropriate cell–ECM interactions result in apoptosis, a phenomenon known as anoikis. These interactions are dependent on the cell surface receptors. Cell adhesion molecules (CAMs) are glycoproteins found on the cell surface. They are accountable for binding with the other cells or with the extracellular matrix in the process called ‘cell adhesion’. These CAMS have been found to have a fundamental role in phagocytosis, locomotion, mitosis and cytokinesis. CAMs have an important role in

diseases such as cancer, thrombosis, autoimmune diseases, bacterial and viral infections.

These transmembrane receptors are composed of 3 domains-

a) Intracellular domain- Interacts with the cytoskeleton.

b) Transmembrane domain.

c) Extracellular domain- Interacts with other similar CAMS (Homophilic binding) or CAM of extracellular matrix (Heterophilic binding).

CAMs are divided into 4 classes- Integrins, cadherins, selectins and immunoglobulin superfamily.

Integrins are a superfamily of cell adhesion receptors binding to extracellular matrix ligands, cell-surface ligands and soluble ligands. These are non-covalently linked heterodimeric molecules containing an α and a β subunit. These are type 1 transmembrane proteins with large extracellular and short cytoplasmic domains. There are altogether 18 α and 8 β subunit genes in the mammalian genomes in total forming 24 α- β combinations at the protein levels. The cytoplasmic domain of integrins coordinates the assembly of cytoskeletal polymers and signaling complexes. The extracellular domains however engage either extracellular matrix macromolecules or counter-receptors on adjacent cell surfaces. In this way , they integrate cells with their microenvironment. The integrin-ligand pairs have been identified either by affinity chromatography or through the ability of subunit- cases, direct protein-protein binding specific monoclonal antibodies to block adhesion of cells to specific ligands. In some assays have been used to support biochemical or cell biological data.

In mammals some integrins are limited to certain cell types-

αIIb β_3 – platelets

α6 β_4 - keratinocytes

αE β_7 - T cells, dendritic cells & mast cells in mucosal tissues

α4 β_1 - Leucocytes

α4 β_7 - Memory T cells

αV β_3 - Widely expressed on the endothelial cells

The mammalian integrins express ligand specificity to a significant extent. Based on this, they can be classified into following categories-

1. Laminin binding integrins- α1 β1, α2 β1, α3 β1 , α6 β1, α7 β1, α6 β4
2. Collagen- binding integrins- α1 β1, α2 β1, α3 β1 , α10 β1, α11 β1
3. Leucocyte integrins- αL β2, αM β2, αX β2, αD β2,
4. RGD recognizing integrins- α5 β1, αV β1, αV β3, αV β5, αV β6, αV β8, αIIb β_3

Some α subunits contain the I (Inserted or Interactive) domain. These are – α1, α2, α10, α11, αL, αM, αX, αD and αE. The non I domain subunits are – α3, α4, α5, α6, α7, α8, α9, αV and αIIb. In I-domain integrins, the I domain plays a vital role in ligand binding and intercellular adhesions. The α and β subunits have distinct domain structures with extracellular domain from each subunit contributing to the ligand binding site as demonstrated in Fig.2.7. The sequence arginine-glycine-aspartic acid (RGD)has been identified as a general integrin-binding motif. On ligand-binding, the integrins transduce signals into the cell interior[75].

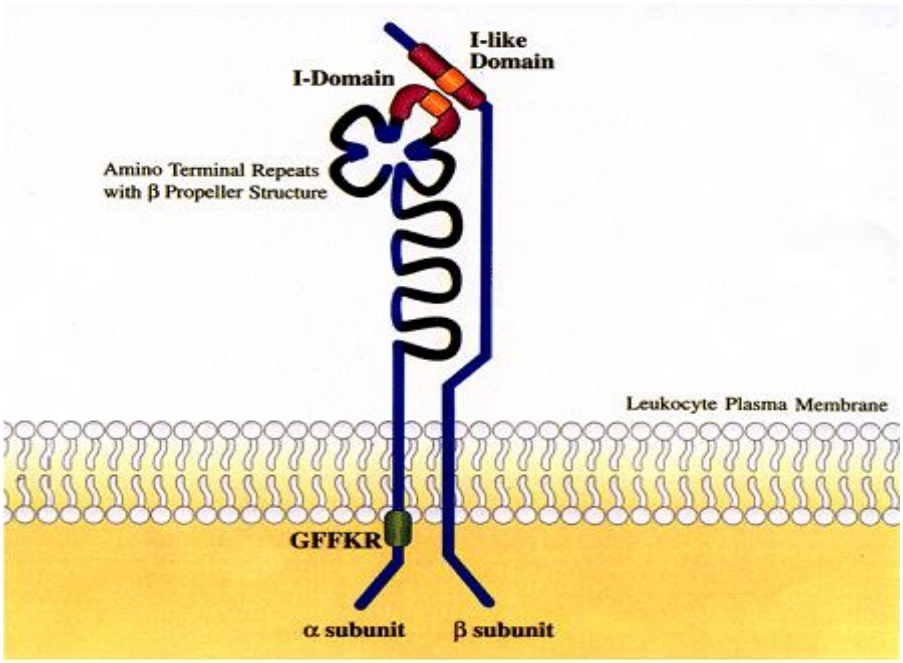

Fig. 2.7 .The leukocyte integrins[76]

RGD binding integrins- All five αV integrins, α5 β1, α8 β1 and αIIb β3 have the ability to recognize ligands containing RGD tripeptide active site. RGD binds at an interface between the α and β subunits, the R residue fitting into a cleft in a β -propeller module in the α subunit, and the D coordinating a cation bound in a von Willebrand factor A-domain in the β subunit[77].

Integrins serve as a transmembrane link between extracellular contacts (other cells or extracellular matrix) and the actin microfilaments of the cytoskeleton. Upon binding the extracellular ligands, the integrins generate intracellular signal, modulate and regulate the cytoskeleton. At the same time, their functioning can be regulated by signals from within the cells.

Integrin-mediated adhesion to ECM triggers intracellular signaling pathways to modulate cell proliferation, morphology, migration, invasion, and survival. Among the various families of cell adhesion molecules, integrin expression patterns appear to

be directly implicated in the progression of malignant disease. During the process of cell aggregation, thrombosis, tumor migration and angiogenesis, integrins bind to various ECM proteins such as fibronectin, vitronectin or cell surface immunoglobulin proteins ICAM-1(intercellular adhesion molecule-1 or VCAM-1(vascular cellular adhesion molecule). During the process of cell locomotion, integrins can continuously undergo the process of endocytosis and exocytosis. During locomotion, the integrins form focal contacts at the front of the cell. This process is usually triggered by vascular endothelial growth factor (VEGF) and controlled by protein kinase C. Polarized distribution of $\alpha_v\beta_3$ has been demonstrated in migrating neutrophils. This process is regulated by Ca^{2+} dependent release of cell adhesion followed by endocytosis of integrins. Thus integrin endocytosis has been proposed as a mechanism for controlling cell signaling pathway which allows the cell to control the location and timing of integrin expression.

GENERAL STRUCTURE OF INTEGRINS-

Arg-Gly-Asp (RGD) tripeptide was originally identified as a motif within the glycoprotein, fibronectin of extracellular matrices mediating cell adhesion. Subsequently the RGD motif has been found in numerous other proteins supporting cell adhesion. All known RGD receptors are members of the integrin family of cell adhesion molecules. The term ‘ integrin’ was first applied to this family by Hynes in 1987 to emphasize the ability of these receptors to integrate the actin containing cytoskeleton from within the cell to the extracellular matrix outside the cell.

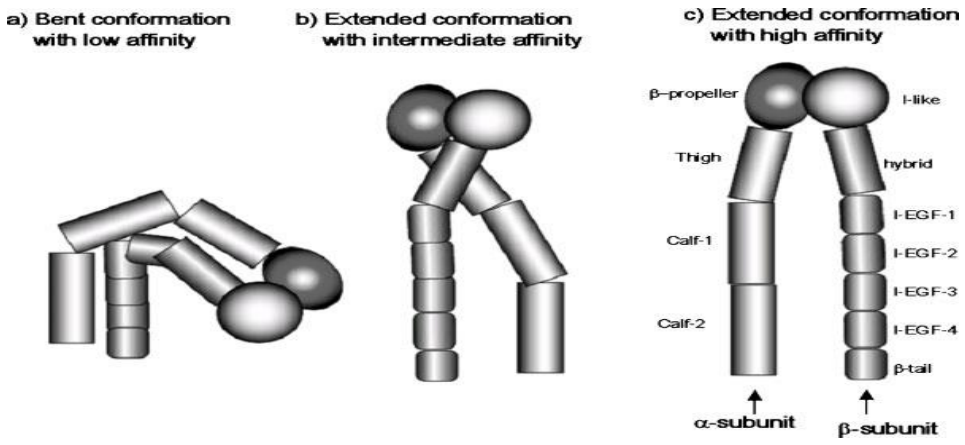

Fig.2.8. The general structure of integrins showing three possible conformations of integrins: (a) a bent conformation with a low affinity for the ligand, (b) an extended conformation with intermediate ligand affinity and closed headpiece, and (c) a high ligand affinity conformation with an extended conformation that has open headpiece when bound to RGD peptide.

As observed in Fig. 2.8, integrins can adapt non-activated, intermediate activated or activated state. Integrins bind to their ligands in the intermediate activated or highly activated state. The activation process involves conformational changes followed by intracellular signaling processes regulating gene expression, cell growth, differentiation and survival.

Historically, cell adhesion peptides were explored for suppressing cell adhesion-mediated diseases such as thrombosis, inflammation, and tumor metastasis. Initially, the roles of ECM proteins were investigated in the adhesion of normal cells to tissues and the process of metastasis of cancer cells. During these investigations, Pierschbacher and Ruoslahti discovered that the RGD sequence found in Fibronectin was responsible for cell adhesion to Fibronectin. They also discovered that small RGD peptides derived from Fibronectin could block cell attachment to Fibronectin. Since then many other ECM proteins such as collagens, laminin, osteonectin, Vitronectin, fibrinogen, von Willebrand Factor and thrombospondin have

been found to have an RGD sequence(s); the cell surface receptors called integrins that recognized the RGD sequences were also discovered, including $\alpha v\beta_3$, $\alpha_v\beta_5$, $\alpha v\beta_6$, $\alpha v\beta_8$, $\alpha_{IIb}\beta_3$, $\alpha_5\beta_1$, and $\alpha_8\beta_1$.

Many synthetic peptides and peptidomimetics bind selectively to specific integrins. This property has been explored to block the cell adhesion to extracellular matrix. The well-known examples are antithrombotic drugs such as Integrilin and Aggarastat which selectively bind to gpIIb/IIIa receptors found on the surface of platelets. During the process of thrombosis, fibrinogen binds to these receptors resulting in platelet aggregation. These drugs Integrilin and aggarastat selectively block the fibrinogen binding to these receptors, preventing platelet aggregation. Similarly, cRGDfK, cRGDyK and RGDC4 selectively block $\alpha v\beta_3$ and $\alpha_v\beta_5$ integrins. So, these RGD peptides have been used to inhibit angiogenesis in solid tumors which overexpress αv integrins that are not detectable in normal blood vessels.

RGD peptide and peptidomimetic drugs are not orally bioavailable due to the presence of positive (guanidinium or amine group) and negative (carboxylic acid group) charges that prevents them from crossing the intestinal mucosal barrier. However cyclic prodrug of RGD peptidomimetics formed by linking the amino group and the carboxylic group via an esterase sensitive linker such as acyloxyalkoxy, trimethyl lock, or coumarinic acid has been found to cross the intestinal mucosal barrier with the anticipation that it can be converted to the drug by esterase found in the blood stream.

Radiolabeled RGD peptides have been used to diagnose the presence of tumor cells in tissues over expressing $\alpha v\beta_3$ and $\alpha_v\beta_5$ integrins.[78] ^{125}I, ^{18}F,^{64}Cu and ^{99m}Tc have been successfully incorporated into Cyclo(RGDxK) and RGD C4 peptides for tumor

diagnosis. In animal experiments, cyclic RGD peptides (RGDyK and RGD4C) after conjugation to paclitaxel and doxorubicin have been successfully demonstrated to suppress tumor progression selectively targeting $\alpha v\beta_3$ and $\alpha_v\beta_5$ on the tumor vasculature during angiogenesis.[79]

The deletion of individual genes by gene knockout in mice has shown that integrins play a critical role in development (the β1 integrins), vasculogenesis (αV integrins), lymphangiogenesis (α9β1), thrombus formation (αIIbβ3), the integrity of the skin (α6β4), and immune responses (the β2 integrins). Knockout of the gene for β3 enhanced tumorigenesis and angiogenesis, enhanced wound healing and enhanced inflammation and atherosclerosis, suggesting that αVβ3 normally suppresses these processes.

Large number of therapeutic drugs has been developed to exploit the properties of integrin binding to various ligands in the pathogenesis of various diseases. A humanized anti-β3 antibody (abciximab) that blocks the binding of platelet integrin αIIbβ3 to fibrinogen has been used to prevent thrombosis. A humanized anti-α4 antibody (natalizumab) that can block the α4β1-VCAM interaction or the α4β7-mucosal addressin cell adhesion molecule (MAdCAM) interaction on mucosal endothelium has been tested in clinical trials. Natalizumab blocks leukocyte trafficking across the blood-brain barrier and thereby moderates inflammation in multiple sclerosis. Anti-α4 antibody is also effective in clinical trials in ameliorating inflammatory bowel diseases such as Crohn's disease. Eptifibatide and tirofiban are being used as inhibitors of αIIbβ3 to reduce platelet aggregation and the formation of blood clots.

The αvb6 integrin does not express itself within the normal epithelial tissues but only in those that have undergone malignant transformation. Research has confirmed that

heterologous expression of αvb6 in colon cancer cells promotes tumour cell growth *in vitro* and *in vivo*, moreover, αvb6 expression in colon cancer cells leads to increased gelatinase B secretion in a protein kinase C (PKC)-dependent manner and that integrin αvb6 up regulates its own expression via PKC mediated signaling as tumour cells become crowded through a system of integrin autoregulation. Inhibition of av integrin activity by monoclonal antibodies (mAbs), cyclic RGD peptide antagonists, and peptidomimetics has been shown to induce endothelial apoptosis, inhibit angiogenesis, and increase endothelial monolayer permeability. Inhibiting av integrin will probably reduce the expression level or block the function of integrin αvb1, αvb3, αvb5, αvb6, and αvb8, so they have a more broad-spectrum anti-integrin effect. In this study, the authors used the monoclonal antibody against integrin αvb6 to block the function of αvb6 integrin so as to investigate the role of integrin αvb6 in apoptosis of colon cancer cells and the related mechanisms in a more specific pathway[80].

Angiogenesis plays a vital role in tumour progression. The tumor angiogenesis is regulated by a fine balance between angiogenic factors and antiangiogenic factors secreted by tumour cells and host infiltrating cells. The clinical implications of tumour angiogenesis include the development of novel strategy of anticancer therapy targeting the tumour vessels instead of cancer cells. Monoclonal antibodies against vascular endothelial growth factor have been successfully used for the treatment of colon cancer in combination with conventional chemotherapy to prolong the patient survival.

During tumour progression, environmental and genetic factors induce an angiogenic switch with either upregulation of angiogenic factors or downregulation of anti-

angiogenic factors. The factors triggering angiogenesis include hypoxia, altered pH, metabolic stress, cytokines from inflammatory response and hormones such as androgens, progesterones & oestrogens in hormone dependent cancers such as breast and prostate cancers. It has been proved that tumour growth depends on angiogenesis, the formation of new blood vessels from the existing host microvasculature. Antiangiogenesis can act synergistically with conventional chemotherapy.

Table 3 provides a comprehensive list of various angiogenic factors. Table 4 provides a list of various anti-angiogenic factors. These factors play a pivotal role in tumor progression.

Table 3. Angiogenic factors

Vascular endothelial growth factor	Acidic and basic fibroblast growth factors
Transforming growth factor	Platelet-derived endothelial cell growth factor
Hepatocyte growth factor	Tumor necrosis factor-
Epidermal growth factor	Placental growth factor
Tissue factor	Interleukin-6/8
Angiogenin	Angiopoietin-1
Cyclooxygenase-2	Nitric oxide

Table 4. Antiangiogenic factors

Thrombospondin-1, 2	Endostatin
Angiostatin	Interferon-α/β
Interleukin-12	Platelet factor 4 fragment
Human macrophage metalloelastase	Tissue inhibitor of metalloproteinase-1/2
Platelet factor 4 fragment	Angiopoietin-2
Vascular endothelial growth inhibitor	Vasostatin
Anti-thrombin III fragment	Osteopontin fragment

Strieth et al in their study demonstrated a significant reduction in the anti-tumoural functional vessel density and regression of microvasculature after treatment with the combination of αV inhibitor cRGD and VEGFR 2 antagonist as compared with antiangiogenic monotherapy[81].

During the process of angiogenesis, the angiogenic factors selectively bind to the specific receptors on the endothelial cells of pre-existing blood vessels. In addition to these factors proteinases such as matrix metalloproteinases and plasminogen activators help the process by dissolving the extracellular matrix surrounding the sprouting blood vessels. Also, endothelial cell adhesion molecules such as $\alpha v\beta_3$ integrins and vascular adhesion molecule-1 help to connect the newly formed vessels to the pre-existing blood vessels in order to produce rich intra-tumoral vascular network.

During the process of angiogenesis, it was presumed that new blood vessels originate from the endothelial cells in the pre-existing blood vessels. However new

evidence suggests that bone marrow derived circulating endothelial precursor cells bone marrow progenitor cells such as haemopoietic progenitor cells may be responsible for this process.

Tumour microvessel density has been proven to be a prognostic factor independent of conventional pathological prognostic factors on recurrence of different cancers after resection and survival. Traditionally, quantification of tumour neovascularization is done by immunohistochemistry using endothelial markers to stain microvessels as these vessels are not seen on conventional histological assessment. The commonly used endothelial markers are CD31, CD34 and von Willibrand factor (vWF). Following immunostaining, the entire tumour section is scanned at low power (x40) to identify the areas of highest neovascularization as 'hot spots'. Individual microvessels are counted under high power (x200). The average microvessel count in 5 'hotspots' is taken as microvessel density (MVD).Though several studies have shown the significance of degree of revascularization as a prognostic indicator in various human cancers, the lack of standardization and inter-observer variation has always been questioned. Automated computerized image analysis as well as selective immunostaining for over expressed integrins has been recommended as a way forward. In order to avoid the bias linked with MVD assessment and to obtain functional information on tumour angiogenic activity, attention has now been focused to the various angiogenic factors. VEGF (vascular endothelial growth factor) has been a widely studied angiogenic factor of clinical significance. Various studies have documented significant relevance between over expression of VEGF and human cancer related prognostic factors such as MVD, tumour invasiveness and advanced stage of the disease.

Majority of angiogenic factors are soluble and diffusible peptides. The measurement of circulating angiogenic factors as a biomarker of tumour is a very convenient and less expensive method to monitor tumour angiogenesis before and after antiangiogenic therapy[82].

2.6. APPLICATION OF QDs FOR CELL LABELING-

Cell based therapeutics has emerged as an innovative tool with its potential applications in stem cells and progenitor cell based research in the regenerative medicine. Stem cells and progenitor cells are able to differentiate into a diverse range of specialized cell types. If harnessed well, they can proliferate and replace or repair the defective cell population. This approach could exhibit their potential benefit in treating patients with degenerative neurological disorders such as demyelinating disorders, spinal cord injuries, Parkinson's disease etc. as well as myocardial regeneration. It even may be possible to augment the antitumor power of immune cells such as Natural Killer cells (NK), T cells, B cells & dendritic cells towards alternative modality of treatment of malignancies. Quantum dots can be bioconjugated to variety of these cells by direct cell labeling method. This is relatively easy and less expensive. Once labeled, cells can be tracked by relevant imaging modality. The limitation include shorter observation period as a result of diminishing signal intensity during cell proliferation.

In this method of optical labeling, cells are labeled with a fluorescent tag *'ex vivo'* and are subsequently grafted to the host site. These cells can be visualized based on the detection of fluorescence and their survival, migration, differentiation & regenerative potential can be tracked and monitored. The depth of tissue penetration

of these fluorescent labels is required to be taken into consideration as tracer more than 4-8 cm from the skin surface may not be detected.

Slotkin et al performed direct QD labeling of *in vivo* mammalian stem cells & progenitor cells by injecting 620nm COOH- conjugated QDs into the ventral telencephalon of mouse embryos *in utero*. QDs were found in the principle cell types generated by these neural stem and progenitor cells substantial distance away from the site of primary injection without interrupting their migration and differentiation during the developmental cycle.

Dendritic cells (DC) present antigens to the T cells in lymphoid organs, thereby initiating an adaptive immune response. Noh et al labeled DCs with QDs and observed dendritic cell migration into lymph nodes in vivo. This labeling did not affect the dendritic cell phenotype or maturation potential as observed by MTT assay and FACS analysis. The researchers observed migration of QD labeled DCs into popliteal and inguinal lymph nodes after injection into the footpad in experimental animals via NIR Fluorescent imaging.

Lim et al labeled Natural Killer (NK) cells with QD 705 and observed that there was no influence on NK cell viability by FACS analysis.

All these studies reliably confirmed that QD labeling can be used as a safe and effective means to facilitate in vivo therapeutic cell trafficking.

2.7.CYTOTOXICITY OF QUANTUM DOTS - CdTe QDs are synthesized from Cadmium and Telluride precursors. Elemental Cadmium gained major interest as a result of range of its technological uses. To protect steel and other alloys from corrosion (such as in aeronautics industry) Cadmium-coating by electroplating has been used consistently. Cadmium is a key component of several alloys as it improves mechanical and thermal properties of materials used in antifriction, soldering and electrical applications. Cadmium chalcogenides express optical properties subsequent to their interaction with photons. As a result their use has been justified as pigments in plastics, paintings, enamels and inks. Emitted light from these chalcogenides has been used in electronics and several display devices.

2.7.1 CADMIUM TOXICITY- Manufacturing and disposing Cadmium containing compounds are the major causes of occupational exposure. Wind driven suspension of cadmium powder present on the surface of earth or dispersion of volcanic gases could result in air pollution. Agricultural activities through the use of fertilizers can introduce the metal into the food chain and water. Thus inhalation and ingestion predominantly become the source of human exposure to elemental cadmium.

Due to the polluted atmosphere, upper respiratory tract and lungs become the major target for Cadmium dust and vapors. However ingested Cadmium generally target intestines, liver and kidneys resulting in toxic insult to these viscera. Once absorbed, cadmium has a very long half- life of more than 20 years in humans. So it can be efficiently trapped in the body and can escape detoxification.

Different mechanisms exist demonstrating transport of Cadmium within the body based on the mode of exposure. Inhaled Cadmium particles are generally transported along the primary olfactory neurons to the olfactory bulb which is where

these particles are accumulated. Inhaled Cadmium particles are also accumulated in the lungs as in smokers. Despite of an efficient barrier for toxic molecules and heavy metals, Cadmium can pass through alveolar cells and enter the circulation. Ingested Cadmium can accumulate in the enterocytes, the process favored in the iron deficient state.

Cadmium is not only mutagenic but is genotoxic and carcinogenic. When the cells are exposed to high concentration of Cadmium in a short duration, there is increased oxidative DNA damage as a result of creation of reactive oxygen species. In addition there is an evidence of inhibition of cellular DNA repair mechanism. Acute exposure to Cadmium results in cell necrosis and apoptosis mediated by various signaling pathways which trigger caspase dependent or caspase independent mechanisms.

Cadmium exposure in humans can cause host of toxic manifestations based on mode of exposure. Inhalation exposure results in injury to the respiratory tract. Emphysema, anosmia and chronic sinusitis have been linked with pulmonary exposure. Large incidence of lung cancer in the occupationally exposed populations led to Cadmium being classified as human pulmonary carcinogen.

Cadmium interferes with mineralization of bones. Toxicity is associated with osteomalacia, osteoporosis and bone fractures. Anaemia and eosinophilia have been associated with Cadmium toxicity. Renal toxicity results in nephropathy and proteinurea[83].

2.7.2 TELLURIUM TOXICITY- Tellurium is a naturally occurring element used in alloys of copper, steel, lead and bronze as it provide more resistance to corrosion. It is also used in vulcanization of rubber to provide increased resistance to heat, abrasion and aging. In addition, Tellurium is used in metal-oxidizing solutions to

blacken or tarnish metals e.g. in jewellery manufacturing.

Elemental tellurium has relatively low toxicity. It is converted in the body to dimethyl telluride which imparts garlic like odor to breath and sweat.

Accidental ingestion is the commonest mode of Tellurium toxicity in human beings which often manifests by metallic taste, nausea, vomiting, headache, drowsiness, garlic odor of the breath blackened oral mucosa & skin and corrosive gastrointestinal tract injury from acid solvent. Toxicity from exposure to hydrogen telluride gas leads to mucous membrane & pulmonary irritation, haemolysis, haemoglobinuria, anuria, jaundice, pulmonary oedema, tremors, convulsions and respiratory arrest[84].

Before the quantum dots can be applied in the clinical setting, it is fundamental that their potential adverse effect on human being is fully established. Understanding the toxicity of QDs is mandatory as it carries significant implications on health of the population, environmental safety and public acceptance. Quantum dots are composed of heavy metals with known toxicity. Also because of their size, they are easily accessible to cells within the vital organs. Once administered, these nanoparticles may either remain adherent to the cell surface or may undergo internalization by diverse pathways such as translocation through the plasma membrane, receptor mediated endocytosis or pinocytosis. Once internalized, they may remain in endosomes, disperse within the cytosol to interact with subcellular organelles or are recycled to the cell surface. The localization of these quantum dots within the cell will eventually determine their cytotoxicity.[85] These promising nanoparticles though possess invaluable diagnostic and therapeutic potentials, they contain heavy metals and demonstrate prolonged tissue retention causing concerns

for toxicity. Some of these quantum dots may be retained in the body for more than 100 days[86].

Large number of *in vitro* studies observed cytotoxicity of QDs. The determinants of cytotoxicity are size, capping material, colour, dose of QDs, surface chemistry , coating bioactivity and processing parameters[11] Besides these oxidative, photolytic and mechanical stability of the QDs contribute to the cytotoxicity potential. Their potential weakness is the very coating that makes them novel. Any compromise in the coating can expose the metalloid core. The toxicity of core elements may either be due to the composite materials such as CdSe / CdTe or to the constituent core element after their dissolution e.g. Cd.

Occasionally the ligands added to render the probe biologically active may have toxic effects on the cells. The coating material such as mercaptoacetic acid, Mercaptopropionic acid has been found to be mildly cytotoxic. MUA, cysteamine and TOPO have all been shown to have the ability to damage DNA in the absence of QD core.

Under proteolytic and oxidative conditions, QDs can become degradable resulting in disruption of core-coating biocomplexes rendering them cytotoxic. Several studies suggested QD cytotoxicity due to photolysis or oxidation. These processes can degrade the QDs , exposing either potentially toxic capping materials or core metal components as a result of dissolution of core complexes[87]. Several mechanisms have been attributed to be responsible for cytotoxicity of QDs which include QD core degradation, free radical formation and interaction of QDs with intracellular components.

Groups III-V QDs may provide a more stable alternative to Groups II-VI QDs due to the presence of a covalent rather than an ionic bond and have been reported to have lower cytotoxicity. However these QDs are difficult to prepare on a competitive time scale and have much lower quantum efficiencies.

Lovric et al studied subcellular localization and cytotoxicity of Cadmium Telluride (CdTe) Quantum dots in PC12 and N9 cell lines and effects of pharmacological agents to prevent cell death. They demonstrated marked cytotoxicity in both these cell lines in the form of chromatin condensation and membrane blebbing along with marked decrease in the metabolic activities observed by calorimetric 3-(4,5-dimethylthiazol-2-yl)-2,5-diphenyl tetrazolium bromide(MTT) assay more pronounced with small (2r = 2.2 ± 0.1 nm) green emitting positively charged QDs than the large (2r = 5.2 ± 0.1 nm) red emitting equally charged QDs. They also noticed that pre-treatment with antioxidants N-acetylcysteine and with bovine serum albumin considerably reduced the QD induced cell death. They couldn't demonstrate similar effect after pre-treatment with Trolox, similar antioxidant, the water soluble analog of vitamin E. The authors proposed that N-acetylcysteine could exert its effect by stabilizing the QDs as a result of its mercapto group being adsorbed on their surfaces or by activating the key antiapoptotic signal transduction pathways leading to transcription of genes involved in cell survival along with its antioxidant properties and its ability to enhance glutathione expression[33].

Yang et al quantitatively studied blood and tissue kinetics of QD 705 in mice following single tail vein injection of 40 pmol dose. Using Inductively Coupled Plasma Mass Spectrometry (ICP-MS),they observed continuously increasing levels of QDs in spleen, liver and kidneys 28 days after the intravenous injection with time dependent redistribution with no fecal or urinary excretion concluding a very long

plasma half-life potentially weeks or even months raising concerns over the health consequences[40].

Derfus et al observed that liver is the primary site of acute injury as a result of cadmium exposure. Even in vitro studies demonstrated significant hepatotoxicity to very low levels (100-400µm) of cadmium ions. More than 25% of administered cadmium in rats was found to be accumulated in liver. The mechanism of injury has been attributed to Cadmium binding to sulfhydryl groups of critical mitochondrial proteins and inefficient detoxification of this Cadmium by relatively small amount of Metallothione protein in the cytoplasm. Authors demonstrated that CdSe core quantum dots are cytotoxic by means of formation of reduced Cd on the QD surface and release of free Cadmium ions. Capping CdSe core with Zns or coating with BSA virtually eliminates the cytotoxicity of QDs due to oxidation.

Male et al utilized the on line and continuous technique based on electric cell substrate impedance (ECIS) sensing to measure the concentration and time response functions of Chinese hamster lung fibroblast V 79 cells to various quantum dots and fluorescent gold particles. The cytotoxicity was estimated by measuring half-inhibition concentration($ECIS_{50}$), the required concentration to attain 50% inhibition of cytotoxic response. The authors noted direct cytotoxicity with cadmium selenide cores using the ECIS assay. They also indicated that cytotoxicity following CdTe quantum was assigned to free Cadmium as well as the QDs themselves. The QDs synthesized with indium gallium phosphide and the fluorescent gold nanoparticles were not cytotoxic[88].

Chen et al used 21.3 nm diameter QDs with CdSeS core coated with a shell of silica, network with multiple hydroxyl groups to promote water solubility and to ensure

biocompatibility. The shell of silica effectively insulated the CdSeS core. During the experiment which lasted for 5 days with a QD dose of 5 nmol / mouse, no death or symptoms of illness were observed in the mice. During the in vitro experiments, the authors observed that the core-shell structure and fluorescent properties of the QDs remain unaltered in the environment of blood and kidney. During in vivo experiments in mice, the authors observed that these QDs coated with multiple Si-OH groups had an affinity for liver, kidney, spleen and lung after tail vein injection. Most of the QDs were metabolized and excreted in the kidney and liver. No Cadmium was demonstrated in the supernatant solution of the homogenized liver and kidney after ultracentrifugation implying stability of the QDs to maintain themselves in the core-shell structure. The authors also state that after intravenous injection of these QDs, unbound QDs are rapidly excreted by the kidneys. Protein bound QDs are translocated to the liver and are excreted in faeces. A small fraction of QDs aggregated to larger particles are retained in the liver tissue for long term[89].

Biological interaction of quantum dots with the porcine skin was observed by Zhang et al using QD 621 nanoparticles containing Cadmium selenide core with Cadmium sulphide shell coated with polyethylene glycol (PEG). They noted that quantum dots were located primarily within the intercellular lipid bilayers of stratum corneum layer of the skin even at the highest concentration. Cell viability assay using human epidermal keratinocyte cells (HEK) using MTT assay revealed statistically significant decrease in the cell viability using higher doses at 24 and 48 hours. The researchers indicated that stratum corneum acts as a primary barrier for the skin and any types of breach in the epithelial integrity in the form of cuts and wounds would expose the QDs to the viable skin cells potentiating the cytotoxic risk[38].

Further possibility of corneal toxicity produced by QDs following penetration of corneal epithelial barrier has been raised posing potential risk of eye exposure to these nanoparticles. Kuo et al studied permeability and distribution of CdSe/Zns QDs both in vitro and in vivo models using two photon microscopic imaging & observed that the fluorescent QDs can easily penetrate & reside within the interlamellar space following injury to the corneal epithelial barrier. They pointed out that corneal stromal viability was inversely proportional to the concentration of these QDs and duration of exposure. During in vivo experiment, they noticed that these QDs can be retained within the cornea for up to 26 days long enough to cause consequential toxicity[90].

Wang et al studied cytotoxic effects of human umbilical vein endothelial cells (HUVEC) & demonstrated the dose dependent inhibitory effects on cell growth by generation of Reactive Oxygen Species(ROS). They also demonstrated that pre-treatment with N-acetyl Cysteine (NAC) , a ROS scavenger inhibited the induction of ROS by QDs & thereby decreasing the QD induced DNA damage[91].

Clift et al published their results of cytotoxic effects of different surface coated QDs such as organic, carboxylated (COOH),amino & PEG coated QDs on J774A1 macrophage cell viability. They analyzed MTT assay & LDH release study to conclude that organic QDs induced significant cytotoxicity up to 48 hours even at a particle concentration as low as 20 nm. Both (COOH & NH2) PEG QDs cause reduced cell viability & cell membrane permeability at a much higher concentration of 80 nm. Also they suggested that surface coating and core material resulted in cytotoxicity[92].

The influence of CdSe QDs on oocyte maturation, fertilization and subsequent pre & post implantation development was studied by Hsieh et al to observe that these QDs demonstrated significant teratogenic influence in the form of decrease in cell number, increased apoptosis and inhibition of post- implantation development. ZnS coated CdSe QDs seemed safer than uncoated ones[93].

In summary, both coated and noncoated QDs can exert their toxicity to various tissues depending on the chemical composition and mode of exposure. Careful evaluation of cytotoxicity potential of QDs is essential prior to their application in human population.

Chapter 3.

Synthesis and characterization of CdTe Quantum dots

3.1 Introduction

To date several methods of preparation of CdTe QDs have been described which include both organic synthesis and aqueous synthesis. The high quality CdTe nanocrystals prepared in the organic solvents cannot be utilized in the biosystems as they are hydrophobic. Several methods have been described to convert hydrophobic QDs into hydrophilic one such as ligand exchange, encapsulation into water soluble shell and arrested precipitation in water. However these processes indeed diminish their photoluminescence quantum yield (PL QY) during the transferring process. The aim of the study was to synthesize highly efficient and stable water soluble CdTe quantum dots from cheaper chemical precursors and to characterize these quantum dots.

3.2 Synthesis of Cadmium Telluride (CdTe) QDs

Water soluble CdTe QDs were prepared using precursors Cadmium Chloride and Sodium Tellurite in presence of buffer solution of Mercaptosuccinic acid.

15 mM solution of Borax ($Na_2B_4O_2$) was prepared by dissolving 1.44 gm of borax to 200 mls of water. 15 mM solution of citrate acid was prepared by dissolving 0.88 gm of sodium citrate in 200 ml of water. All the reactions proceeded in the buffer solution composed of $Na_2B_4O_2$ and citric acid adjusted to different pH values with 1 M Hydrochloric acid) (HCL) or 1 M Sodium Hydroxide (NaOH). The precursor solution was prepared by mixing a solution of 1 mM Cadmium chloride ($CdCL_2$ – 18.3 mg in 50 mls), 0.25 mM Sodium Tellurite (Na2TeO3- 6 mg in 50 mls) and 3 mM Mercaptosuccinic acid (MSA – 45 mg in 50 ml) in 50 ml of the above buffer solution in one-neck flask at room temperature (16 ± 2^0C) at pH ~ 7.0. The molar ratio of

Cd:Te:MSA was 4:1:12..After vigorously stirring for 5 minutes, 20 mg of Sodium tetrahydridoborate (NaBH4) powder was added to the precursor solution. The flask was attached to a condenser and refluxed at 100^0C under open air conditions as revealed in Fig. 3.1.

Fig. 3.1. Experimental setup in the preparation of water soluble QDs.

Once the development of CdTe nanocrystals was completed, the growth of CdTe nanocrystals during the refluxing was controlled by the Ostwald ripening process in which smaller particles dissolve and the monomers released are consumed by the larger once[24]. The emission spectrum of quantum dots was precisely determined by size of the QDs. The preparation of QDs with different emission spectrums can be controlled by regulating the duration of condensation and refluxation of the mixture of QD precursors. The QDs thus prepared were water soluble and stable at room temperature.

Fig. 3.2 demonstrate different colour emitting QDs in the ultraviolet scanner. These semiconductor nanoparticles emit fluorescence depending upon size of these particles as explained in Fig. 3.3.

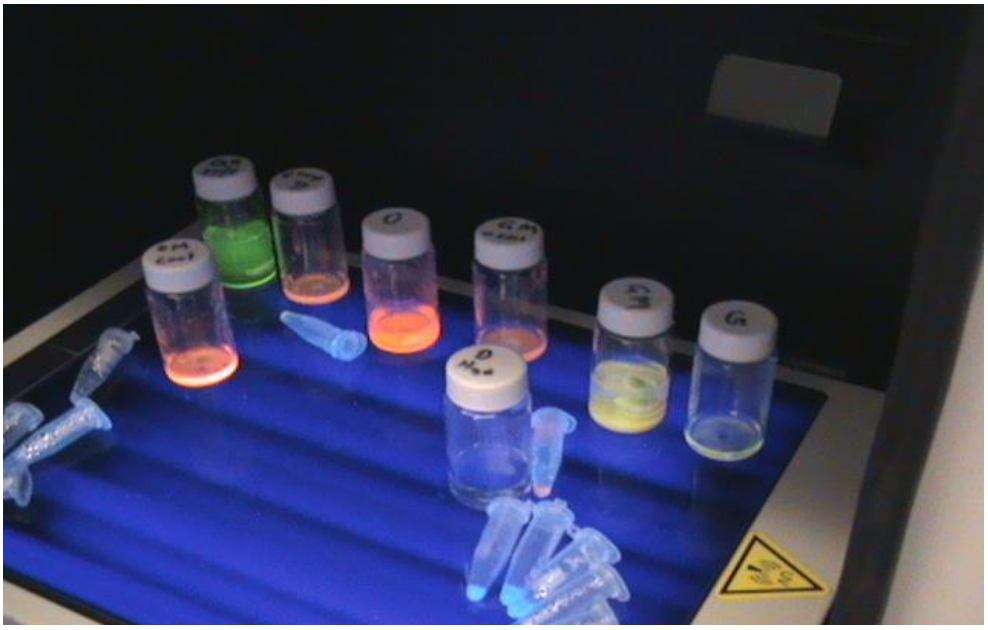

Fig.3.2 QDs in ultraviolet scanner. Fluorescence of difference colour based on size of the QDs.

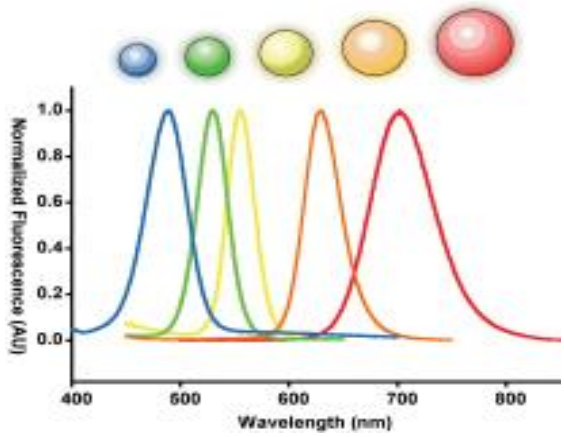

Figure 3.3 Size dependent fluorescence of semiconductor nanoparticles.2 nm quantum dots emit blue fluorescence but at 6 nm, they emit in the red. The size is inversely related the bandgap energy which dictates the fluorescence emission[85]

During the process of synthesis of CdTe QDs, in the initial phase when $NaBH_4$ powder was added to the precursor solution, this solution turned green within few seconds depending upon the pH value of the precursor solution, the concentration of the solution and the reaction temperature. It was noted that lowering the pH value , increasing the concentration of the precursor solution or increasing the reaction temperature accelerated the formation of the CdTe nanocrystals. During the initial stage, no photoluminescence was observed from the crude solution presumably as a result of smaller size of the QDs. Weaker luminescence was noted after prolonged boiling when the solution turned dark green in colour. With prolonging of the reflux time, the absorption spectra as well as PL emission spectra shifted to longer wavelength with increase in the size of the CdTe nanocrystals due to quantum confinement effect. These MSA- CdTe nanocrystals remained stable for months when stored in the refrigerator at 4ºC indicating attractive bio-labeling and bio-imaging applications.

3.3 Excitation and emission spectrum

An *excitation spectrum* (a plot of absorbance as a function of wavelength) was determined to select the optimal wavelength for analyzing a given compound. The optimal wavelength (A_{max}) for measuring absorbance is the wavelength that is most absorbed by the compound in question.

The spectrophotometer analysis of excitation spectrum and emission spectrum of red photoluminescent mercaptosuccinic acid stabilized CdTe nanocrystals thus prepared in aqueous solution was analyzed.

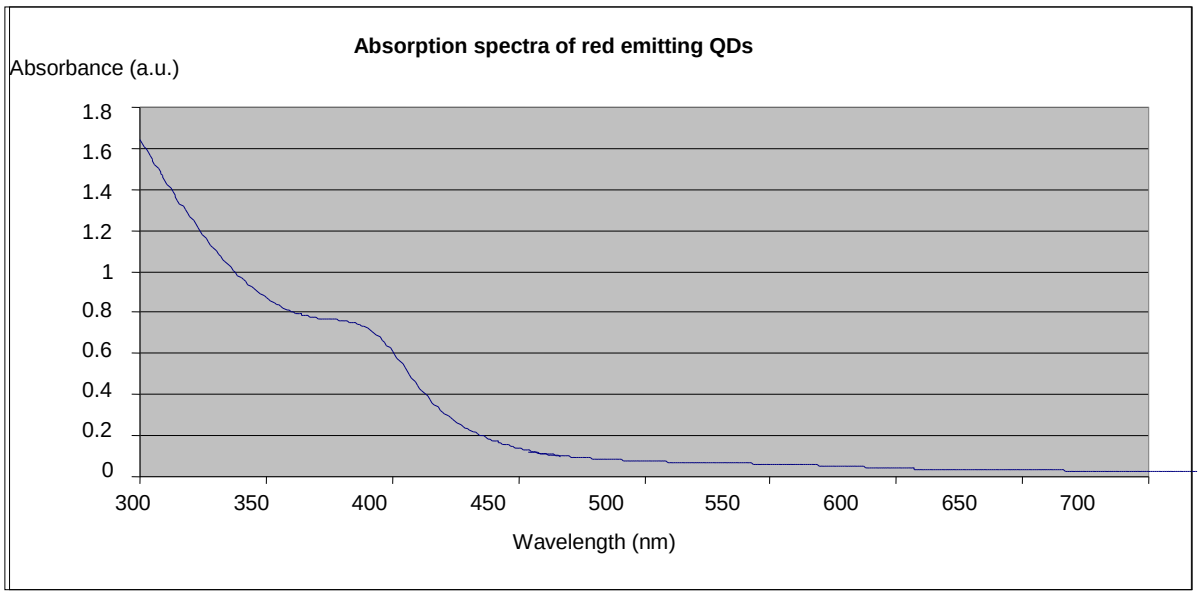

Fig 3.4. Excitation spectrum of red emitting CdTe QDs

When these QDs were subjected to spectrophotometry, the broad absorption spectrum was observed. The graph of absorbance vs. wavelength for CdTe quantum dots was plotted which demonstrated a wider range of absorbance with an excitonic absorption peak at 380 nm as shown in fig. 3.4.

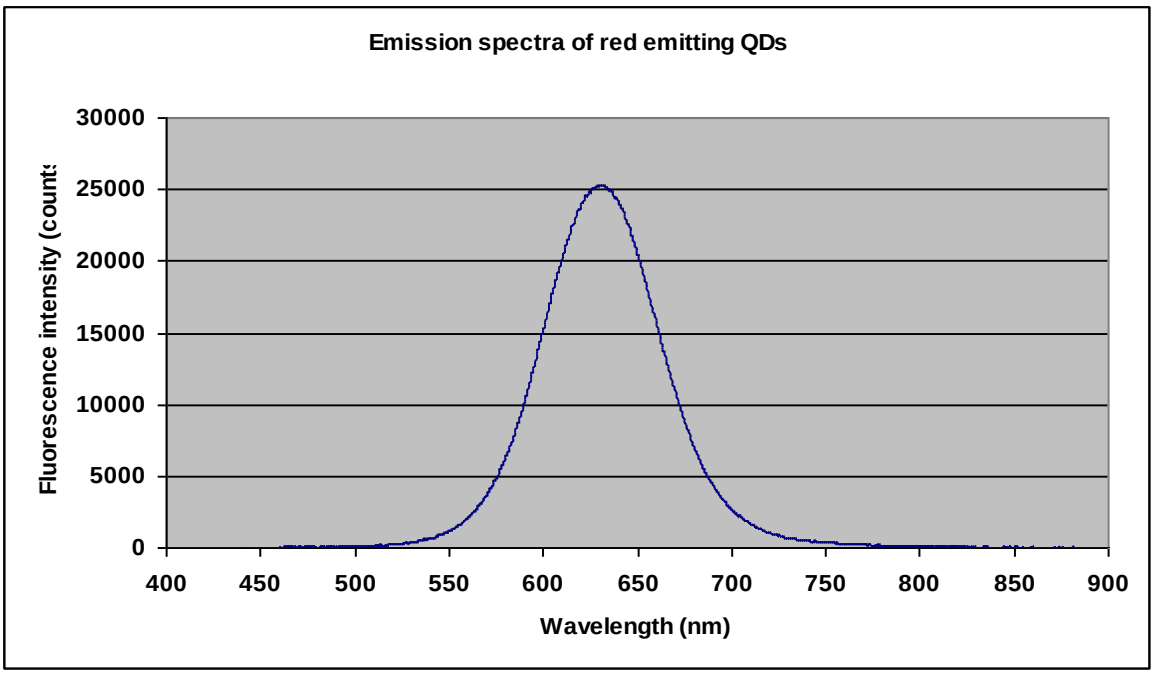

Fig.3.5. Emission spectra of red emitting QDs

These red emitting water soluble CdTe quantum dots exhibited narrow and symmetrical emission. The emission spectrum suggests an emission peak at 630 nm and is characterized by good symmetry and narrow spectral width as demonstrated in fig. 3.5. During the synthesis of quantum dots it was observed that the these quantum dots demonstrated size dependent fluorescence emission. In the initial stages of QD synthesis, smaller diameter QDs revealed emission peak at lower wavelength however they were symmetrical with narrow spectral width. Progressively, larger diameter CdTe QDS as in this study were red emitting ones at an emission peak of 630nm.

3.4 QD size

The transmission electron microscopic appearance of CdTe nanocrystals was analyzed. These quantum dots were observed to be present in different sizes and shapes. Majority of these nanocrystals were contain single or clusters of these quantum dots measuring 5nm to 10 nm.in diameter. Fig. 3.6 and 3.7 display transmission electron microscopic images of CdTe QDs.

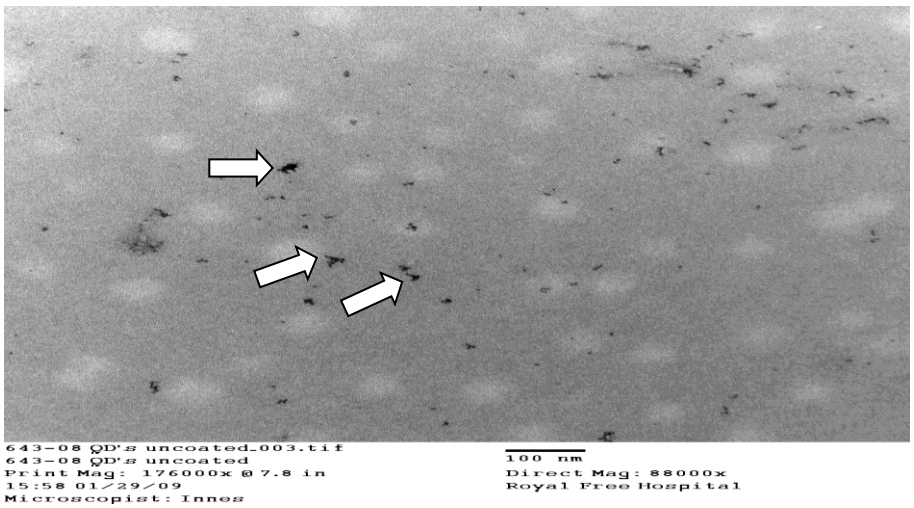

Fig.3.6. Transmission electron microscopic appearance of CdTe Quantum dots. (white arrows indicate CdTe quantum dots),

Figure 3.6 indicate TEM appearance of CdTe quantum dots. The image was obtained at a magnification of 88000X. The uncoated Qds are randomly dispersed and appear in the form of single crystals or multiple clusters. White arrow indicate the presence of QDs.

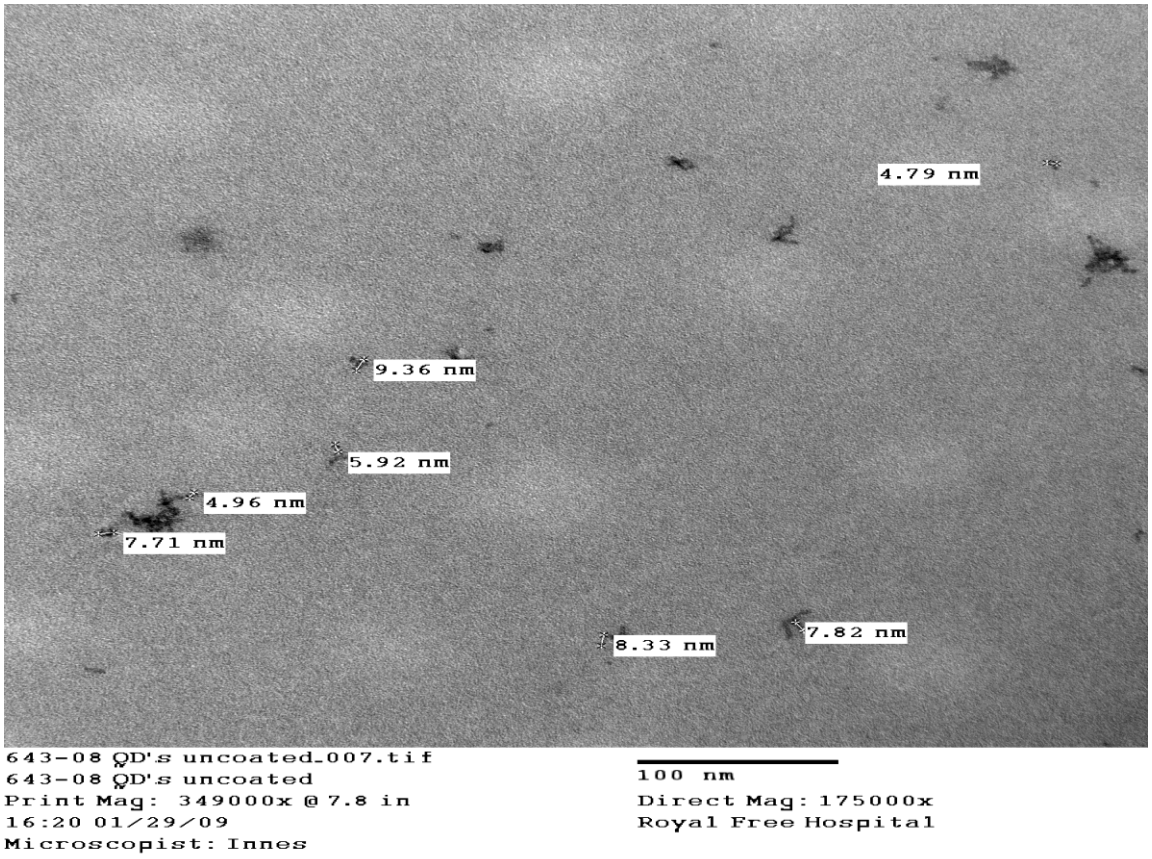

Fig. 3.7 Size of CdTe nanocrystals

The QDs were sized according to TEM criteria as demonstrated in fig. 3.7. Each single QDs measured between 5-10nm in diameter. As observed in the figure, the tendency to form clusters was noted. These QDs were then subjected to X-ray microanalysis using transmission electron microscopy to establish the constituents of these QDs as observed in fig. 3.8.

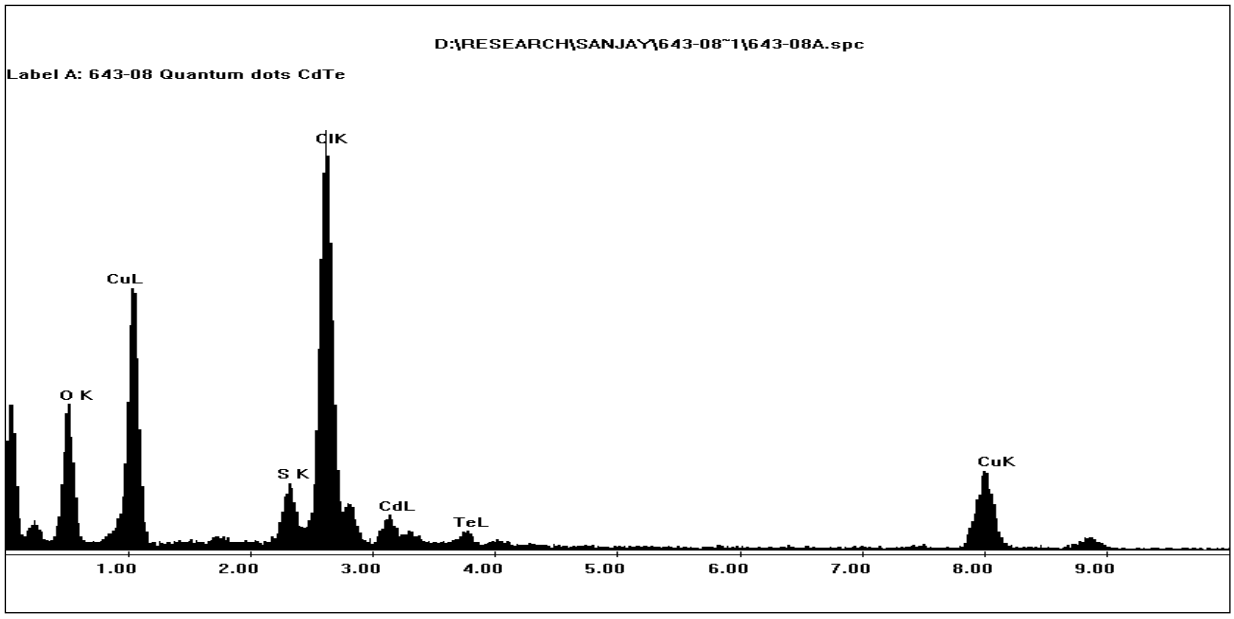

Fig.3.8. X-Ray Microanalysis of Quantum Dots

Further analysis of these quantum dots was performed using X-ray microanalysis in order to establish and confirm the chemical composition of these nanocrystals. X-ray microanalysis is a technique used by electron microscopist to get an insight into elemental localization at cellular or even subcellular level. This technique is based upon spectral analysis of the scattered x-ray emission from the specimen induced by the electron beam.This does confirm the presence of Cadmium and Tellurite in addition to chloride, copper and sulphur most probably contributed by mercaptosuccinic acid as observed in Fig.3.8. Though quantitative elemental analysis is feasible, the facilities to do so were unavailble.

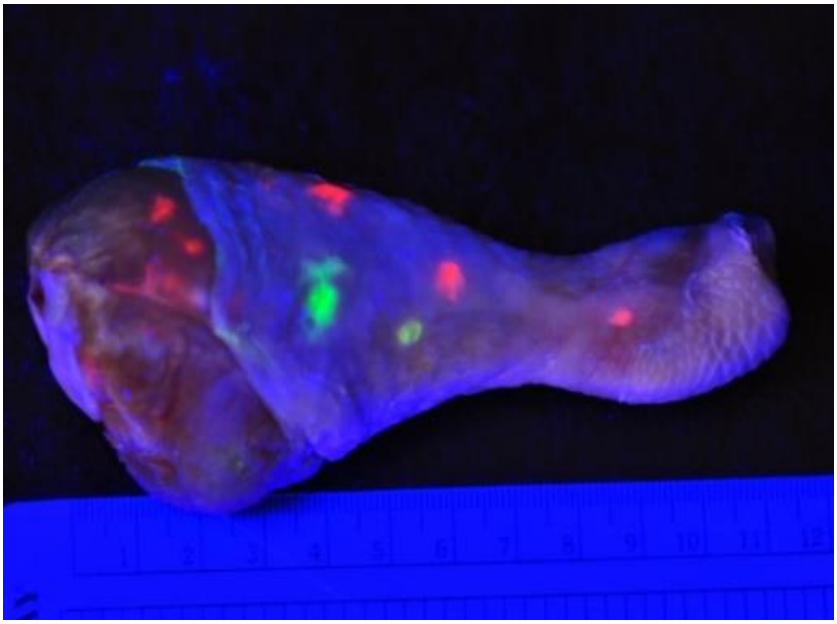

Fig. 3.9. Fluorescence emitted by different colour emitting QDs in an experimental chicken leg under ultraviolet light.

Above figure 3.9 demonstrates fluorescence emitted by different colour emitting QDs after injecting them in different muscle compartments of chicken leg and viewed under ultraviolet light. The fluorescence decay was extremely slow and persisted several days after storing the specimen in the deep freezer.

3.5 Conclusion

It is possible to synthesize water soluble CdTe QDs form their presursors Cadmium Chloride and Sodium Tellurite in presence of Mercaptosuccinic acid acting as a buffer solution. These QDs are stable at room temperature for several days and can be used for *in vitro* and *in vivo* experiments. Spectroscopic analysis revealed that these Qds have a wider absorbance with an excitonic absorption peak at 380nm and a narrow spectral emission peak at 630nm.These Qds measure between 5-10nm in

diameter.X-ray microanalysis of these nanocrystals confirm the presence of elemental Cadmium and Tellurite.

Chapter 4.

Materials and methods

Introduction

This chapter describes the experimental evaluation of cultures of HT29 colon cancer cells used to provide evidence of cancer cells binding of CdTe QD. Parallel experiments were conducted on C2C12 mouse skeletal muscle cells as normal controls. The chapter elaborates the method of water soluble CdTe QD synthesis, their conjugation to commercially purchased RGD peptides and transmission electron microscopic studies. Subsequent overview of cytotoxicity methodology of both nonconjugated and conjugated QDs concludes this chapter.

4.1 Cell culture

4.1.1 Culture of HT29 colon cancer cells lines

HT29 cells were originally purchased from the European collection of cell cultures (ECACC, Sigma, and Dorset, UK). These cells were initially isolated from a primary tumor in a 44 year old Caucasian female. The cells form a well differentiated adenocarcinoma consistent with colony primary grade 1.The cells possesses the HLA profile of A1, 3; B12, 17; Cw5.

4.1.1.1 Resuscitation of frozen HT29 cells

HT29 cells were removed from the storage (Liquid Nitrogen) and quickly thawed in a water bath at 37ºC. 1 ml volume of the cell suspension containing 1 million cells was added to 15ml of McCoy's 5A growth medium containing GlutaMAX (GIBCO).This solution was supplemented with 10% Fetal bovine serum and 1% Penicillin-Streptomycin in tissue culture grade flasks with surface area of 96 cm^2 and incubated

at 37ºC & 5%CO_2 .in a humidified atmosphere $_{to}$ allow uniform cell growth for 3-5 days.

4.1.1.2 Cell Passaging of HT29 cells

The procedure was carried out under sterile technique in a laminar flow cabinet to avoid contamination with bacteria, yeast or other cell lines. The previous growth media was removed. Cells were washed three times with phosphate buffered saline (PBS) – GIBCO. 3ml of 0.25% Trypsin- EDTA was added to detach the cells from the bottom of the flask. To optimize the function of trypsin, the flask was incubated at 37ºC for 5 minutes. 10 mls of fully supplemented McCoy's 5A growth medium was added to the flask to neutralize the effects of trypsin. The cells in the suspension of trypsin and growth medium were centrifuged with 350 revolutions per minute (RPM) at 4ºC for 5 minutes. The supernatant was discarded and the remaining cell pellets were re-suspended in 5 ml fresh growth medium. After counting the cells, appropriate numbers of cells were transferred in a new sterile flask with an area of 96 cm^2 and fresh medium was added. The flask was subsequently maintained in an incubator to allow cell growth. Once the cells achieved approximately 85% confluence, they were passaged and counted for further experiment.

4.1.2 Tissue culture of mouse skeletal muscle (C2C12) cell lines as a control

Mouse skeletal muscle C2C12 cell lines were used as a normal control in the experiment for the study of bioconjugation of QDs and QD cytotoxicity. The original cell lines were obtained by subcloning of mouse myoblast cell lines conserved in the frozen storage.

4.1.2.1 Resuscitation of frozen C2C12 cells

C2C12 cells were removed from the frozen storage and quickly thawed in a water bath at 37ºC. 1 ml volume of the cell suspension containing 1 million cells was added to 15ml of Dulbecco's Modified Eagle Medium (DMEM) - GIBCO, supplemented with 10% fetal bovine serum and 1% Penicillin-Streptomycin in a flask with surface area of 96 cm^2 and incubated at 37ºC & 5%CO_2 in a humidified to allow uniform cell growth.

4.1.2.2 Cell passaging of C2C12 cells

The procedure was carried out under sterile technique in a laminar flow cabinet to avoid contamination with bacteria, yeast or other cell lines. The previous growth media was removed from the flask. Cells were washed three times with phosphate buffered saline (PBS). 3ml Trypsin was added to detach the cells from the bottom of the flask. To optimize the function of trypsin, the flask was incubated at 37ºC for 5 minutes. Fully supplemented Dulbecco's Modified Eagle Medium (DMEM) was added to the flask to neutralize the effects of trypsin. The cells in the suspension of trypsin and growth medium were centrifuged at 350 revolutions per minute, 4ºC for 5 minutes. The resulting supernatant was discarded and the remaining cells from the bottom of the centrifuge tube were re-suspended in 5 ml fresh growth medium. After counting the cells, appropriate number of cells was transferred in a new sterile flask with an area of 96 sq.cm and fresh medium added. The flask was subsequently maintained in an incubator to allow cell growth. Once the cells achieved approximately 85% confluence, they were passaged and counted.

4.1.3. Counting of cells prior to transferring into the 24 well plates

The cells were counted in order to provide uniform monolayer of cells when grown in the 24 well plates and to avoid bias during *in vitro* experiments. Conventional haemocytometer containing counting chamber was used to count the number of cells per unit volume in cell suspension. A thick, specially designed coverslip was placed over the polished surface of the counting chamber. 20µl. solution of the cell suspension was placed into the V shaped wells with a fine pipette. The gap under the coverslip was noted to fill by capillary action. The charged counting chamber was placed on the microscope stage. The microscope was focused on the counting grid at low power. The cells were counted in the 4 larger corner squares. As each square has surface area of 1mm-squared and a depth of 0.1mm giving it a volume of 0.1 mm^3. The average cell count of 4 corner cells multiplied by 10000 provided the exact value of cell count per ml. The volume of cells was calculated accordingly in order to set up to 80,000 cells in each well of 24 well plate. The 24 well plate was then

labeled and incubated at 37ºC and 5% CO2 to allow uniform cell growth. The 24 well plates prepared in this manner were used for subsequent serial experiments on semiconductor quantum dots.

4.2 Interaction of RGD bioconjugated QDs with HT29 cells

RGD PEPTIDES –

Three types of RGD peptides were commercially ordered from Peptides International, Inc., Louisville, USA. They were-

a. Cyclo (Arg-Gly-Asp-D-Phe-Lys) - c (RGDfK) (M.W. 603.68) C27H41N9O7-alphavbeta3 Integrin Binding RGD Peptide.

This peptide has been proven to bind specifically and with high affinity to αvβ3 receptors on neovascular blood vessel sections of different major human cancers. The integrin alpha(IIb)beta(3)-specific cyclic hexapeptide contains an Arg-Gly-Asp (RGD) sequence.

b. Cyclo(Arg-Gly-Asp-D-Phe-Cys*)* c(RGDfC) (M.W. 578.65) C24H34N8O7S RGD

This is a cyclic RGDfC sequence, an integrin avb3-affine peptide. (linker additions via Cys)

c. Cyclo(Arg-Ala-Asp-D-Phe-Val)- c(RADfV) (M.W. 588.68) C27H40N8O7

This was used as a negative control.

HT 29 cells were cultured in flasks with a surface area of 96 cm^2. When the cells were 85% confluent, they were trypsinized for 5 minutes. Fully supplemented McCoy's 5A growth medium was added to the flask to neutralize the effects of trypsin. The cells in the suspension of trypsin and growth medium were centrifuged at 350 revolutions per minute, 4ºC for 5 minutes. The resulting supernatant was discarded and the remaining cells from the bottom of the centrifuge tube were diluted with McCoy's 5A growth medium. Cells were counted using the haemocytometer containing counting chamber. Cell suspension was prepared with a concentration of 20,000cellls in 200 µl.solution. 96 well plate were prepared seeding 20,000 cells in each well (200 µl. solution per well). The first row contained only HT 29 cells without an addition of quantum dots. 20µl.solution of CdTe quantum dots was added to the second row. 20µl.solution of CdTe quantum dots bound to c (RGDfK) αvβ3 Integrin Binding RGD peptide was introduced in the third row. 20µl.solution of CdTe quantum

dots bound to c (RGDfC) RGD Tumor Targeting Peptide was introduced in the fourth row. 20 µl.solution of CdTe quantum dots bound to c (RADfV) Negative Control was added to the fifth row. The cells were incubated at 37ºC & 5%CO_2 for 2 hours. Images were obtained with inverted microscope.

4.3 TRANSMISSION ELECTRON MICROSCOPIC (TEM) STUDIES OF THE QUANTUM DOTS -

10 µl solution of Red emitting CdTe QDs was collected in an eppendorph tube. The solution was centrifuged at 350rpm for 10 minutes. This resulted in aggregation of the QDs at the bottom of the eppendorph tube. HT29 colon cancer cells were passaged and transferred into 3 flasks with a surface area 96$cm^{2.}$Cells were allowed to grow in incubator at 37ºC & 5%$CO_{2.}$ When cells were grown to 85% confluence, they were trypsinized for 5 minutes. Fully supplemented McCoy's 5A growth medium was added to the flask to neutralize the effects of trypsin. The cells in the suspension of trypsin and growth medium were centrifuged at 350 revolutions per minute, 4ºC for 5 minutes. The resulting supernatant was discarded and the remaining cells from the bottom of the centrifuge tube were kept ready to be mixed with QDs alone as well as different RGD peptide bound QDs. The first flask was used as a control flask containing only HT29 cells with no added QDs. 10 µl solution of CdTe QDs was added to the second flask. 10 µl solution of c (RGDfC) - RGD Tumour Targeting Peptide bound to the CdTe QDs. was added to the third flask. Eppendorph tube containing only CdTe QDs

With no cells was used as another control. All 4 flasks were incubated at 37ºC & 5%CO_2 for 2 hours. The cells were fixed in 1.5% glutaraldehyde for a minimum of 2 hours, before being centrifuged to form a pellet in a 0.5 ml eppendorf. The cell

pellets were washed with two changes of phosphate buffer [Oxoid] and postfixed using osmium tetroxide. The cells were resuspended after each change of solution and allowed to stand for 10 minutes, before centrifugation and removal of the supernatant and addition of the next processing solution. Cells were washed using several changes of distilled water to remove the osmium tetroxide and dehydrated using alcohol 30%, 50%, 70%, 90% and 100%. The samples were left in 50% alcohol/50% Lemix (Taab) epoxy resin mixture on a mixer overnight to infiltrate with resin. They were then placed in 100% Lemix resin for a minimum of 4 hours, embedded in fresh Lemix Resin and polymerized at 70^{o} C overnight. Semithin (1µm) sections were cut using glass knives on a Reichert-Jung ultracut microtome, collected on glass microscope slides and stained using 1% toluidene blue. Ultrathin sections were cut using a diamond knife (Diatome) and collected on 300HS, 3.05mm copper grids (Gilder). The ultrathin sections were stained using saturated alcoholic uranyl acetate (TAAB) for 5 mins. followed by Reynold=s lead citrate, also for 5 mins. The ultrathin sections were viewed and photographed using a Philips CM120 transmission electron microscope.

Reagents used were as follows-

a) Glutaraldehyde

(20mls 20% paraformaldehyde [Analar BDH] + 16mls 25% glutaraldehyde [TAAB] + 59mls phosphate buffered saline [Oxoid])

b) Osmium tetroxide

1% osmium tetroxide [Analar BDH] + 1.5% potassium ferricyanide [BDH] in PBS [Oxoid]

c)Toluidene blue stain

1% toluidine blue [Raymond Lamb] with 0.2% pyronine [Raymond Lamb] in 1% sodium tetraborate [Analar BDH].

d) Reynolds lead citrate

Dissolve 1.33g lead nitrate [BDH] in 15mls distilled water and 1.76g sodium citrate [BDH] in 15mls distilled water, mix solutions together and dissolve the resulting precipitate with 8 mls of 1M sodium hydroxide [BDH], make up to final volume of 50mls

e)Lemix epoxy resin

Lemix A (25mls) + Lemix B (55mls) + Lemix D (20mls). Pour into plastic resin bottle and add 2 mls of BDMA, mix well.

4.4 CYTOTOXICITY STUDIES

4.4.1 Cytotoxicity of elemental Cadmium and Tellurium to cells

C2 C12 cells were trypsinized from sub confluent cultures by adding 3 ml. of trypsin to 96 cm^2. falcon culture flask with confluent cells. The flask was incubated at 37°C for 5 minutes with regular gentle shaking. The trypsin reaction was stopped by addition of 10 mls of fully supplemented Dulbecco's Modified Eagle's Medium (DMEM). Cell suspension was then centrifuged at 350rpm for 5min at 4°C. The cell pellet was resuspended in 20 mls. DMEM solution. Cells were counted with Fuchs-Rosenthal haemocytometer and brought to a concentration of 1,00,000 cells /ml. By serial dilution, cell suspension was prepared containing $2x10^4$ cells to be added to each well. Two 96 well plates were taken- one designated to test the cytotoxicity of

Cadmium and the second to investigate the cytotoxicity of Tellurium. After excluding the wells in the margin of the plate , total 10 columns of 6 rows of wells were used (total 60 wells on each of the two plates). 200µl cell suspension containing 20,000 cells was introduced in each well used for the experiment. Both 96 well plates were incubated at 37°C and 5%CO_2 for 24 hours to allow uniform growth of cells . Cadmium Chloride and Sodium Telluride solution was prepared in sterile condition containing 1mg /ml. of Cadmium and Tellurium. Both solutions were passed through Sterile filters Scleicher & Schuell 0.45µm , 7 bar. Max. Serial dilution of Cadmium and Tellurium solutions in the growth medium were prepared to obtain the concentration of 0µg/ml, 0.01µg/ml, 0.05µg/ml, 0.1µg/ml, 0.5µg/ml, 1µg/ml, 5µg/ml, 10 µg/ml, 50µg/ml and 100 µg/ml. After 24 hours in the incubator, both 96 well plates were removed and previous growth medium emptied. Each strength of Cadmium was added to each column of 6 wells. All 10 strengths of Cadmium was added to a total of 60 wells on one 96 well plate. Same procedure was carried out on the second 96 well plate with serially diluted Tellurium. Both plates were further incubated for 24 hours at 37°C and 5%CO_2. Cell Titer Blue Reagent G 808A (Promega) was used as an indicator of cell survival. 20 µl solution of this reagent was added to the upper 3 rows containing total 30 wells of each 96 well plates (First containing Cadmium and the second containing Tellurium). Yo Pro-1 Iodide (491/509)-Invitrogen 1mM solution in DMSO was diluted to obtain 20µM strength solution. This was used as an indicator of cell death. 20 µl solution of the reagent was added to the lower 3 rows containing total 30 wells of each of these two 96 well plates. The reagents were thoroughly mixed with the cells by placing the plates on R 100 Rotatest shaker for 5 minutes. Both plates were incubated at 37°C and 5%CO_2 for 4 hours. Fluoroscan was used to calculate the percentage of cell survival and cell

death respectively for these 2 reagents. For cell Titer Blue reagent, filter containing excitation of 530nm and emission of 620nm was used. For Yo Pro 1 Iodide reagent, filter containing excitation of 485nm and emission of 510nm was used. The results were analyzed by Ascent software for Fluoroscan.

4.4.2 Cytotoxicity of nonconjugated and bioconjugated CdTe QDs

C2C12 cells were trypsinized from subconfluent cultures by adding 3 ml. of trypsin to 96 cm^2 falcon culture flask with confluent cells. The flask was incubated at 37°C for 5 minutes with regular gentle shaking. The trypsin reaction was stopped by addition of 10 mls of fully supplemented Dulbecco's Modified Eagle's Medium (DMEM). Cell suspension was then centrifuged at 800 rpm for 5 min at 4°C. The cell pellet was resuspended in 20 mls. of medium. Cells were counted with Fuchs-Rosenthal haemocytometer and brought to a concentration of 1,00,000 cells /ml. By serial dilution, cell suspension was prepared containing 20,000 cells to be added to each well. Two 96 well plates were taken. 200µl cell suspension containing 20,000 cells was introduced in each well used for the experiment. Both 96 well plates were incubated at 37°C and 5%CO_2 for 24 hours to allow uniform growth of cells. After 24 hours in the incubator, both 96 well plates were removed and previous growth medium emptied. Only Dulbecco's Modified Eagle's Medium (DMEM) medium was used in the outermost rows and columns. One row was designated for CdTe QDs. Second row was selected for RGD (Lysine) bound CdTe QDs. Third row was allocated for RGD (Cysteine) bound CdTe QDs. The fourth one selected for c(RGDfV) negative control bound CdTe QDs. And the last one for the POSS polymer coated QDs. Serial dilution of these naked QDs and conjugated QDs in the growth medium were prepared to obtain the concentration of 0µg/ml, 0.01µg/ml,

0.05µg/ml, 0.1µg/ml, 0.5µg/ml, 1µg/ml, 5µg/ml, 10 µg /ml, 50µg/ml and 100 µg/ml. which was added to each column. Both plates were further incubated for 24 hours at 37°C and 5%CO_2 After 24 hours in the incubator, both 96 well plates were removed and previous medium emptied. Cell Titer Blue Reagent G 808A (Promega) was used as an indicator of cell survival. 20 µl solution of this reagent was added to all the rows in the first 96 well plate. Yo Pro-1 Iodide (491/509)-Invitrogen 1mM solution in DMSO was diluted to obtain 20 µM strength solution. This was used as an indicator of cell death. 20 µl solution of the reagent was added to all the rows in the second 96 well plate. The reagents were thoroughly mixed with the cells by placing the plates on R 100 Rotatest shaker for 5 minutes. Both plates were incubated at 37°C and 5%CO_2 for 4 hours. Fluoroscan was used to calculate the percentage of cell survival and cell death respectively for these 2 reagents. For cell Titer Blue reagent, filter containing excitation of 530nm and emission of 620nm was used. For Yo Pro 1 Iodide reagent, filter containing excitation of 485nm and emission of 510nm was used. The results were analyzed by Ascent software for Fluoroscan.

Conclusion-

This chapter summarizes cell studies in the laboratory setting. It elaborates detail methodology of culture of HT29 colon cancer cells and C2C12 mouse skeletal muscle cells including method of cell counting prior to preparation of uniform sheet of cells in order to optimize and assess binding of QDs. After synthesis of water soluble CdTe QDs in the laboratory, these were bound to 3 RGD peptides, two of which mainly C(RGDfK) and c(RGDfC) have affinity to integrins overexpressed by the colon cancer cells. C(RADfV) was used as a negative control. Transmission Electron Microscopic studies were performed on the unbound and bound QDs. Following this,

the chapter explains method of evaluating cytotoxicity of elemental Cadmium, Tellurium, nonconjugated and bioconjugated CdTe QDs.

Chapter 5

Cytotoxicity of quantum dots

5.1 Introduction - As Cadmium and Tellurium are the key components of CdTe QDs, the aim of the study was to evaluate minimal concentration of elemental Cadmium and elemental Tellurium that result in the cytotoxicity to the mouse skeletal muscle cells. Use of mouse skeletal muscle cells in this study formed the basis of subsequent *in vivo* study using these QDs. The study evaluated cytotoxicity of nonconjugated CdTe QDs, RGD bound CdTe QDs, RAD bound CdTe QDs (negative control) and polymer coated CdTe QDs.

5.2 Materials and methods- In order to study the cytotoxicity of elemental Cadmium to the C2C12 mouse skeletal muscle cells, graded concentration of elemental Cadmium was prepared with concentration of 0 µg/ml, 0.01µg/ml, 0.05 µg/ml, 0.1 µg/ml, 0.5 µg/ml, 1 µg/ml, 5 µg/ml, 10 µg/ml, 50 µg/ml and 100 µg/ml. Equal number of cells ($2x10^4$) were added to each well of 96 well plate. At the end of 24 hours of incubation period, Cadmium in graded concentration was added to the wells containing equal number of cells and incubated for further 4 hours following which both cell viability and cell death assay was performed and analyzed. The same procedure was applied to elemental Tellurium to assess baseline toxicity assay prior to utilizing CdTe QDs within this study.

Subsequently equivalent assessments were performed using nonconjugated CdTe QDs, RGD bound CdTe QDs, RAD bound CdTe QDs (negative control) and polymer coated CdTe QDs for comparison. The detailed methodology has been explained in chapter 4.4.2.

5.3 Results-

5.3.1 Cytotoxicity of elemental cadmium

Cell viability assay with cadmium

Graded concentration of elemental Cadmium ranging from 0.01µg/ml to 100µg/ml prepared by serial dilution in Dulbecco's Modified Eagle Medium (DMEM) was used to assertain the cell viablility studies to mouse skeletal C2C12 cells. Only medium was used in the first column as a control. Cells were incubated for a period of 24 hours, Fluoroscan analysis after incubation with Cell Titer-Blue reagent for 4 hours revealed no obvious toxicity to these cells from 0.01 µg/ml to the concentration of 1 µg/ml. At concentration of 5 µg/ml, obvious toxicity was evident. Further increasing the concentration from 10 µg/ml to 100 µg/ml revealed persistently significant toxicity as shown in table 5.1 and fig.5.1. Statistical analysis using one way ANOVA and Dunnett's multiple comparison test revealed statistically significant difference in the cytotoxicity at the concentration of of 5 µg/ml as shown in Appendix table 1, page 199.

Table 5.1 Cell viability assay of mouse skeletal C2C12 cells with elemental Cadmium. Fluoroscan readings with graded concentration of elemental Cadmium

Medium only	**0.01 µg/ml**	**0.05 µg/ml**	**0.1 µg/ml**	**0.5 µg/ml**	**1 µg/ml**	**5 µg/ml**	**1.0 µg/ml**	**50 µg/ml**	**100 µg/ml**
98.28	119.40	121.30	114.80	127.00	115.20	64.76	17.29	13.57	13.45
86.04	126.40	99.17	115.20	107.40	99.13	64.61	18.70	14.27	14.28
134.70	114.40	99.92	99.03	93.31	98.86	67.61	20.16	15.79	14.28
Mean 106.35	120.09	106.79	109.70	109.22	104.41	65.66	18.72	14.54	14.00

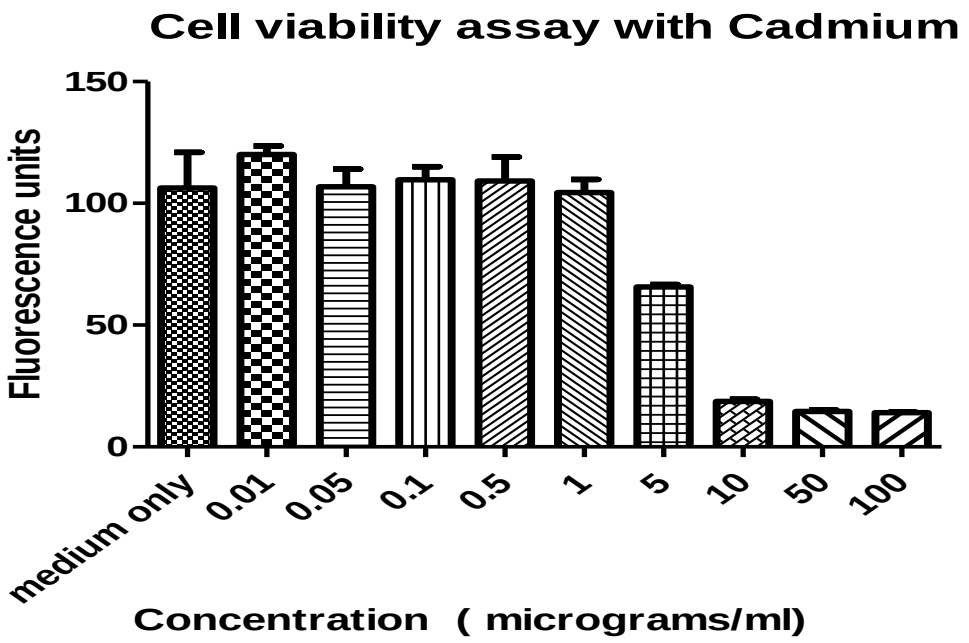

Fig. 5.1 Percentage of mouse skeletal C2C12 cell survival using graded concentration of Cadmium at fluoroscan analysis.

Cell death assay with cadmium

Graded concentration of elemental Cadmium ranging from 0.01µg/ml to 100µg/ml prepared by serial dilution in Dulbecco's Modified Eagle Medium (DMEM) was used to assertain the cell death studies to mouse skeletal C2C12 cells. Only medium was used in the first column as a control. Cells were incubated for a period of 24 hours, Fluoroscan analysis after incubation with Yo Pro-1 Iodide (491/509)-Invitrogen reagent for 4 hours revealed no obvious toxicity to these cells from 0.01 µg/ml to the concentration of 5 µg/ml. At concentration of 10 µg/ml, obvious toxicity was evident. Further increasing the concenration 100 µg/ml revealed persistently significant toxicity as shown in table 5.2 and fig.5.2. Statistical analysis using one way ANOVA and Dunnett's multiple comparison test revealed statistically significant difference in the cytotoxicity at the concentration of of 10µg/ml as revealed in Appendix,table 2 Page 200.

Table 5.2. Cell death assay of mouse skeletal C2C12 cells with elemental Cadmium. Fluoroscan readings at graded concentration of elemental Cadmium

Medium only	0.01 µg/ml	0.05 µg/ml	0.1 µg/ml	0.5 µg/ml	1 µg/ml	5 µg/ml	10 µg/ml	50 µg/ml	100 µg/ml
1.359	1.350	1.306	1.440	1.328	1.622	1.953	2.602	2.574	2.956
1.367	1.436	1.279	1.473	1.423	0.765	2.088	3.364	2.608	2.976
1.581	1.563	1.461	1.529	1.615	0.779	2.369	3.932	3.669	2.724
Mean 1.435	1.450	1.349	1.481	1.455	1.055	2.137	3.299	2.950	2.885

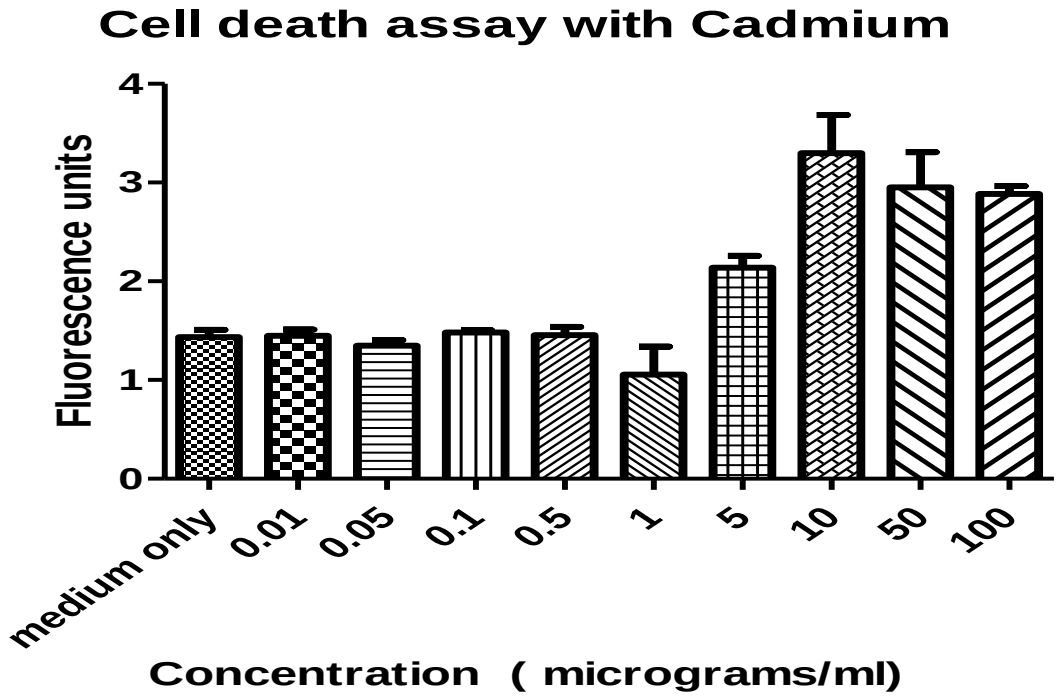

Fig.5.2 Percentage of mouse skeletal C2C12 cell death using graded concentration of Cadmium at fluoroscan analysis.

The above studies using two reagents (one to study the cell viability and the other to study cell death) revealed similar results. Both studies confirmed that elemental

Cadmium was safe to mouse skeletal C2C12 cells only below the concentration of 5 µg/ml. Any further increase in the concentration proved toxic to these cells.

5.3.2 CYTOTOXICITY OF ELEMENTAL TELLURIUM

Cell viability assay with Tellurium

Graded concentration of elemental Tellurium ranging from 0.01µg/ml to 100µg/ml prepared by serial dilution in Dulbecco's Modified Eagle Medium (DMEM) was used to assertain the cell viablility studies to mouse skeletal C2C12 cells using Cell Titer-Blue reagent as an indicator of cell survival. Only medium was used in the first column as a control. Cells were incubated with graded concentration of tellurium for a period of 24 hours. Fluoroscan analysis after incubation with Cell Titer-Blue reagent for 4 hours followed by sstatistical analysis using one way ANOVA and Dunnett's multiple comparison tests revealed statistically significant difference in the cytotoxicity at the concentration of 0.1 µg/ml as shown in Appendix table 3 page 201.This is demonstrated in table 5.3 and fig.5.3.

Table 5.3 Cell viability assay of mouse skeletal C2C12 cells with elemental Tellurium –fluoroscan readings with graded concentration of elemental Tellurium

Medium only	**0.01 µg/ml**	**0.05 µg/ml**	**0.1 µg/ml**	**0.5 µg/ml**	**1 µg/ml**	**5 µg/ml**	**10 µg/ml**	**50 µg/ml**	**100 µg/ml**
120.60	134.30	117.10	115.60	104.30	104.40	94.99	99.01	14.62	18.08
139.80	134.70	130.80	121.00	112.40	110.80	104.50	96.56	15.60	18.79
145.00	126.00	129.50	115.80	107.70	116.20	98.34	99.16	16.04	20.73
Mean 135.12	131.68	125.80	117.47	108.10	110.46	99.27	98.24	15.42	19.20

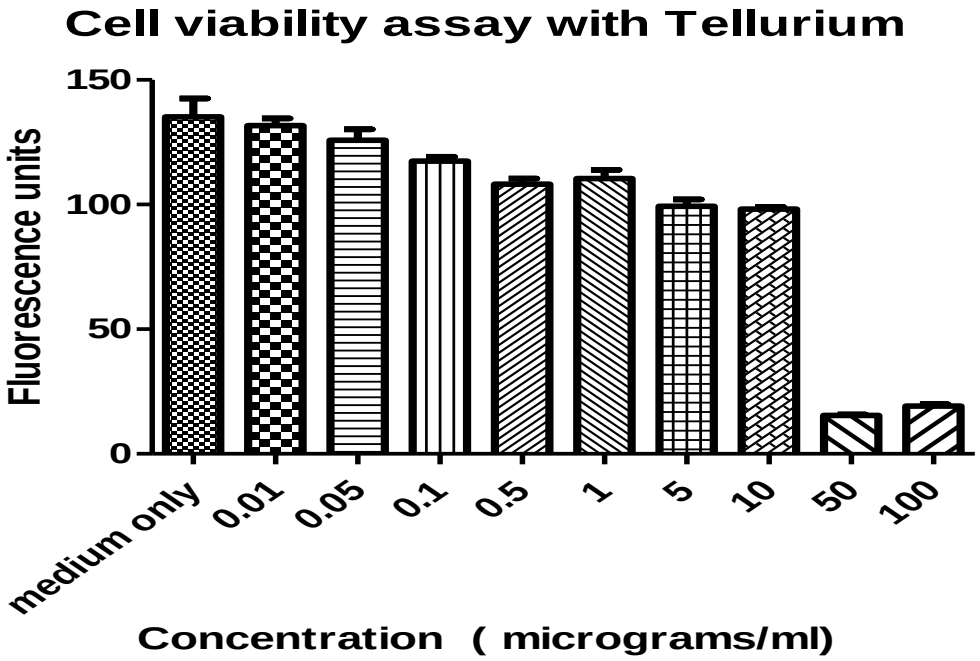

Fig. 5.3. Percentage of mouse skeletal C2C12 cell survival using graded concentration of Tellurium at fluoroscan analysis.

Cell Death assay with Tellurium

Graded concentration of elemental Tellurium ranging from 0.01µg/ml to 100µg/ml was used to assertain the cell viablility studies to mouse skeletal C2C12 cells using Yo Pro-1 Iodide (491/509)-Invitrogen reagent as an indicator of cell survival. Only medium was used as a control. Fluoroscan analysis confirmed that elemental Tellurium was toxic at the concentration of 50µg/ml as demonstrated in table 5.4 and fig 5.4. This was confirmed by Statistical analysis using one way ANOVA and Dunnett's multiple comparison tests which revealed statistically significant difference in the cytotoxicity at the concentration of 50µg/ml as shown in Appendix, table 4, page 202.

Table 5.4 Cell death assay of mouse skeletal C2C12 cells with elemental tellurium. Fluoroscan readings at graded concentration of elemental Tellurium

Medium only	0.01 µg/ml	0.05 µg/ml	0.1 µg/ml	0.5 µg/ml	1 µg/ml	5 µg/ml	10 µg/ml	50 µg/ml	100 µg/ml
1.352	1.445	1.497	1.497	1.506	1.589	1.569	1.644	2.881	3.227
1.449	1.526	1.472	1.409	1.541	1.605	1.545	1.631	3.234	3.544
1.636	1.522	1.621	1.624	1.652	1.683	1.841	1.739	2.957	3.927
Mean 1.479	1.497	1.530	1.510	1.566	1.626	1.652	1.671	3.024	3.566

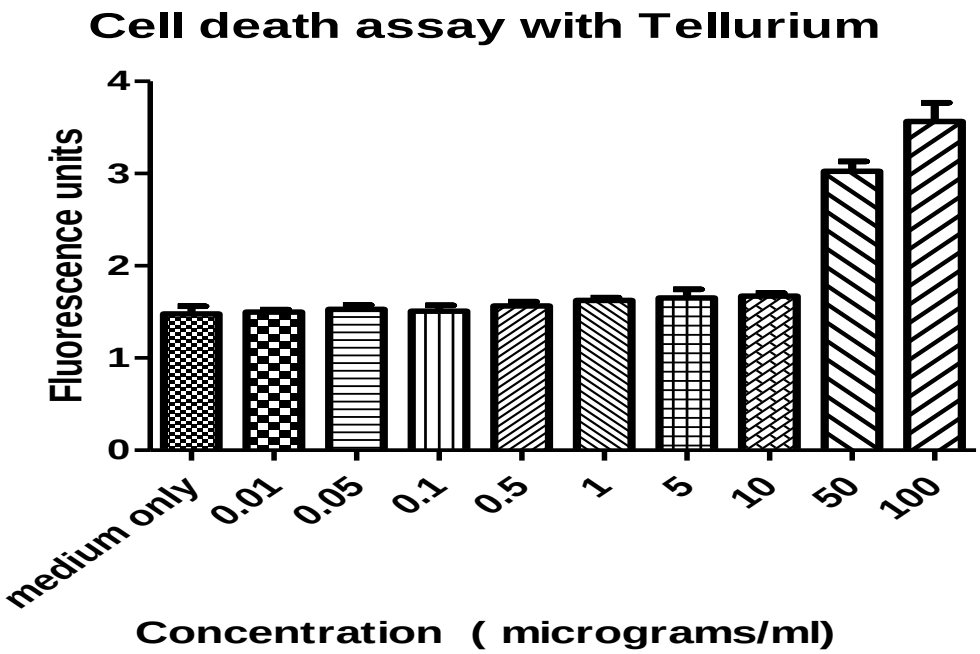

Fig. 5.4. Percentage of mouse skeletal C2C12 cell death using graded concentration of tellurium at fluoroscan analysis.

Following this analysis, it was demonstrated that both elemental Cadmium and Tellurium were toxic to mouse skeletal C2C12 cell lines using both cell survival and

cell death assay at fluoroscan analysis. This study was a baseline analysis to compare cytotoxicity of both unconjugated and conjugated CdTe Qds to the C2C12 cells.

5.3.3 Cytotoxicity of CdTe QDs

Cell Viability Assay with CdTe QDs – Sample 1.

Graded concentration of unconjugated CdTe QDs ranging from 0.01µg/ml to 50µg/ml as described above was used to assertain the cell viablility of QDs to C2C12 mouse skeletal muscle cells using Cell Titer-Blue reagent as an indicator of cell survival. Only Dulbecco's Modified Eagle Medium (DMEM) was used as a control and elemental Cadmium was used at a concentration of 50µg /ml to compare the toxicity of QDs with Cadmium. Cells were incubated with graded concentration of CdTe QDs for a period of 24 hours. Fluoroscan analysis after incubation with Cell Titer-Blue reagent for 4 hours confirmed obviously significant toxicity of nonconjugated CdTe QDs at 50µg /ml. However, CdTe Qds were nontoxic below the concentration of 50µg /ml as shown in table 5.5 and fig 5.5. Statistical analysis using one way ANOVA and Dunnett's multiple comparison tests revealed statistically significant difference in the cytotoxicity at the concentration of 50µg/ml as shown in Appendix, table 5 page 203.

Cell Viability Assay with CdTe QDs – Sample 1.

Table 5.5 Cell viability assay of mouse skeletal C2C12 cells with nonconjugated CdTe QDs. fluoroscan readings with graded concentration of nonconjugated CdTe QDs

Medium only	QD0.01 µg/ml	QD0.05 µg/ml	QD0.1 µg/ml	QD0.5 µg/ml	QD1 µg/ml	QD5 µg/ml	QD10 µg/ml	QD50 µg/ml	Cadmium 50 µg/ml
78.84	89.11	85.63	92.88	88.20	84.56	78.04	69.82	39.46	11.25
79.49	85.18	82.31	81.50	82.53	89.90	87.35	78.41	49.41	12.60
82.82	83.08	88.71	81.88	85.56	84.32	87.31	75.83	48.56	11.65
Mean 80.38	85.79	85.55	85.42	85.43	86.26	84.23	74.69	45.81	11.83

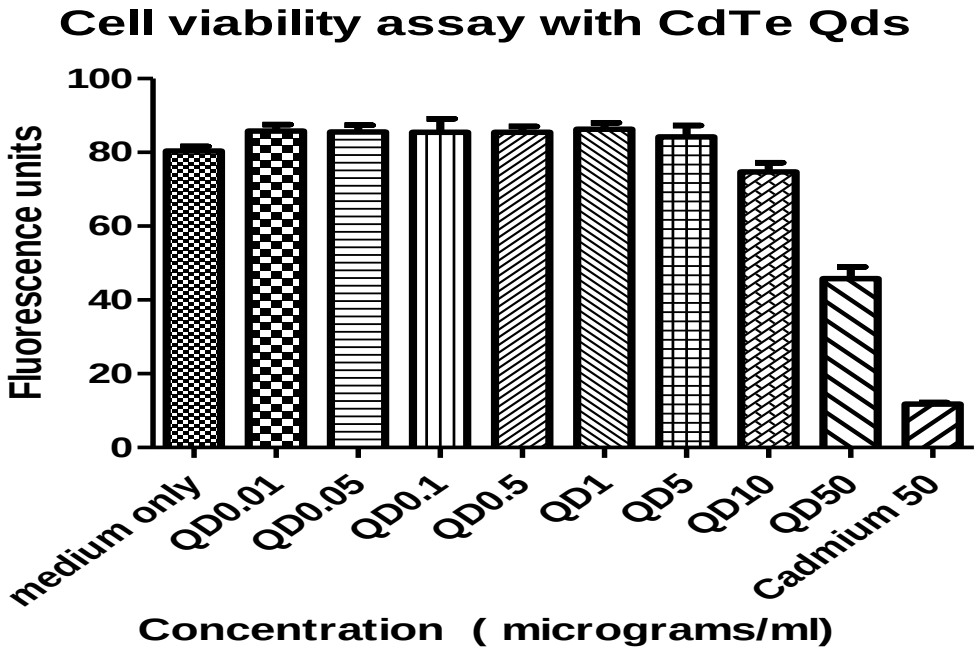

Fig. 5.5. Percentage of mouse skeletal C2C12 cell survival using graded concentration of nonconjugated QDs at fluoroscan analysis.

Cell Viability Assay with CdTe QDs – Sample 2

The experiment was repeated on a completely different batch of cells separately grown from their precursors. Exactly similar number of cells were harvested and used for this experiment. The graded concentrations as described previously for sample 1 were used and the toxicity analysis performed in comparison with toxicity of elemental Cadmium at the concentration of 50µg /ml. The results are revealed in table 5.6 and fig. 5.6. Statistical analysis using one way ANOVA and Dunnett's multiple comparison tests revealed statistically significant difference in the cytotoxicity at the concentration of 0.1 µg/ml as shown in table 6 on page 204. However it was observed that the toxicity pattern was not uniform.

Table 5.6 Cell viability assay of mouse skeletal C2C12 cells with nonconjugated CdTe QDs. Fluoroscan readings with graded concentration of nonconjugated CdTe QDs.

Medium only	**QD0.01 µg/ml**	**QD0.05 µg/ml**	**QD0.1 µg/ml**	**QD0.5 µg/ml**	**QD1 µg/ml**	**QD5 µg/ml**	**QD10 µg/ml**	**QD50 µg/ml**	**Cadmium 50 µg/ml**
67.54	76.07	80.18	91.19	90.35	104.4	88.71	69.96	42.39	11.94
75.80	86.07	83.26	90.56	65.03	94.02	84.73	72.58	37.63	11.78
82.29	78.41	81.48	86.68	88.00	93.13	89.54	80.56	36.29	11.18
Mean 75.21	80.18	81.64	89.48	81.13	97.18	87.66	74.37	38.77	11.64

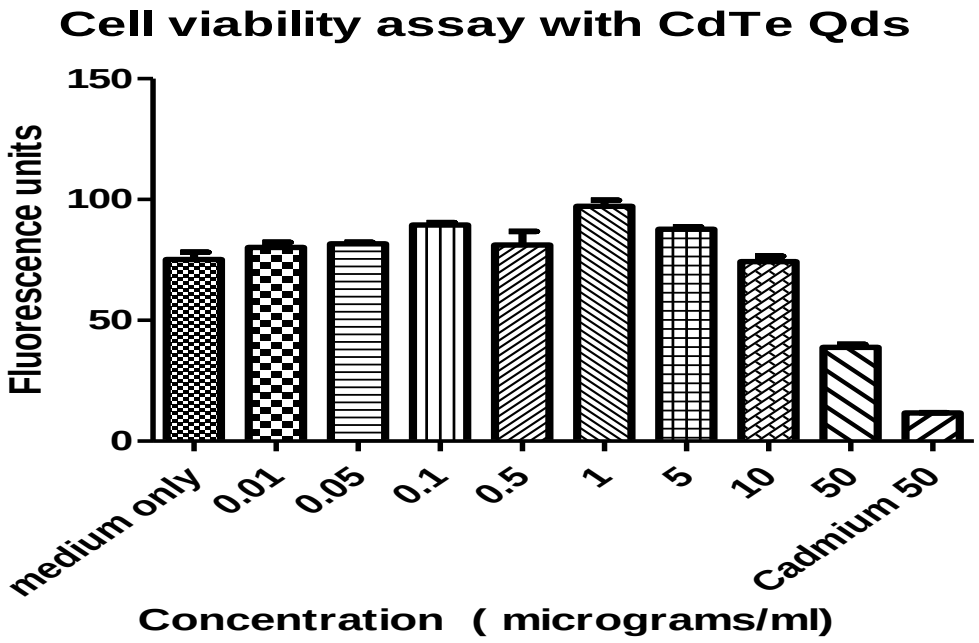

Fig.5.6.Percentage of mouse skeletal C2C12 cell survival using graded concentration of nonconjugated QDs. compared with Cadmium alone at 50 µg/ml at fluoroscan analysis.

Cell Death Assay with CdTe QDs – Sample 1.

Cell death analysis using Yo Pro-1 Iodide (491/509)-Invitrogen reagent confirmed similar findings to cell viability assay. The quantum dots were nontoxic even at the concentration of 50 µg/ml to mouse skeletal C2C12 cells. Cadmium toxicity was obviously noted at similar concentration as shown in table 5.7 and Fig. 5.7. Statistical analysis using one way ANOVA and Dunnett's multiple comparison test revealed no statistically significant difference in the cytotoxicity even at the maximum concentration of 50 µg/ml as shown in Appendix table 7, page 205.

Table 5.7. Cell death assay of mouse skeletal C2C12 cells with nonconjugated QDs. compared with Cadmium alone at 50 µg/ml at fluoroscan analysis.

Medium only	QD0.01 µg/ml	QD0.05 µg/ml	QD0.1 µg/ml	QD0.5 µg/ml	QD1 µg/ml	QD5 µg/ml	QD10 µg/ml	QD50 µg/ml	Cadmium 50 µg/ml
1.417	1.477	1.356	1.487	1.670	1.410	1.116	1.743	1.795	3.567
1.342	1.472	1.377	1.463	1.415	1.439	1.389	1.705	1.727	3.787
1.540	1.339	1.475	1.482	1.461	2.045	1.960	2.057	2.317	3.937
Mean 1.433	1.429	1.402	1.477	1.515	1.631	1.488	1.834	1.946	3.763

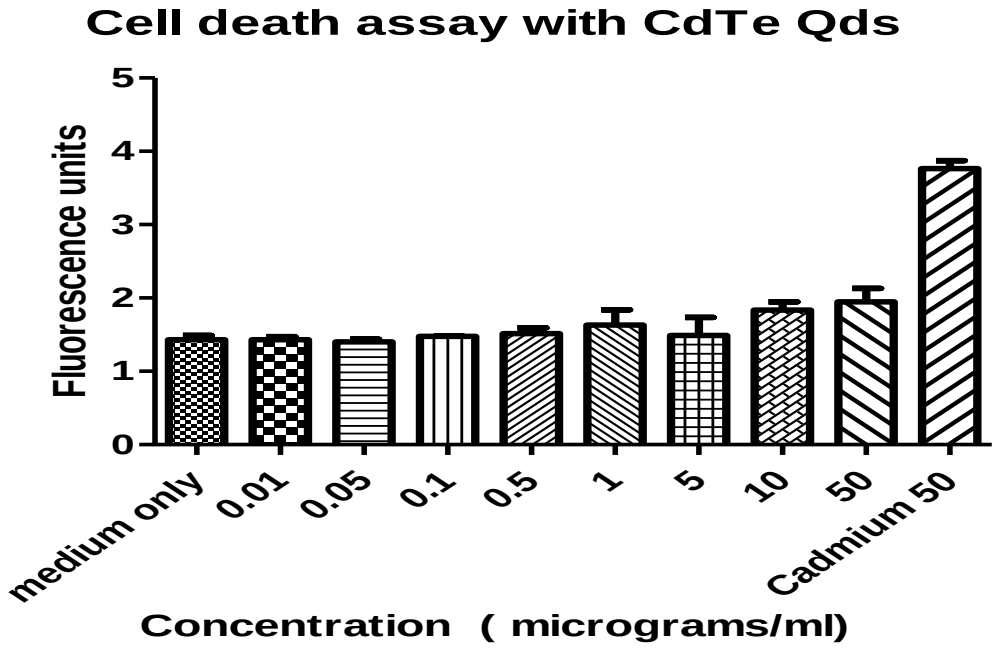

Fig. 5.7. Percentage of mouse skeletal C2C12 cell death using graded concentration of nonconjugated CdTe QDs at fluoroscan analysis.

Cell death assay with CdTe QDs – Sample 2.

Cell death assay using second sample at the same concentration gradient revealed following results. For statistical analysis, only medium was used for comparison. Cadmium at the concentration of 50 µg/ml with an obvious toxicity was used at the other extreme. No obvious toxicity was observed below the concentration of 50 µg/ml as shown in table 5.8 and fig. 5.8. Statistical analysis using one way ANOVA and Dunnett's multiple comparison tests revealed no statistically significant difference in the cytotoxicity at the maximum concentration of 50 µg/ml as shown in Appendix, table 8 page 206.

Table 5.8. Cell death assay of mouse skeletal C2C12 cells with nonconjugated QDs. compared with Cadmium alone at 50 µg/ml . Fluoroscan readings at graded concentration of nonconjugated QDs.

Medium only	**QD0.01 *µg/ml***	**QD0.05 *µg/ml***	**QD0.1 *µg/ml***	**QD0.5 *µg/ml***	**QD1 *µg/ml***	**QD5 *µg/ml***	**QD10 *µg/ml***	**QD50 *µg/ml***	**Cadmium 50 *µg/ml***
1.320	1.407	1.316	1.426	1.339	1.657	1.582	1.744	1.605	2.876
1.306	1.420	1.258	1.384	1.301	1.439	1.337	1.502	1.718	3.118
1.411	1.385	1.687	1.419	1.439	1.658	1.358	1.559	1.594	2.936
Mean 1.346	1.404	1.420	1.409	1.360	1.585	1.425	1.601	1.639	2.977

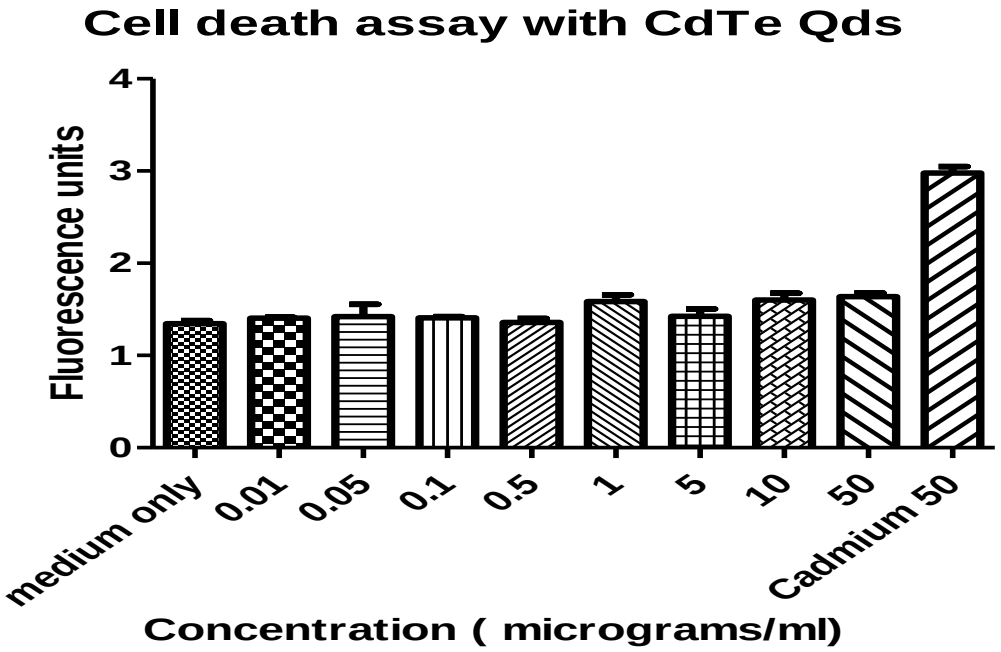

Fig.5.8. Percentage of mouse skeletal C2C12 cell death using graded concentration of nonconjugated CdTe compared with Cadmium alone at 50 µg/ml at fluoroscan analysis

5.3.4 Cytotoxicity of conjugated CdTe QDs

Cell Viability Assay with RGD (Lysine) bound CdTe QDs- Sample1

After establishing the relatively nontoxic nature of CdTe QDs to the mouse skeletal C2C12 cells, the experiment was focused on RGD bound quantum dots as these were the basis of *in vitro* and *in vivo* studies involving colon cancer cells. In order to prove nontoxic nature of RGD (Lysine) bound CdTe complexes, the same experiment was repeated using graded concentration of these complexes and toxicity assay performed using Cell Titer- Blue reagent. This study was able to prove that CdTe –RGD(Lysine) compound was nontoxic at the concentration of 5 µg/ml as compared to elemental Cadmium at the concentration of 50 µg/ml. CdTe-RGD (Lysine)compound was nontoxic to C2C12 cells from the concentration of 0.01µg/ml

to 5 µg/ml. Table 5.9 and fig. 5.9 confirm the above mentioned observations. Statistical analysis using one way ANOVA and Dunnett's multiple comparison tests revealed statistically significant difference in the cytotoxicity at the concentration of 5 µg/ml as shown in Appendix, table 9, page 207.

Table 5.9. Cell viability assay of mouse skeletal C2C12 cells with conjugated CdTe QDs.. Fluoroscan readings with graded concentration of CdTe QDs conjugated to RGD (Lysine).

Medium only	**QD0.01 *µg/ml***	**QD0.05 *µg/ml***	**QD0.1 *µg/ml***	**QD0.5 *µg/ml***	**QD1 *µg/ml***	**QD5 *µg/ml***	**QD10 *µg/ml***	**QD50 *µg/ml***	**Cadmium 50 *µg/ml***
72.10	72.59	81.20	83.24	78.03	91.15	78.15	96.45	112.10	13.84
73.18	88.19	86.78	88.19	87.80	86.02	87.63	105.40	104.80	12.95
73.07	74.65	86.64	84.44	85.67	87.24	105.60	92.27	95.47	12.96
Mean 72.78	78.48	84.87	85.29	83.83	88.13	90.47	98.05	104.13	13.25

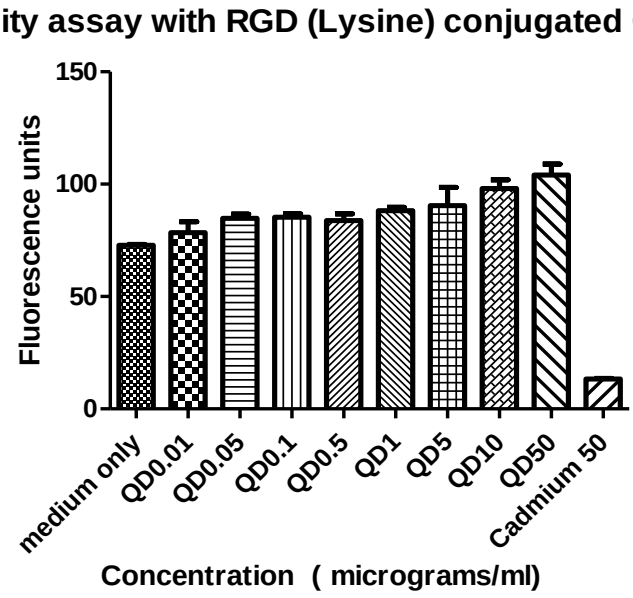

Fig 5.9 Percentage of mouse skeletal C2C12 cell survival using graded concentration of RGD (Lysine) conjugated QDs. compared with Cadmium alone at 50 µg/ml at fluoroscan analysis..

Cell Viability Assay with RGD (Lysine) bound CdTe QDs- Sample 2

The experiment was repeated using second batch of cells with graded concentration of RGD (Lysine) bound CdTe QDs and toxicity assay was performed using Cell Titer- Blue reagent. The pattern of cell viability assay has been shown in table 5.10 and fig. 5.10. Statistical analysis using one way ANOVA and Dunnett's multiple comparison tests revealed no statistically significant difference in the cytotoxicity even at the maximum concentration of 50 µg/ml as shown in Appendix, table 10, page 208.

Table 5.10. Cell viability assay of mouse skeletal C2C12 cells with (Lysine) conjugated CdTe QDs.. Fluoroscan readings with graded concentration of CdTe QDs conjugated to RGD (Lysine).

Medium only	**QD0.01 µg/ml**	**QD0.05 µg/ml**	**QD0.1 µg/ml**	**QD0.5 µg/ml**	**QD1 µg/ml**	**QD5 µg/ml**	**QD10 µg/ml**	**QD50 µg/ml**	**Cadmium 50 µg/ml**
89.18	85.04	77.52	86.70	89.09	87.10	100.4	99.15	101.1	12.94
95.31	99.66	92.47	93.13	55.52	89.30	86.72	101.1	98.49	13.87
96.36	86.53	83.67	84.09	85.94	90.11	90.31	92.48	102.1	13.12
Mean 93.62	90.41	84.55	87.97	76.85	88.84	92.47	97.56	100.58	13.31

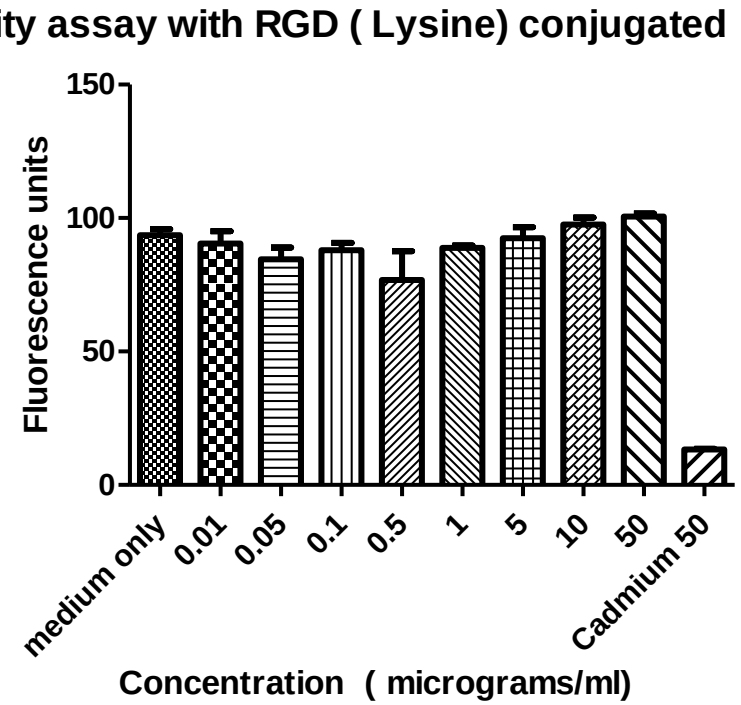

Fig 5.10. Percentage of mouse skeletal C2C12 cell survival using graded concentration of RGD (Lysine) conjugated QDs compared with Cadmium alone at 50 µg/ml at fluoroscan analysis.

Cell Death Assay with RGD (Lysine) bound CdTe QDs-Sample 1

Comparative results were obtained using cell death analysis with Yo Pro-1 Iodide (491/509)-Invitrogen reagent to substantiate nontoxic nature of CdTe QD + RGD (Lysine).The toxicity of elemental Cadmium was stationary at the reference range as demonstrated in table 5.11 and fig. 5.11. Statistical analysis using one way ANOVA and Dunnett's multiple comparison tests revealed no statistically significant difference in the cytotoxicity even at the maximum concentration of 50 µg/ml as shown in Appendix, table 11, page 209.

Table 5.11 Cell death assay of mouse skeletal C2C12 cells with RGD (Lysine) conjugated QDs. compared with Cadmium alone at 50 µg/ml. Fluoroscan readings at graded concentration of RGD (Lysine) conjugated QDs.

Medium only	**QD0.01 µg/ml**	**QD0.05 µg/ml**	**QD0.1 µg/ml**	**QD0.5 µg/ml**	**QD1 µg/ml**	**QD5 µg/ml**	**QD10 µg/ml**	**QD50 µg/ml**	**Cadmium 50 µg/ml**
1.204	1.347	1.162	1.373	1.108	1.351	1.222	1.341	1.310	2.889
1.204	1.335	1.150	1.343	1.323	1.343	1.271	1.590	1.250	3.018
1.327	1.331	1.321	1.325	1.247	1.092	1.306	1.280	1.284	3.041
Mean 1.245	1.338	1.211	1.347	1.226	1.262	1.266	1.404	1.281	2.983

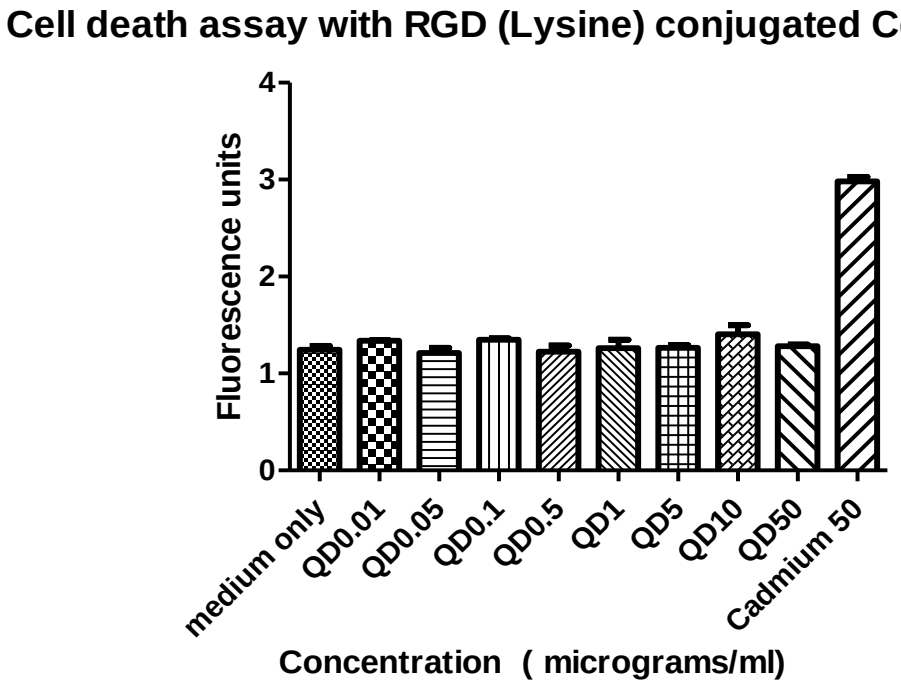

Fig 5.11. Percentage of mouse skeletal C2C12 cell death using graded concentration of RGD (Lysine) conjugated CdTe QDs. Fluoroscan analysis of CdTe QD compared with Cadmium alone at 50 µg/ml.

Cell Death Assay with RGD (Lysine) bound CdTe QDs- Sample 2

In this study, second batch of cells were used with similar number of C2 C12 cells at graded concentration. Cell death assay was analyzed using Yo Pro-1 Iodide (491/509)-Invitrogen reagent. The comparison was made to control cells not exposed to QDs. Elemental Cadmium was used at a concentration of 50 µg/ml for comparison being aware of its cytotoxic nature. The results are shown in table 5.12 and fig. 5.12.

Statistical analysis using one way ANOVA and Dunnett's multiple comparison tests revealed no statistically significant difference in the cytotoxicity even at the maximum concentration of 50 µg/ml as shown in Appendix, table 12, page 210.

Table 5.12 Cell death assay of mouse skeletal C2C12 cells with RGD (Lysine) conjugated QDs. compared with Cadmium alone at 50 µg/ml at fluoroscan analysis. Fluoroscan readings at graded concentration of RGD (Lysine) conjugated QDs.

Medium only	**QD0.01 *µg/ml***	**QD0.05 *µg/ml***	**QD0.1 *µg/ml***	**QD0.5 *µg/ml***	**QD1 *µg/ml***	**QD5 *µg/ml***	**QD10 *µg/ml***	**QD50 *µg/ml***	**Cadmium 50 *µg/ml***
1.204	1.347	1.162	1.373	1.108	1.351	1.222	1.341	1.310	2.889
1.204	1.335	1.150	1.343	1.323	1.343	1.271	1.590	1.250	3.018
1.327	1.331	1.321	1.325	1.247	1.092	1.306	1.280	1.284	3.041
Mean 1.245	1.338	1.211	1.347	1.226	1.262	1.266	1.404	1.281	2.983

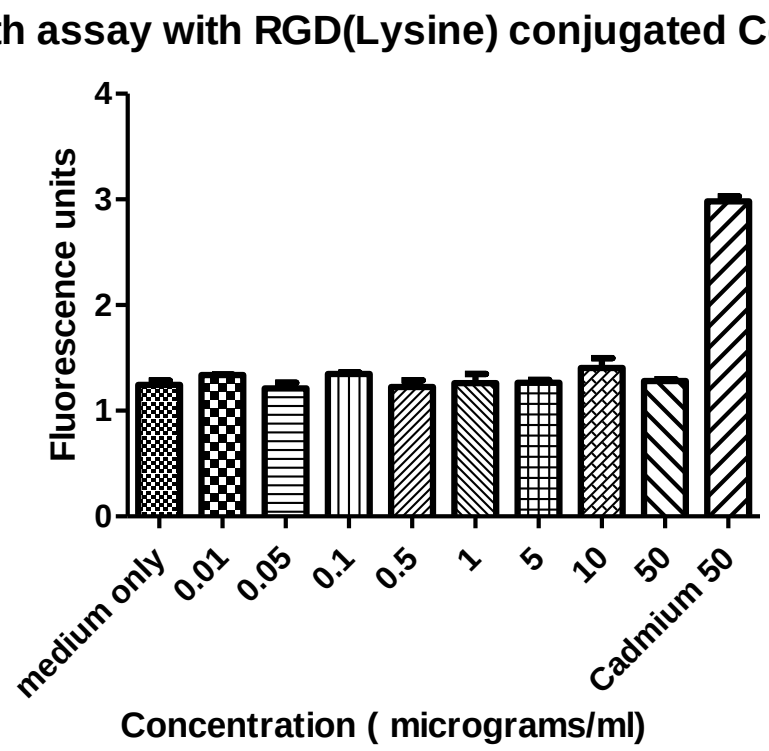

Fig 5.12. Percentage of mouse skeletal C2C12 cell death using graded concentration of RGD (Lysine) conjugated CdTe QDs. Fluoroscan analysis using graded concentration of CdTe QD compared with Cadmium alone at 50 µg/ml.

.

Cell Viability Assay with RGD (Cysteine) bound CdTe QDs-Sample 1

Graded concentration of RGD (Cysteine) conjugated to CdTe quantum dots from 0.01µg/ml to 50µg/ml prepared by serial dilution in the Dulbecco's Modified Eagle Medium (DMEM) was used to assertain the cell viablility studies to mouse skeletal C2C12 cell lines. Only medium was used in the first column as a control. Elemental Cadmium at a concentration of 50 µg/ml was used in the last column to compare the toxicity. Fluoroscan analysis after incubation with Cell Titre Blue reagent revealed no obvious toxicity to these cells from 0.01 µg/ml to the concentration of 5 µg/ml as shown in table 5.13 and fig. 5.13.

Statistical analysis using one way ANOVA and Dunnett's multiple comparison tests revealed statistically significant difference in the cytotoxicity at the concentration of 5 µg/ml as shown in Appendix, table 13, page 211.

Table 5.13. Cell viability assay of mouse skeletal C2C12 cells with RGD (Cysteine) conjugated CdTe QDs. Fluoroscan readings with graded concentration of CdTe QDs.conjugated to RGD (Cysteine).

Medium only	**QD0.01 *µg/ml***	**QD0.05 *µg/ml***	**QD0.1 *µg/ml***	**QD0.5 *µg/ml***	**QD1 *µg/ml***	**QD5 *µg/ml***	**QD10 *µg/ml***	**QD50 *µg/ml***	**Cadmium 50 *µg/ml***
88.06	89.34	91.39	99.14	93.93	92.05	96.87	98.42	117.20	14.59
89.76	89.07	88.36	94.42	90.52	96.30	107.30	109.0	114.1	13.02
87.29	91.88	87.01	88.47	88.88	91.68	101.50	96.00	99.18	12.95
Mean 88.37	90.10	88.92	94.01	91.11	93.35	101.87	101.15	110.14	13.52

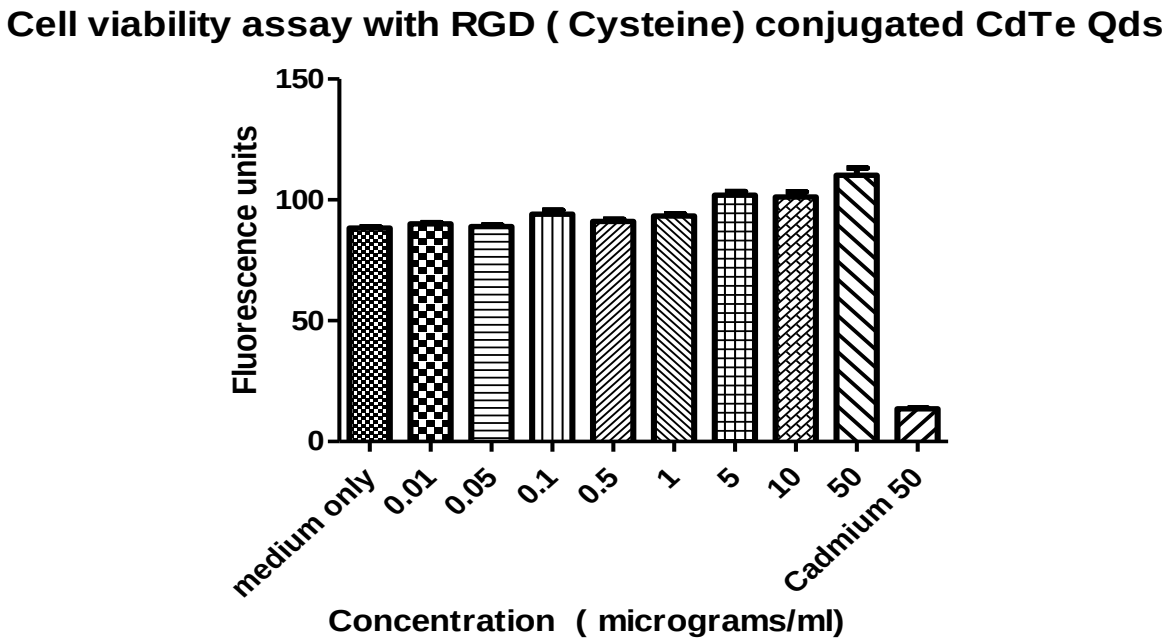

Fig.5.13. Percentage of mouse skeletal C2C12 cell survival using graded concentration of RGD (Cysteine) conjugated QDs. compared with Cadmium at 50 µg/ml at fluoroscan analysis

Cell Viability Assay with RGD (Cysteine) bound CdTe QDs-Sample 2

Graded concentration of RGD (Cysteine) conjugated to CdTe quantum dots from 0.01µg/ml to 50µg/ml prepared by serial dilution in the Dulbecco's Modified Eagle Medium (DMEM) was used to assertain the cell viablility studies to mouse skeletal C2C12 second batch of cells. Only medium was used in the first column as a control. Elemental Cadmium at a concentration of 50 µg/ml was used in the last column to compare the toxicity. No obvious toxicity was noted at the maximum concentration of 50 µg/ml using Cell Titer- Blue reagent as shown in table 5.14 and fig. 5.14. Statistical analysis using one way ANOVA and Dunnett's multiple comparison tests revealed no statistically significant difference in the cytotoxicity even at the maximum concentration of 50 µg/ml as shown in Appendix, table 14,page 212.

Table 5.14. Cell viability assay of mouse skeletal C2C12 cells with (Cysteine) conjugated CdTe QDs. Fluoroscan readings with graded concentration of CdTe QDs. conjugated to RGD (Cysteine).

Medium only	**QD0.01 *µg/ml***	**QD0.05 *µg/ml***	**QD0.1 *µg/ml***	**QD0.5 *µg/ml***	**QD1 *µg/ml***	**QD5 *µg/ml***	**QD10 *µg/ml***	**QD50 *µg/ml***	**Cadmium 50 *µg/ml***
79.79	77.26	75.05	97.60	86.44	93.60	95.49	103.0	80.39	14.42
77.03	83.22	94.04	95.99	98.61	96.93	90.86	108.7	104.7	13.67
88.88	86.13	107.8	80.45	107.0	87.22	70.44	89.94	110.0	12.85
Mean 81.90	82.20	92.30	91.35	97.33	92.58	85.60	100.54	98.34	13.64

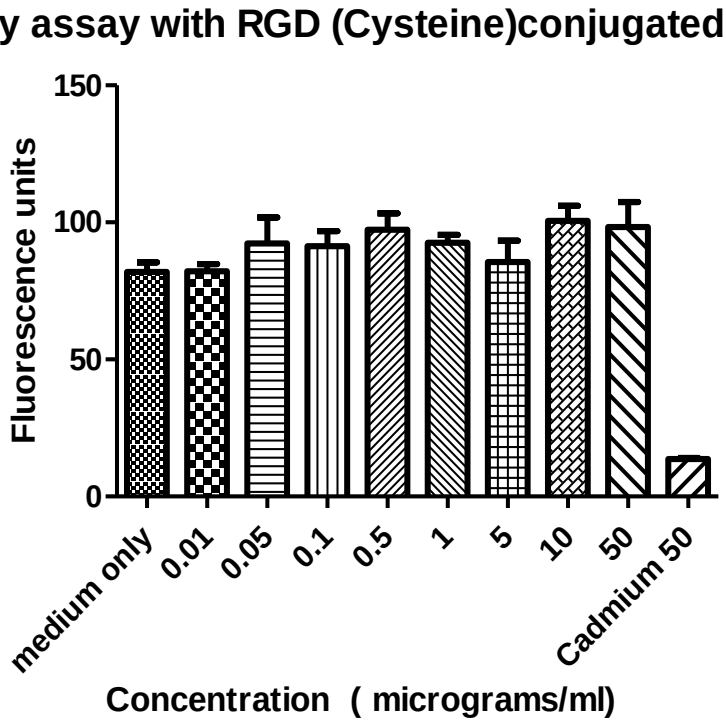

Fig 5.14. Percentage of mouse skeletal C2C12 cell survival using graded concentration of RGD (Cysteine) conjugated QDs compared with Cadmium alone at 50 µg/ml at fluoroscan analysis.

Cell Death Assay with RGD (Cysteine) bound CdTe QDs- Sample 1

In this study, graded concentration of RGD (Cysteine) conjugated CdTe QDs was used to assess cytotoxicity to C2C12 cells. Cell death assay was analyzed using Yo Pro-1 Iodide (491/509)-Invitrogen reagent. The comparison was made with cells immersed in the DMEM (Dulbecco's Modified Eagle Medium). Elemental Cadmium was used at a concentration of 50 µg/ml for comparison being aware of its cytotoxic nature. The result of cell death assay revealed nontoxic nature of this complex at a concentration of 50 µg/ml. The elemental Cadmium continued to prove its toxicity at similar concentration as shown in table 5.15 and fig. 5.15.

Statistical analysis using one way ANOVA and Dunnett's multiple comparison tests revealed no statistically significant difference in the cytotoxicity even at the maximum concentration of 50 µg/ml as shown in Appendix, table 15, page 213.

Table 5.15. Cell death assay of mouse skeletal C2C12 cells with RGD (Cysteine) conjugated QDs compared with Cadmium alone at 50 µg/ml at fluoroscan analysis. Fluoroscan readings at graded concentration of RGD (Cysteine) conjugated QDs.

Medium only	**QD0.01 *µg/ml***	**QD0.05 *µg/ml***	**QD0.1 *µg/ml***	**QD0.5 *µg/ml***	**QD1 *µg/ml***	**QD5 *µg/ml***	**QD10 *µg/ml***	**QD50 *µg/ml***	**Cadmium 50 *µg/ml***
1.225	1.334	1.131	1.295	1.135	1.338	1.159	1.329	1.382	2.982
1.268	1.331	1.241	1.349	1.229	1.397	1.251	1.401	1.329	3.067
1.365	1.350	1.323	1.349	1.339	1.401	1.365	1.454	1.477	3.510
Mean 1.286	1.338	1.232	1.331	1.235	1.379	1.258	1.395	1.396	3.186

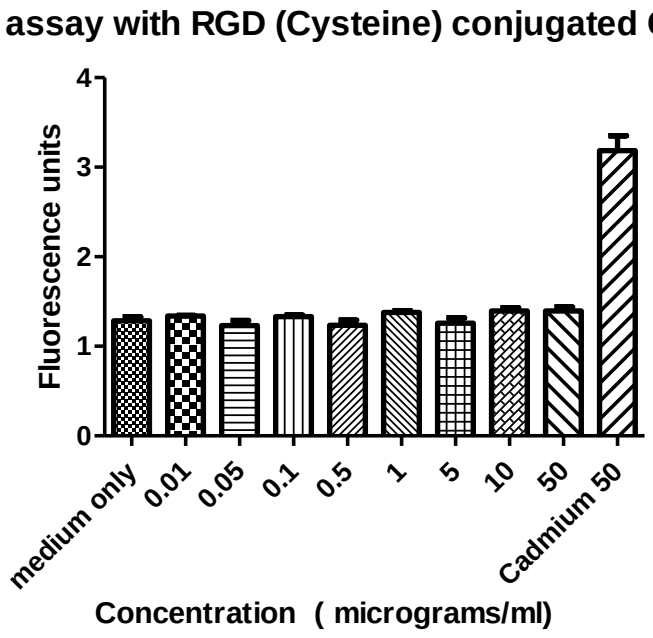

Fig. 5.15. Percentage of mouse skeletal C2C12 cell death using graded concentration of RGD (Cysteine) conjugated CdTe QDs. Fluoroscan analysis using graded concentration of CdTe QD compared with Cadmium alone at 50 µg/ml.

.

Cell Death Assay with RGD (Cysteine) bound CdTe QDs- Sample 2

In this study, graded concentration of RGD (Cysteine) conjugated CdTe QDs was used to assess cytotoxicity to the second sample of mouse C2C12 cells. Cell death assay was analyzed using Yo Pro-1 Iodide (491/509)-Invitrogen reagent. The comparison was made with cells immersed in the DMEM (Dulbecco's Modified Eagle Medium). Elemental Cadmium was used at a concentration of 50 µg/ml for comparison being aware of its cytotoxic nature. The result of cell death assay revealed no obvious cytotoxicity at a concentration of 50 µg/ml. The elemental Cadmium continued to prove its toxicity at similar concentration. The results are shown in table 5.16 and fig. 5.16.

Statistical analysis using one way ANOVA and Dunnett's multiple comparison tests revealed no statistically significant difference in the cytotoxicity even at the maximum concentration of 50 µg/ml as shown in Appendix, table 16, page 214.

Table 5.16. Cell death assay of mouse skeletal C2C12 cells with RGD (Cysteine) conjugated QDs. compared with Cadmium alone at 50 µg/ml at fluoroscan analysis. Fluoroscan readings at graded concentration of RGD (Cysteine) conjugated QDs.

Medium only	**QD0.01 *µg/ml***	**QD0.05 *µg/ml***	**QD0.1 *µg/ml***	**QD0.5 *µg/ml***	**QD1 *µg/ml***	**QD5 *µg/ml***	**QD10 *µg/ml***	**QD50 *µg/ml***	**Cadmium 50 *µg/ml***
1.235	1.354	1.192	1.348	1.169	1.297	1.270	1.487	1.359	2.809
1.267	1.369	1.089	1.377	1.412	1.327	1.348	1.420	1.411	2.717
1.400	1.324	1.363	0.9504	1.568	1.324	1.362	1.478	1.521	2.965
Mean 1.301	1.349	1.215	1.225	1.383	1.316	1.327	1.461	1.430	2.830

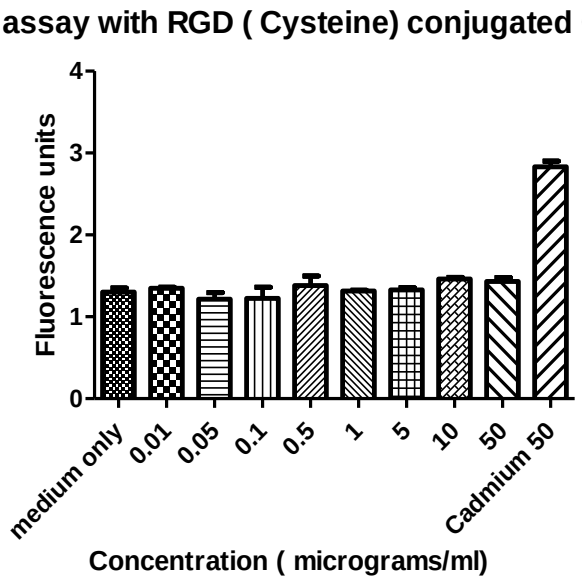

Fig. 5.16. Percentage of mouse skeletal C2C12 cell death using graded concentration of RGD (Cysteine) conjugated CdTe QDs. Fluoroscan analysis using graded concentration of CdTe QD compared with Cadmium alone at 50 µg/ml.

Cell viability assay with negative control c (RADfV) bound CdTe QDs- Sample 1

c (RADfV) was used as a negative control in the experiment. They do not bind to integrins overexpressed by the colon cancer cells. Graded concentration of RAD conjugated to CdTe quantum dots from 0.01µg/ml to 50µg/ml prepared by serial dilution in the Dulbecco's Modified Eagle Medium (DMEM) was used to assertain the cell viablility studies to mouse skeletal C2C12 cells. Only medium was used in the first column as a control. Elemental Cadmium at a concentration of 50 µg/ml was used in the last column to compare the toxicity. Fluoroscan analysis after incubation with Cell Titre Blue reagent revealed no obvious toxicity to these cells from 0.01 µg/ml to the concentration of 0.5 µg/ml as demonstrated in table.5.17 and fig. 5.17.

Statistical analysis using one way ANOVA and Dunnett's multiple comparison tests revealed statistically significant difference in the cytotoxicity at the concentration of 0.5 µg/ml as shown in Appendix, table 17, page 216.

Table 5.17. Cell viability assay of mouse skeletal C2C12 cells with c (RADfV) conjugated CdTe QDs. fluoroscan readings with graded concentration of CdTe QDs. conjugated to negative control c (RADfV)

Medium only	**QD0.01 *µg/ml***	**QD0.05 *µg/ml***	**QD0.1 *µg/ml***	**QD0.5 *µg/ml***	**QD1 *µg/ml***	**QD5 *µg/ml***	**QD10 *µg/ml***	**QD50 *µg/ml***	**Cadmium 50 *µg/ml***
79.39	85.39	86.50	84.66	95.14	103.20	99.08	104.60	105.20	14.40
78.65	80.34	93.76	88.19	97.04	86.26	101.00	106.80	96.04	13.18
79.70	84.56	85.87	84.18	86.35	88.66	95.25	88.60	96.92	12.87
Mean 79.24	83.43	88.71	85.68	92.84	92.70	98.43	99.99	99.37	13.48

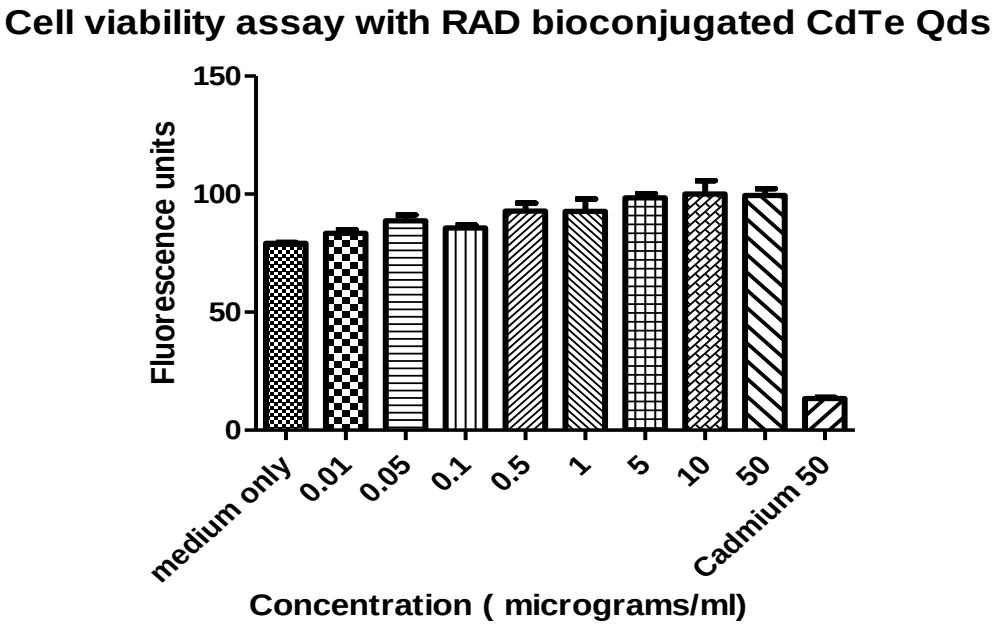

Fig. 5.17 Percentage of mouse skeletal C2C12 cell survival using graded concentration of RAD conjugated QDs compared with Cadmium alone at 50 µg/ml at fluoroscan analysis.

Cell viability assay with negative control c (RADfV) bound CdTe QDs- Sample 2

Graded concentration of RAD conjugated to CdTe quantum dots from 0.01µg/ml to 50µg/ml prepared by serial dilution in the Dulbecco's Modified Eagle Medium (DMEM) was used to assertain the cell viablility studies to mouse skeletal C2C12 cell lines of the second batch of sample. Only medium was used in the first column as a control. Elemental Cadmium at a concentration of 50 µg/ml was used in the last column to compare the toxicity. Fluoroscan analysis after incubation with Cell Titre Blue reagent revealed no obvious toxicity to these cells from 0.01 µg/ml to the concentration of 0.5 µg/ml as shown in table 5.18 and fig. 5.18.

Statistical analysis using one way ANOVA and Dunnett's multiple comparison tests revealed statistically significant difference in the cytotoxicity at the concentration of 0.5 µg/ml as shown in Appendix, table 18, page 216.

Table 5.18. Cell viability assay of mouse skeletal C2C12 cells with c (RADfV) conjugated CdTe QDs. Fluoroscan readings with graded concentration of CdTe QDs. conjugated to negative control c (RADfV)

Medium only	**QD0.01 *µg/ml***	**QD0.05 *µg/ml***	**QD0.1 *µg/ml***	**QD0.5 *µg/ml***	**QD1 *µg/ml***	**QD5 *µg/ml***	**QD10 *µg/ml***	**QD50 *µg/ml***	**Cadmium 50 *µg/ml***
79.39	85.39	86.50	84.66	95.14	103.2	99.08	104.6	105.2	14.40
78.65	80.34	93.76	88.19	97.04	86.26	101.0	106.8	96.04	13.18
79.70	84.56	85.87	84.18	86.35	88.66	95.25	88.60	96.92	12.87
Mean 79.24	83.43	88.71	85.68	92.84	92.70	98.43	99.99	99.37	13.48

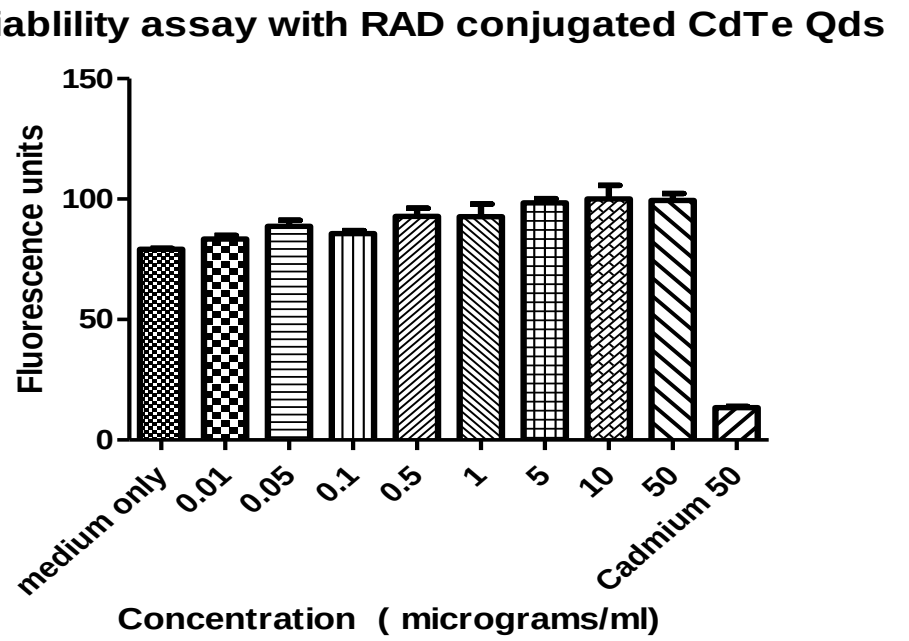

Fig. 5.18 Percentage of mouse skeletal C2C12 cell survival using graded concentration of RAD conjugated QDs. compared with Cadmium alone at 50 µg/ml at fluoroscan analysis

Cell death assay with negative control c (RADfV) bound CdTe QDs-Sample 1

In this study, graded concentration of RAD conjugated CdTe QDs was used to assess cytotoxicity to the mouse C2C12 cells. Cell death assay was analyzed using Yo Pro-1 Iodide (491/509)-Invitrogen reagent. The comparison was made with cells immersed in the DMEM (Dulbecco's Modified Eagle Medium). Elemental Cadmium was used at a concentration of 50 µg/ml for comparison being aware of its cytotoxic nature. Cell death assay for QD-RAD complexes equally proved nontoxic at the study concentration level up to 50 µg/ml. Elemental Cadmium continued its trend of cytotoxicity to the skeletal muscle cells at similar concentration of 50 µg/ml. as shown in table 5.19 and fig.5.19.

Statistical analysis using one way ANOVA and Dunnett's multiple comparison tests revealed no statistically significant difference in the cytotoxicity even at the maximum concentration of 50 µg/ml as shown in Appendix, table 19, page 217.

Table 5.19 Cell death assay of mouse skeletal C2C12 cells with RAD conjugated QDs. compared with Cadmium alone at 50 µg/ml at fluoroscan analysis. Fluoroscan readings at graded concentration of RAD conjugated QDs.

Medium only	**QD0.01 *µg/ml***	**QD0.05 *µg/ml***	**QD0.1 *µg/ml***	**QD0.5 *µg/ml***	**QD1 *µg/ml***	**QD5 *µg/ml***	**QD10 *µg/ml***	**QD50 *µg/ml***	**Cadmium 50 *µg/ml***
1.196	1.331	1.257	1.338	1.219	1.321	1.203	1.375	1.436	3.573
1.286	1.441	1.080	1.394	1.347	1.423	1.303	1.473	1.462	3.681
1.386	1.414	1.416	1.388	1.557	1.377	1.366	1.461	1.453	2.900
Mean 1.289	1.395	1.251	1.373	1.374	1.374	1.290	1.436	1.450	3.385

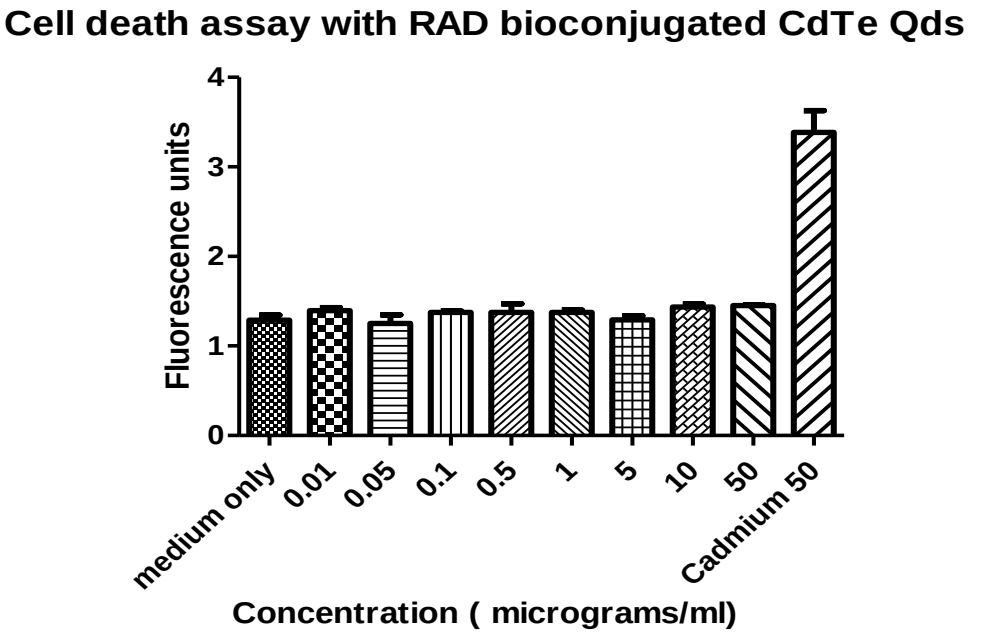

Fig. 5.19. Percentage of mouse skeletal C2C12 cell death using graded concentration of RAD conjugated CdTe QDs. Fluoroscan analysis compared with Cadmium alone at 50 µg/ml

Cell Death Assay with Negative control c (RADfV) bound CdTe QDs-Sample 2

In this study, graded concentration of RAD conjugated CdTe QDs was used to assess cytotoxicity to the second sample of mouse C2C12 cells. Cell death assay was analyzed using Yo Pro-1 Iodide (491/509)-Invitrogen reagent. The comparison was made with cells immersed in the DMEM (Dulbecco's Modified Eagle Medium). Elemental Cadmium was used at a concentration of 50 µg/ml for comparison being aware of its cytotoxic nature. The result of cell death assay revealed no obvious cytotoxicity at a concentration of 50 µg/ml. The elemental Cadmium continued to prove its toxicity at similar concentration. The results are shown in table 5.20 and fig. 5.20.

Statistical analysis using one way ANOVA and Dunnett's multiple comparison tests revealed no statistically significant difference in the cytotoxicity even at the maximum concentration of 50 µg/ml as shown in Appendix, table 20, page 218.

Table 5.20. Cell death assay of mouse skeletal C2C12 cells with RAD conjugated QDs compared with Cadmium alone at 50 µg/ml at fluoroscan analysis. Fluoroscan readings at graded concentration of RAD conjugated QDs.

Medium only	**QD0.01 *µg/ml***	**QD0.05 *µg/ml***	**QD0.1 *µg/ml***	**QD0.5 *µg/ml***	**QD1 *µg/ml***	**QD5 *µg/ml***	**QD10 *µg/ml***	**QD50 *µg/ml***	**Cadmium 50 *µg/ml***
1.272	1.400	1.346	1.382	1.224	1.365	1.217	1.403	1.392	3.257
1.207	1.344	1.162	1.414	1.696	1.364	1.233	1.401	1.392	3.391
1.351	1.360	1.386	1.473	1.716	1.420	1.264	1.496	1.559	3.570
Mean 1.277	1.368	1.298	1.423	1.545	1.383	1.238	1.433	1.448	3.406

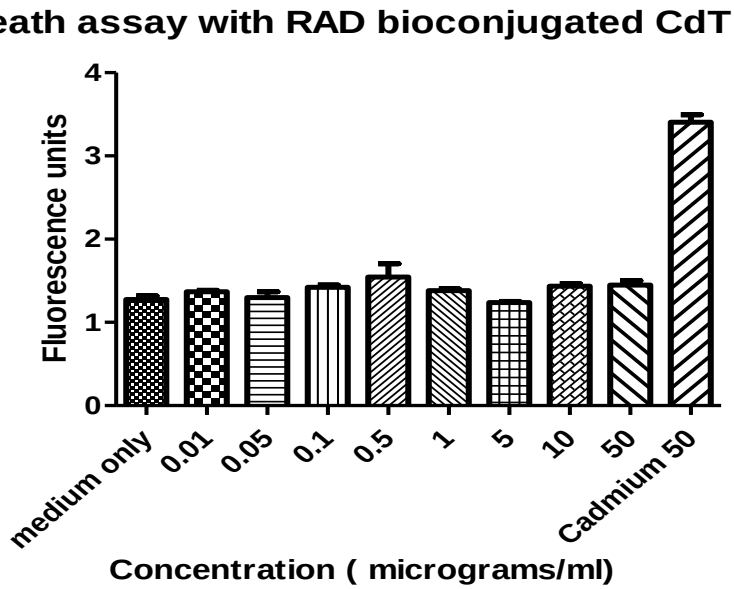

Fig. 5.20. Percentage of mouse skeletal C2C12 cell death using graded concentration of RAD conjugated CdTe QDs. Fluoroscan analysis using graded concentration of CdTe QD compared with Cadmium alone at 50 µg/ml.

Cell viability assay with POSS polymer coated CdTe- Sample 1

Polymer coating has proven to improve photophysical properties including stability, In order to study the range of cytotoxicity, POSS polymer coated CdTe quantum dots were bound to the mouse skeletal muscle cells in ascending concentration gradient. Graded concentration of polymer conjugated to CdTe quantum dots from 0.01µg/ml to 50µg/ml prepared by serial dilution in the Dulbecco's Modified Eagle Medium (DMEM) was used to assertain the cell viablility studies to mouse skeletal C2C12 cell lines. Only medium was used in the first column as a control. Elemental Cadmium at a concentration of 50 µg/ml was used in the last column to compare the toxicity. Fluoroscan analysis after incubation with Cell Titre Blue reagent revealed no obvious toxicity to these cells from 0.01 µg/ml to the concentration of 50 µg/ml in

comparison to the elemental Cadmium at similar concentration as observed in table 5.21 and fig.5.21.

Statistical analysis using one way ANOVA and Dunnett's multiple comparison tests revealed inconsistent cytotoxicity which was being evident from the concentration of 0.05 µg/ml as demonstrated in Appendix, table 21, page 219.

Table 5.21. Cell viability assay of mouse skeletal C2C12 cells with POSS polymer coated CdTe QDs. fluoroscan readings with graded concentration of CdTe QDs. conjugated to POSS polymer.

Medium only	**QD0.01 *µg/ml***	**QD0.05 *µg/ml***	**QD0.1 *µg/ml***	**QD0.5 *µg/ml***	**QD1 *µg/ml***	**QD5 *µg/ml***	**QD10 *µg/ml***	**QD50 *µg/ml***	**Cadmium 50 *µg/ml***
79.52	95.00	99.22	89.96	85.80	91.16	99.86	103.40	94.56	14.82
80.74	100.10	102.60	97.90	98.75	115.40	106.90	107.90	101.90	14.17
87.64	91.39	109.90	100.70	125.20	100.30	103.70	96.22	92.90	14.98
Mean 82.63	95.49	103.92	96.18	103.26	102.31	103.48	102.52	96.43	14.66

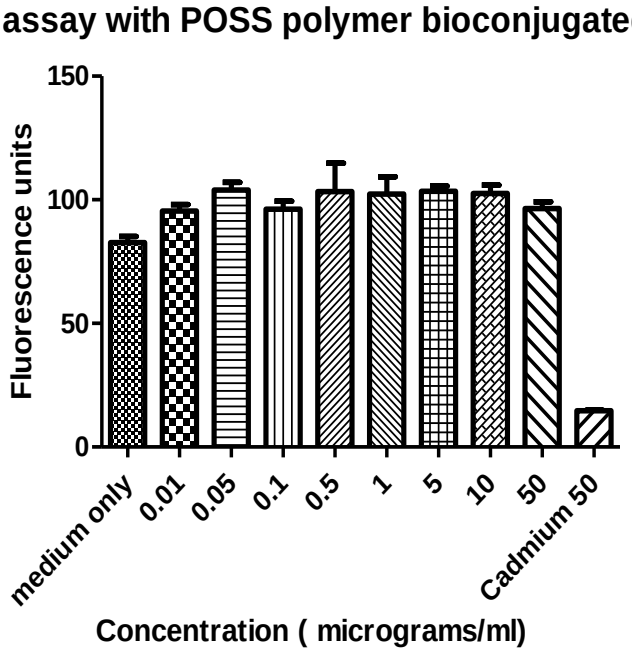

Fig. 5.21. Percentage of mouse skeletal C2C12 cell survival using graded concentration of POSS polymer conjugated QDs compared with Cadmium alone at 50 µg/ml at fluoroscan analysis

Cell Viability Assay with POSS Polymer coated CdTe- Sample 2

Graded concentration of polymer conjugated to CdTe quantum dots from 0.01µg/ml to 50µg/ml prepared by serial dilution in the Dulbecco's Modified Eagle Medium (DMEM) was used to assertain the cell viablility studies to mouse skeletal C2C12 cell lines within the second sample of cells. Only medium was used in the first column as a control. Elemental Cadmium at a concentration of 50 µg/ml was used in the last column to compare the toxicity. Fluoroscan analysis after incubation with Cell Titre Blue reagent revealed no obvious toxicity to these cells from 0.01 µg/ml to the concentration of 50 µg/ml in comparison to the elemental Cadmium at similar concentration as observed in table 5.22 and fig.5.22.

Statistical analysis using one way ANOVA and Dunnett's multiple comparison tests revealed inconsistent cytotoxicity which was being evident from the concentration of 0.05 µg/ml as demonstrated in Appendix, table 22, page 220.

Table 5.22. Cell viability assay of mouse skeletal C2C12 cells with POSS polymer coated CdTe QDs. Fluoroscan readings with graded concentration of CdTe QDs. conjugated to POSS polymer.

Medium only	**QD0.01** µg/ml	**QD0.05** µg/ml	**QD0.1** µg/ml	**QD0.5** µg/ml	**QD1** µg/ml	**QD5** µg/ml	**QD10** µg/ml	**QD50** µg/ml	**Cadmium 50**
79.52	95.00	99.22	89.96	85.80	91.16	99.86	103.4	94.56	14.82
80.74	100.1	102.6	97.90	98.75	115.4	106.9	107.9	101.9	14.17
87.64	91.39	109.9	100.7	125.2	100.3	103.7	96.22	92.90	14.98
Mean 82.63	95.49	103.92	96.18	103.26	102.31	103.48	102.52	96.43	14.66

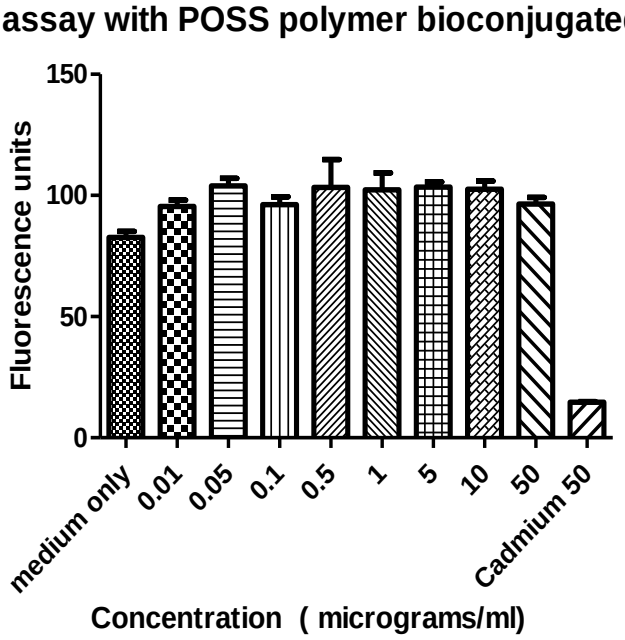

Fig. 5.22. Average cell survival using graded concentration of POSS polymer coated CdTe QD compared with Cadmium alone at 50 µg/ml at fluoroscan analysis

Cell death Assay with POSS Polymer coated CdTe- Sample 1

In this study, graded concentration of polymer conjugated CdTe QDs were used to assess cytotoxicity to the mouse C2C12 cells. Cell death assay was analyzed using Yo Pro-1 Iodide (491/509)-Invitrogen reagent. The comparison was made with cells immersed in the DMEM (Dulbecco's Modified Eagle Medium). Elemental Cadmium was used at a concentration of 50 µg/ml for comparison being aware of its cytotoxic nature. Cell death assay for polymer coated QDs equally proved nontoxic at the study concentration level up to 50 µg/ml. Elemental Cadmium continued its trend of cytotoxicity to the skeletal muscle cells at similar concentration of 50 µg/ml. as shown in table 5.23 and fig.5.23.

Statistical analysis using one way ANOVA and Dunnett's multiple comparison tests revealed no statistically significant difference in the cytotoxicity even at the maximum concentration of 50 µg/ml as shown in Appendix, table 23, page 221.

Table 5.23. Cell death assay of mouse skeletal C2C12 cells with POSS polymer conjugated QDs. compared with Cadmium alone at 50 µg/ml at fluoroscan analysis. Fluoroscan readings at graded concentration of RGD (Lysine) conjugated QDs.

Medium only	**QD0.01 *µg/ml***	**QD0.05 *µg/ml***	**QD0.1 *µg/ml***	**QD0.5 *µg/ml***	**QD1 *µg/ml***	**QD5 *µg/ml***	**QD10 *µg/ml***	**QD50 *µg/ml***	**Cadmium 50 *µg/ml***
1.470	1.503	1.347	1.508	1.307	1.374	1.298	1.432	1.497	3.752
1.332	1.442	1.336	1.440	1.306	1.433	1.308	1.470	1.510	3.531
1.374	1.386	1.387	1.396	1.350	1.372	1.390	1.448	1.607	4.395
Mean 1.392	1.444	1.357	1.448	1.321	1.393	1.332	1.450	1.538	3.892

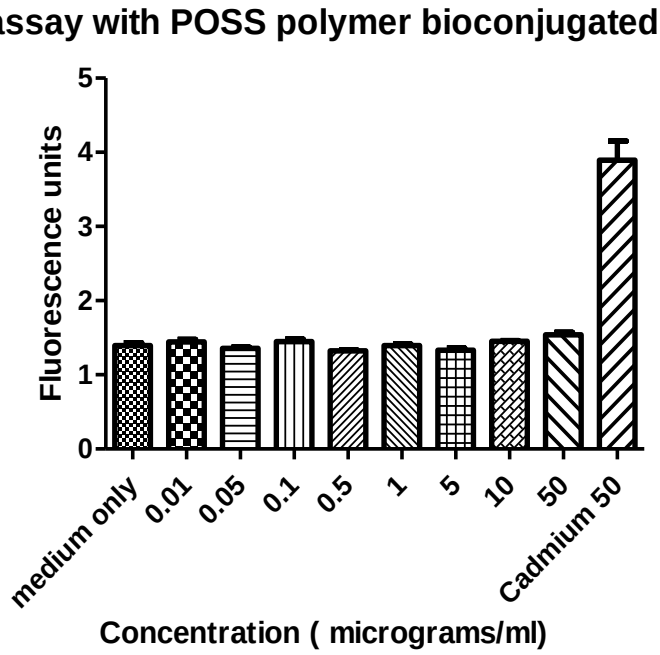

Fig. 5.23. Percentage of mouse skeletal C2C12 cell death using graded concentration of POSS polymer conjugated CdTe QDs. Fluoroscan analysis using graded concentration of CdTe QD compared with Cadmium alone at 50 µg/ml.

Cell death Assay with POSS Polymer coated CdTe- Sample 2

In this study, graded concentration of polymer conjugated CdTe QDs were used to assess cytotoxicity to the second sample of mouse C2C12 cell lines. Cell death assay was performed using Yo Pro-1 Iodide (491/509)-Invitrogen reagent. Comparison was made with cells immersed in the DMEM (Dulbecco's Modified Eagle Medium). Elemental Cadmium was used at a concentration of 50 µg/ml for comparison being aware of its cytotoxic nature. Cell death assay for polymer coated QDs equally proved nontoxic at the study concentration level up to 50 µg/ml. Elemental Cadmium continued its trend of cytotoxicity to the skeletal muscle cells at similar concentration of 50 µg/ml. as shown in table 5.24 and fig.5.24.

Statistical analysis using one way ANOVA and Dunnett's multiple comparison tests revealed no statistically significant difference in the cytotoxicity even at the maximum concentration of 50 µg/ml as shown in Appendix, table 24,page 222.

Table 5.24. Cell viability assay of mouse skeletal C2C12 cells with POSS polymer conjugated CdTe QDs. fluoroscan readings with graded concentration of CdTe QDs. conjugated to POSS polymer

Medium only	**QD0.01**	**QD0.05**	**QD0.1**	**QD0.5**	**QD1**	**QD5**	**QD10**	**QD50**	**Cadmium 50**
1.312	1.415	1.275	1.441	1.237	1.394	1.268	1.388	1.471	2.974
1.352	1.416	1.313	1.403	1.309	1.445	1.338	1.474	1.498	3.711
1.453	1.433	1.425	1.450	1.440	1.409	1.422	1.547	1.613	3.701
Mean 1.372	1.421	1.338	1.431	1.329	1.416	1.343	1.470	1.527	3.462

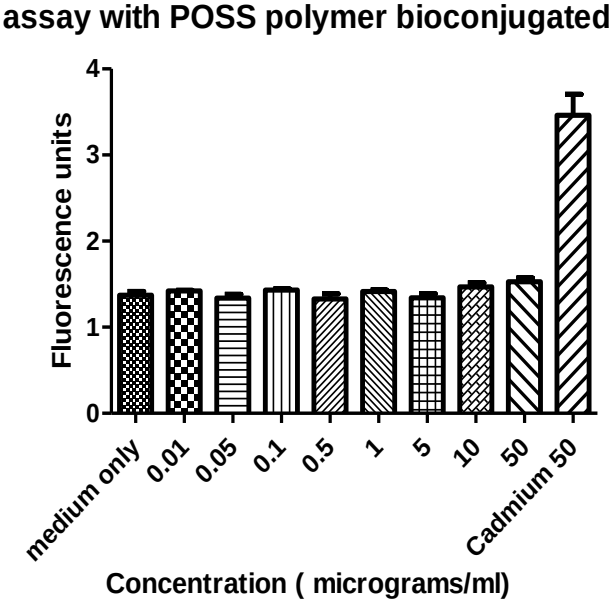

Fig. 5.24. Percentage of mouse skeletal C2C12 cell death using graded concentration of POSS Polymer conjugated CdTe QDs. Fluoroscan analysis concentration of CdTe QD compared with Cadmium alone at 50 µg/ml.

5.4 Discussion - Elemental Cadmium and Tellurium are known to be cytotoxic to the living cells. Prior to the analysis of cytotoxicity of CdTe quantum dots, it was deemed necessary to quantify the minimum concentration required to produce toxicity to the C2C12 mouse skeletal muscle cells by the individual QD components. Elemental Cadmium was found to be toxic to these cells at a concentration of 5 µg/ml. Using Yo Pro-1 Iodide reagent and Cell titre blue reagent, elemental Tellurium was found to be cytotoxic at a concentration of 0.1 µg/ml.

Nonconjugated CdTe quantum dots were nontoxic to the cells below the concentration of 50 µg/ml. QDs conjugated to RGD (Lysine) and RGD (Cysteine) were nontoxic to mouse C2C12 cells below the concentration of 50 µg/ml.

Negative control RAD conjugated QDs revealed inconsistent results in cell survival studies from both samples but also revealed no cytotoxicity in cell death assay below the concentration of 50 µg/ml.

POSS Polymer coated peptides also revealed inconsistent results in the cell survival studies with toxicity evident from concentration as low as 0.05 µg/ml. Cell death studies however suggested these to be safe below the concentration of 50 µg/ml.

5.5 Conclusion- Unconjugated water soluble CdTe QDs are safe below the concentration of 50 µg/ml to be applied for in vitro studies involving noncancer cells and *in vivo* studies. RGD Lysine and RGD Cysteine conjugated QDs are safe below the concentration of 50 µg/ml. and can be applied for in vitro and in vivo experiments.

RAD and Polymer coated QDs revealed inconsistent results with discrepancy between cell viability and cell death assay.

Further studies involving systemic biodistribution of these QDs in animal experiments and long term follow up studies will have to prove nontoxic nature of these QDs prior to their application in human population.

Chapter 6

Interaction of quantum dots with HT-29 cells *in vitro*

6.1 Introduction - The aim of the study was to demonstrate that QDs are capable of binding to HT29 colon cancer cells. As these cells overexpress integrins, the study was aimed to exploit this property for significant and stable binding using RGD (Lysine) and RGD (Cysteine) peptides.

6.2 Materials and Methods- RGD peptides were commercially obtained as discussed in details in chapter 4.2. RGD bound CdTe QDs were bioconjugated with HT29 colon cancer cells. Their interaction with the cells were studied using inverted microscope and transmission electron microscope (TEM) as explained in chapter 4.3

6.3 Results- Fig.6.1 and 6.2 illustrate inverted microscopic image of HT29 colon cancer cells at 10X and 40X magnification respectively at approximately 80-85% confluence. The monolayer of cells was studies after fixed number of cells were used in each well for optimal visualization of the QDs and to avoid bias. The cell growth was observed on daily basis. Generally 85% confluence of cell growth was observed on day 4 after maintaining these flasks containing HT29 cells at 37^0 C, 5% CO2 in a humidified atmosphere.

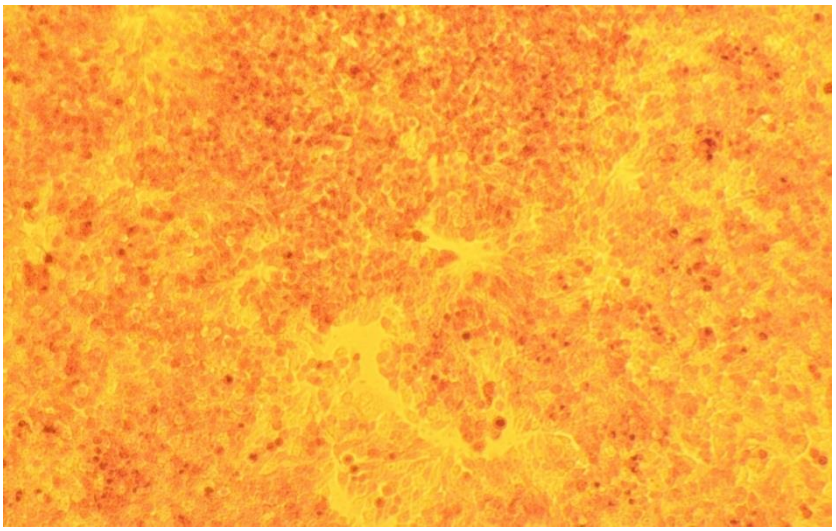

Fig. 6.1 Inverted microscopic image of HT29 cells (10x)

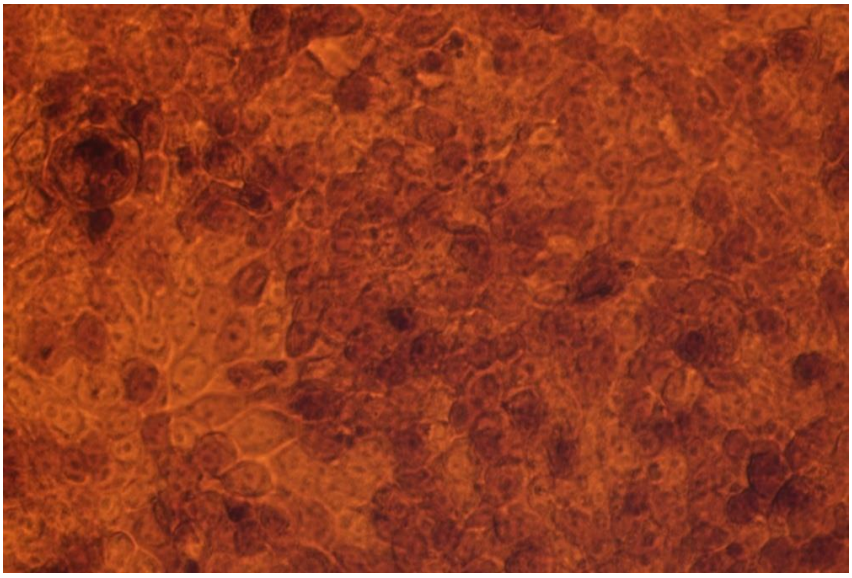

Fig. 6.2 Inverted microscopic image of HT29 cells (40x)

After the CdTe QDs were conjugated to HT29 cells for a period of 2 hours in the incubator, inverted microscopic appearance at a magnification of 40X revealed presence of sparse fluorescent QDs as noted in fig.6.3.

As the HT29 cells overexpress integrins[95-98], RGD tumour targeting peptides showed more significant binding in comparison to passive binding noted after addition of CdTe QDs alone. Fig.6.4 demonstrates more significant binding of RGD (Lysine) bioconjugated QDs to colon cancer cells. Similar stable and prolonged binding was noted after the use of RGD (Cysteine) for bioconjugation with the QDs as illustrated in fig.6.5.

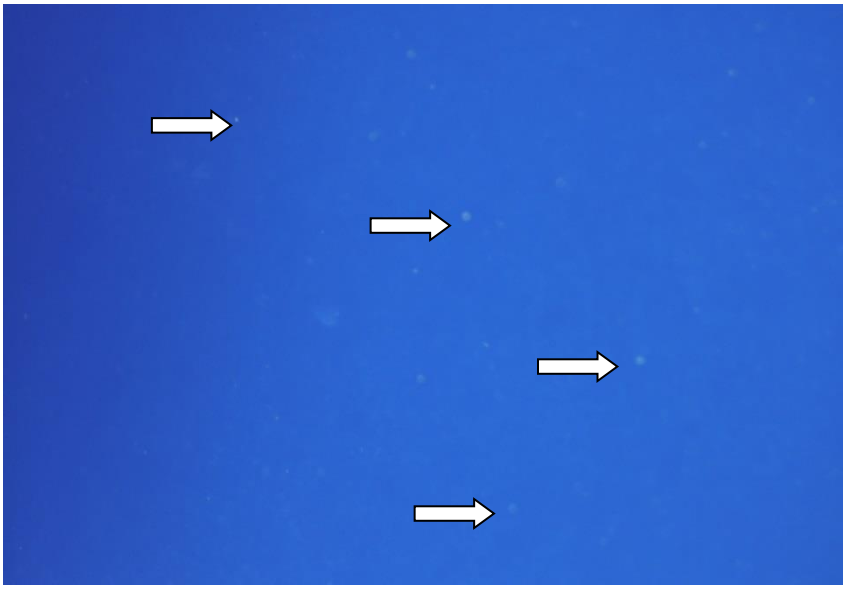

Fig.6.3. Inverted microscopic image of HT-29 cells-(40x) with CdTe QDs. (Arrows indicate the fluorescent QDs)

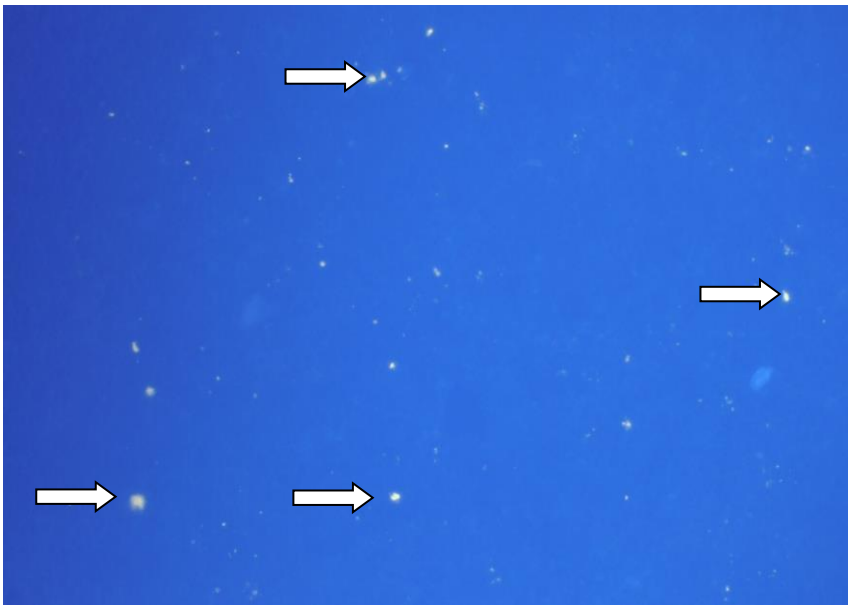

Fig.6.4 Inverted microscopic image of HT-29 cells-(40x) with CdTe QDs bound to c(RGDfK) αVβ3 Integrin binding RGD peptide. (Arrow indicate the fluorescent QDs)

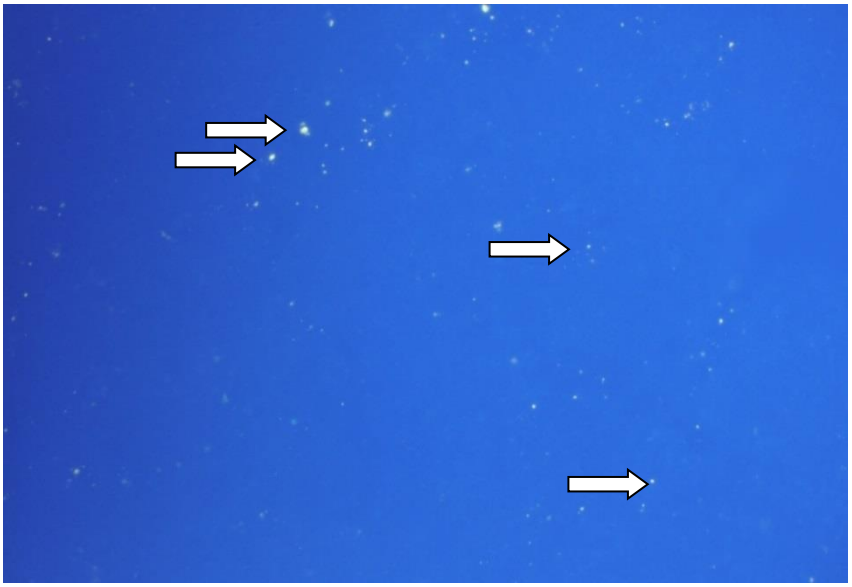

Fig.6.5 Inverted microscopic image of HT-29 cells-(40x) with CdTe QDs bound to c(RGDfC) RGD tumour targeting peptide. (Arrow indicate the QDs)

The binding of conjugated QDs to the HT29 colon cancer cells were noted to be more abundant, prolonged and stable than unconjugated QDs. After 24 hours of further incubation, and washing with PBS solution, when these flasks were observed under inverted microscope, the flasks with QDs bound to RGD peptides demonstrated unchanged appearance. Scanty QDs were noted in the flask containing unconjugated QDs passively bound to HT 29 colon cancer cells.

Fig.6.6, 6.7 and 6.8 illustrates TEM appearance of HT 29 cells with magnifications from 2650 to 40,000.These were used as baseline prior to comparison with QD labeled cells.

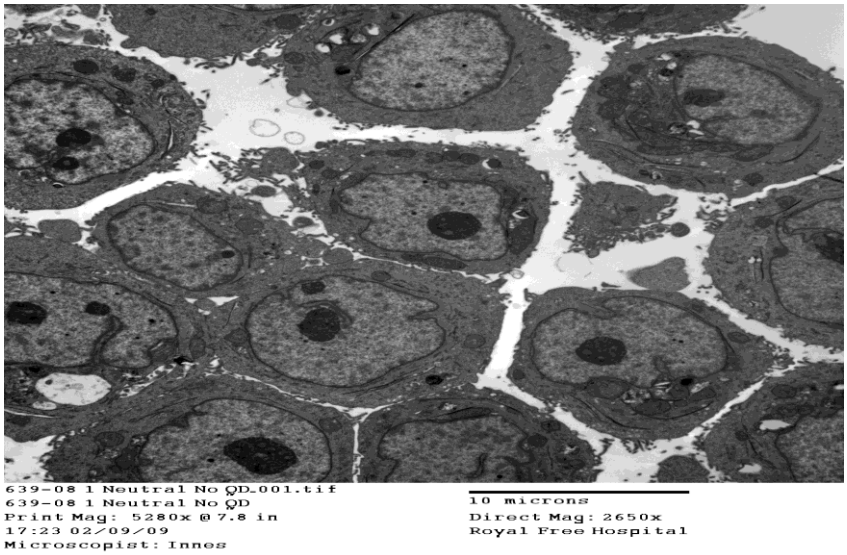

Fig. 6.6 TEM (Transmission Electron Microscopic) Appearance of HT29 Cells (Magnification -2650x),

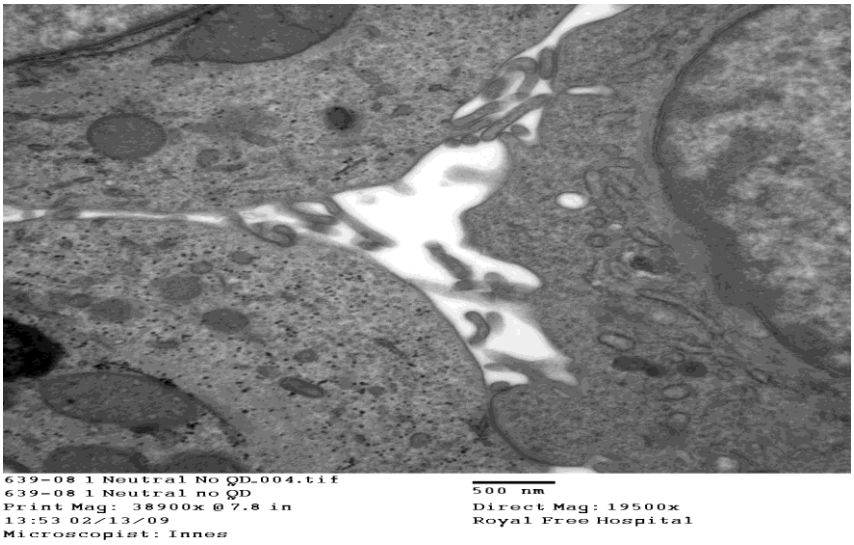

Fig.6.7 TEM (Transmission Electron Microscopic) appearance of HT29 Cells (Magnification -19,500x)

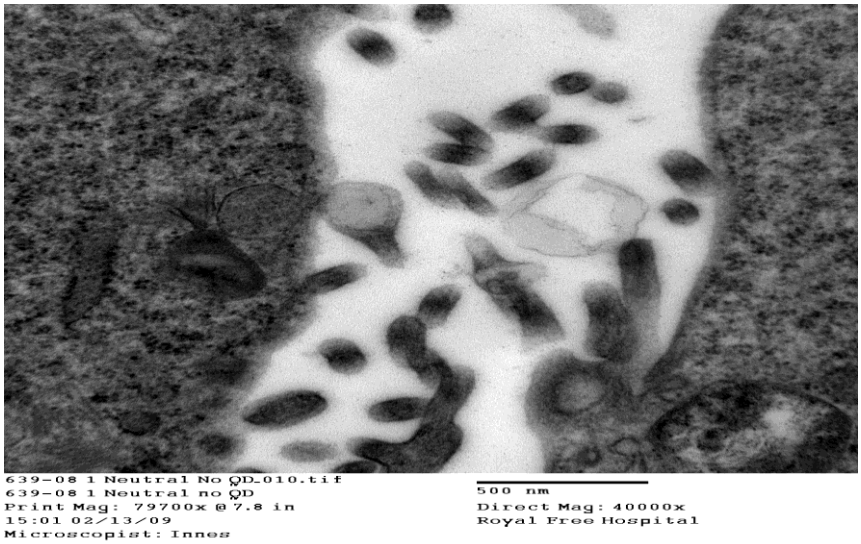

Fig. 6.8. Transmission electron microscopic appearance of HT29 cells (Magnification -40,000 x)

Fig.6.9 and 6.10 represents TEM appearance of HT 29 cells after labeling with CdTe QDs. These were obtained with magnifications ranging from 2650 to 19,500 times normal. Studying these images and comparing them with baseline images of cells, visible presence of quantum dots were noted along the cell membranes. These were confirmed with X-ray microanalysis as well.

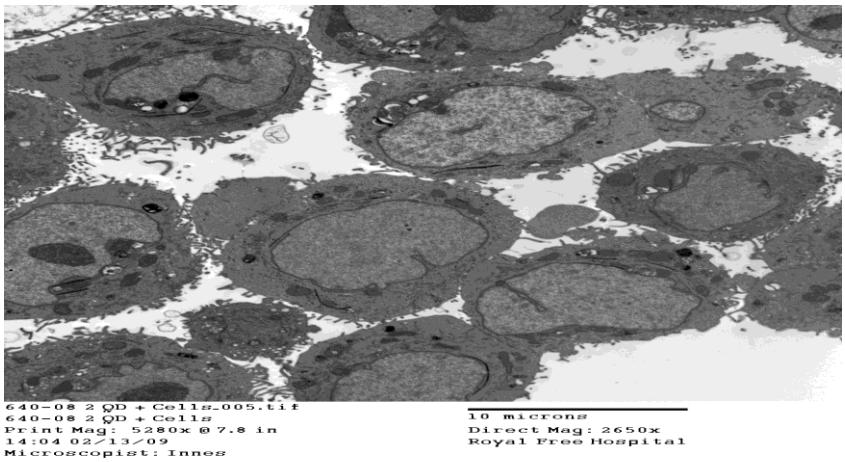

Fig.6.9 Transmission electron microscopic appearance of HT 29 cells with CdTe QDs (Magnification -2650x)

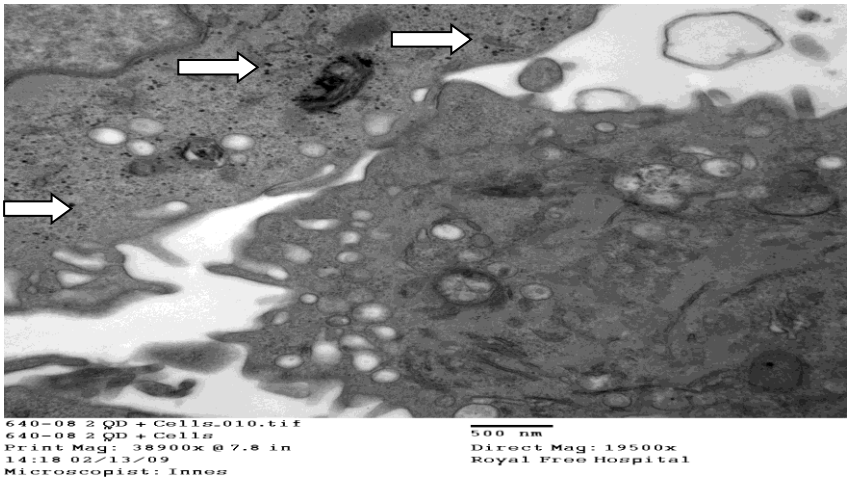

Fig.6.10. Transmission electron microscopic appearance of HT 29 cells with CdTe QDs (Magnification -19,500 x)

Further magnification of QDs labeled HT29 cells at 40,000 and 88,000 times normal was obtained for further delineation of QDs as demonstrated in Fig. 6.11 and 6.12. Abundant presence of QDs was observed as labeled with white arrows. X-ray microanalysis confirmed these dots to be CdTe QDs.

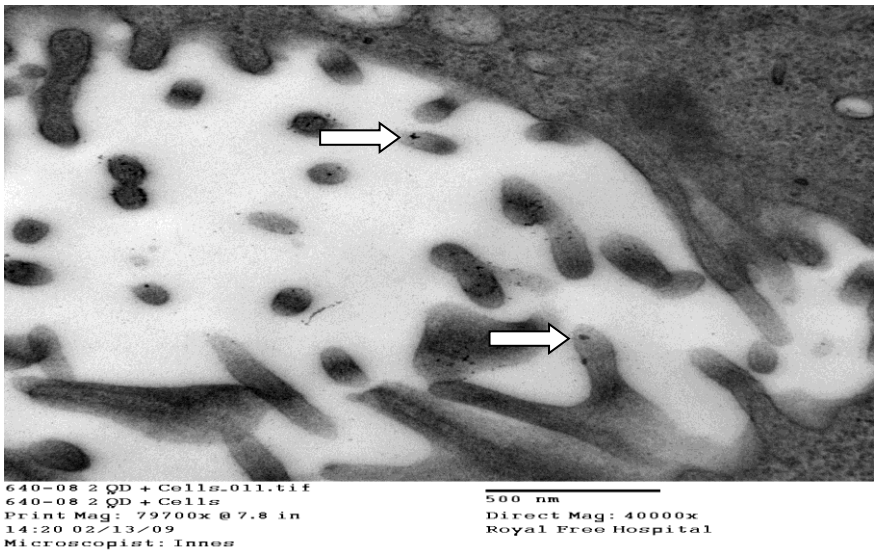

Fig. 6.11. Transmission electron microscopic appearance of HT 29 cells with CdTe QDs. (Magnification -40,000 x)

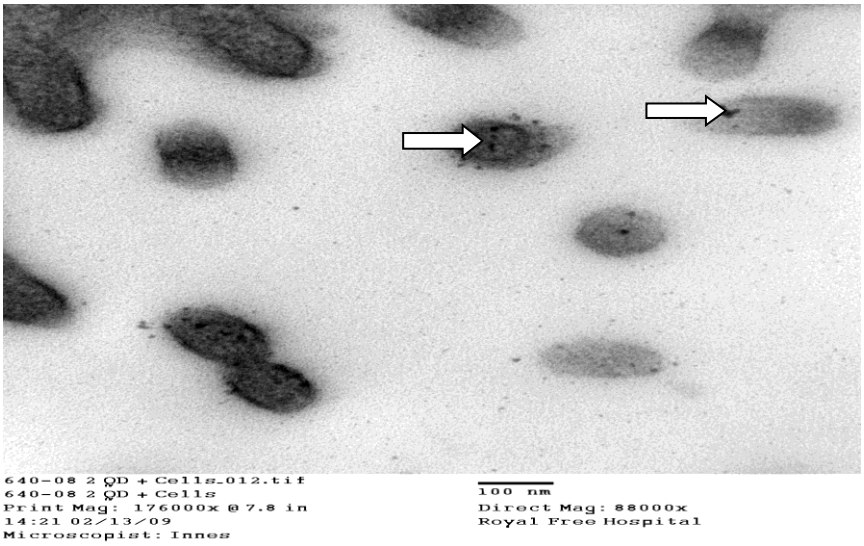

Fig. 6.12. Transmission electron microscopic appearance of HT 29 cells with CdTe QDs (Magnification -88,000 x) (Arrow indicate presence of QDs)

HT29 cells were then labeled with RGD tumour targeting peptide bound to the CdTe QDs and TEM images were obtained with magnifications varying from 2650 to 19,500 times normal as demonstrated in Fig.6.13 and 6.14.RGD labeled peptides confirmed more significant binding of QDs to the cell membrane of HT 29 cells.

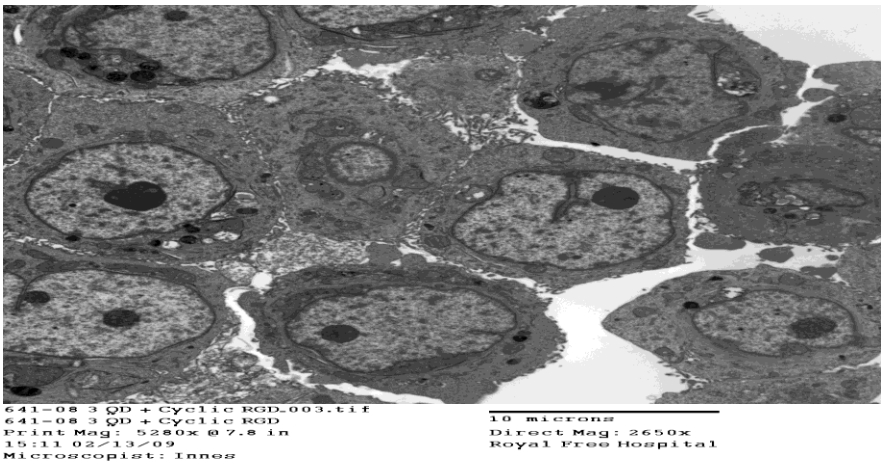

Fig. 6.13 Transmission electron microscopic appearance of HT- 29 cells with c(RGDfC)- RGD tumour targeting peptide bound to the CdTe QDs (Magnification –2650X)

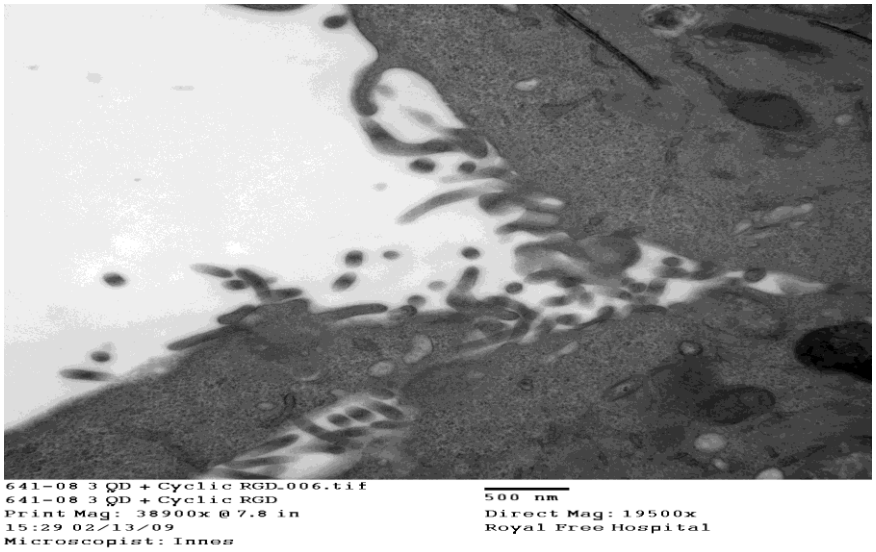

Fig. 6.14. *Transmission electron microscopic appearance of HT- 29 cells with c (RGDfC) - RGD tumour targeting peptide bound to the CdTe QDs – (Magnification –19,500X)*

Further magnification of RGD bound QD labeled HT 29 cells at 40,000 and 88,000 times normal was obtained for further delineation of QDs as demonstrated in Fig.6.15 and 6.16. Abundant presence of QDs was observed as labeled with white arrow. X-ray microanalysis confirmed these dots to be CdTe QDs.

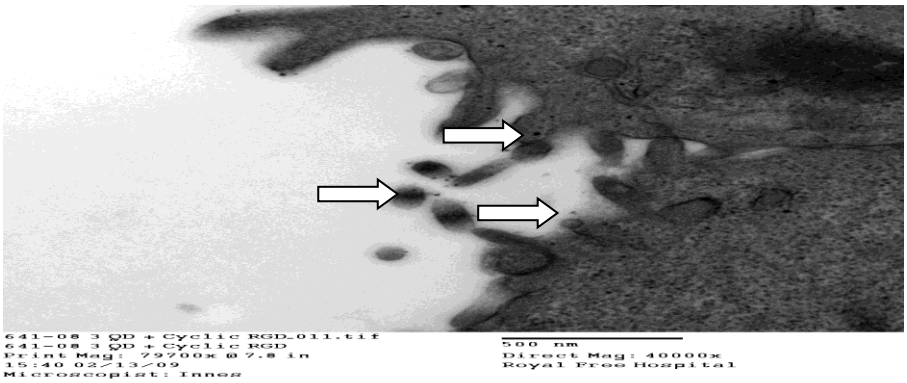

Fig. 6.15 Transmission electron microscopic appearance of HT29 cells with c(RGDfC)- RGD tumour targeting peptide bound to the CdTe QDs (Magnification –40000 X)

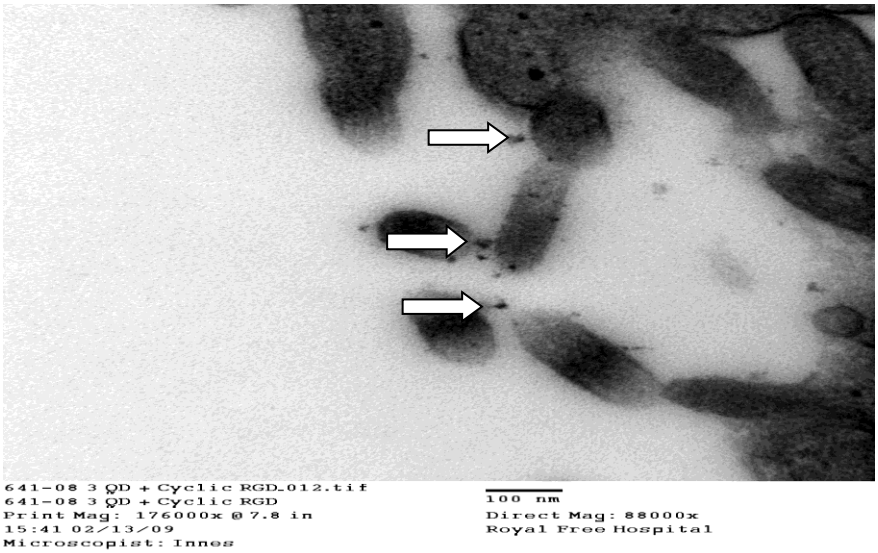

Fig. 6.16 Transmission electron microscopic appearance of HT29 cells with c(RGDfC)- RGD tumour targeting peptide bound to the CdTe QDs – (Magnification –88,000 X)(Arrow indicate presence of QDs)

6.4 Discussion - CdTe QDs were able to conjugate to the HT29 colon cancer cells during *in vitro* experiment. Passive binding was less stable and marginal. Application of RGD peptide conjugated QDs resulted in more stable and prolonged binding to the HT29 colon cancer cells. This was observed under both inverted and transmission electron microscopy confirmed by X-ray microanalysis.

6.5 Conclusion – CdTe QDs were able to bind to the HT29 colon cancer cells. Minimal binding was noted after the cells were washed with phosphate buffered saline (PBS).More significant stable and prolonged binding of QDs was noted to these colon cancer cells after bioconjugation with RGD (Lysine) and RGD (Cysteine).

Chapter 7

Feasibility of quantum dots for *in vivo* application

7.1 Introduction – Several studies have demonstrated successful application of QDs in animal experiments for sentinel lymph node identification based on their biodistribution properties. As the cytotoxicity assay concluded nontoxic nature of these CdTe QDs to normal cells at low concentration, it was decided to study biodistribution properties of these water soluble QDs in animal experiments. The aim of this procedure was to assess the feasibility of these synthetic water soluble CdTe QDs for the purpose of identification of sentinel node lymph nodes after subcutaneous injection of QDs *in vivo*.

7.2 Materials and methods- To observe the distribution of red emitting CdTe QDs *in vivo*, animal experiment was performed using SD (Sprague Dawley) rat. The Sprague Dawley rat is an outbred multipurpose breed of albino rat used extensively in medical research. Its main advantage is calmness and ease of handling. The animal handling was in accordance with standard animal husbandry practice and regulation. The animal was treated humanely and with regard for alleviation of suffering throughout the study. The rat used for this purpose was under 12 hour light-dark cycle, 23 ± 1°C, 39–43% relative humidity; water and food was available *ad libitum.*

The animal experiment was carried out in the animal lab at the University Department of Surgery, University College Medical School, Royal Free Campus in accordance with the Animal (scientific procedures) Act 1986 (ASPA) regulation implemented by the home office in England. The experiment was conducted by the supervisor holding personal license to carry out procedure on animals.

The rat was anaesthetized with isofluorane using a face mask and transferred into the UV chamber. The animal was placed supine. Vital parameters were monitored

throughout the procedure. QD conjugates were injected in the interdigital web space of hind limb. Evidence of uptake by the inguinal nodes in the groin was observed using Ultraviolet probe. Dissection of groin performed and lymph node fluorescence observed as a result of red emitting QDs.

Fig.7.1 Anaesthetized rat using isofluorene with face mask.

7.3 Results- As demonstrated in Fig 7.1 the experiment was conducted in the animal laboratory under aseptic technique. The caged SD rat was obtained and anaesthetized using isofluorene via well-fitting face mask. Continuous monitoring of vital parameters such as heart rate, blood pressure and temperature was performed throughout the experiment. Red emitting CdTe QDs were used at a concentration of 10µg / ml. The aim of this experiment was to trace the QDs after injection into the subcutaneous tissue till the fluorescence is demonstrated within the regional lymph node. The experiment was performed under ultraviolet radiation exposure. Efforts were made to observe live tracking of QDs within the lymphatics. The QDs were injected in the interdigital web space. The total volume of QD solution used was 1 ml.

Fig. 7.2 and 7.3 observe the procedure of QD injection in the interdigital web space. Red emission is obtained from the solution of QDs in the syringe used for injection at the background of external source of ultraviolet irradiation.

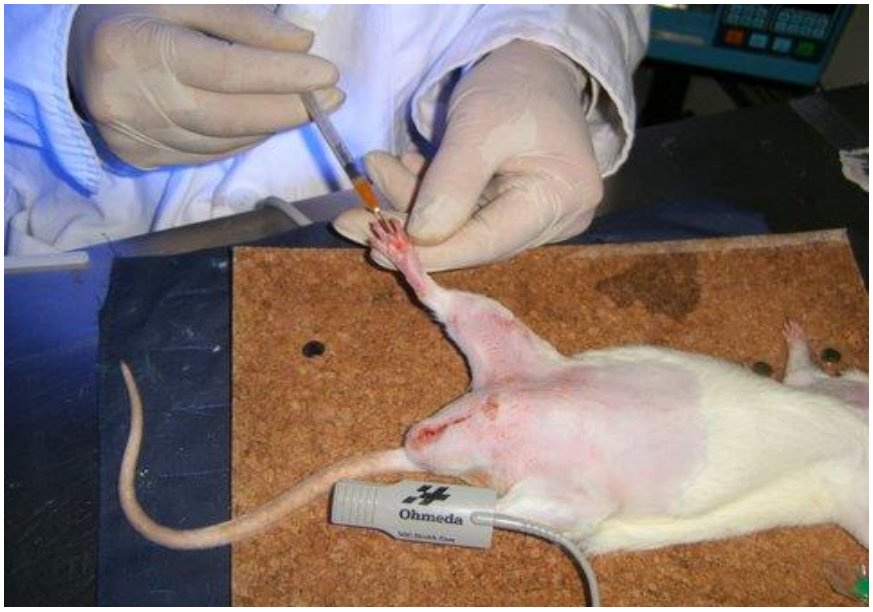

Fig. 7.2 Injection of red emitting CdTe quantum dots in the interdigital web space of the rat.

Fig 7.3 Red Fluorescence under UV exposure

Fig 7.4 Fluorescence due to injected quantum dots at the primary site and sentinel lymph node

As seen in Fig. 7.3 and fig.7.4, red emitting QDs were noted at the site of primary injection in the interdigital web space with subsequent glow in the right groin under UV exposure indicating the uptake by the regional lymph node, 10 minutes after primary injection of the quantum dots. The lymph node was dissected off following skin incision in the groin and was observed under ultraviolet exposure to demonstrate red emission as seen in Fig. 7.5.

Fig 7.5 Dissected sentinel lymph node under UV exposure.

Tail vein injection of the quantum dot conjugates done with a concentration of 10µg / ml. performed. Distribution of fluorescence was observed by careful dissection of the rat 60 minutes after injection. No obvious systemic distribution of the QDs could be demonstrated as illustrated in fig. 7.6.

QDs were injected in the small bowel wall and the distribution of quantum dots to the mesenteric nodes analyzed. After 60 minutes, there was no obvious evidence of sentinel node uptake of quantum dots was observed. The procedure was terminated after 4 hours and the animal was killed by high dose of isofluorane humanely.

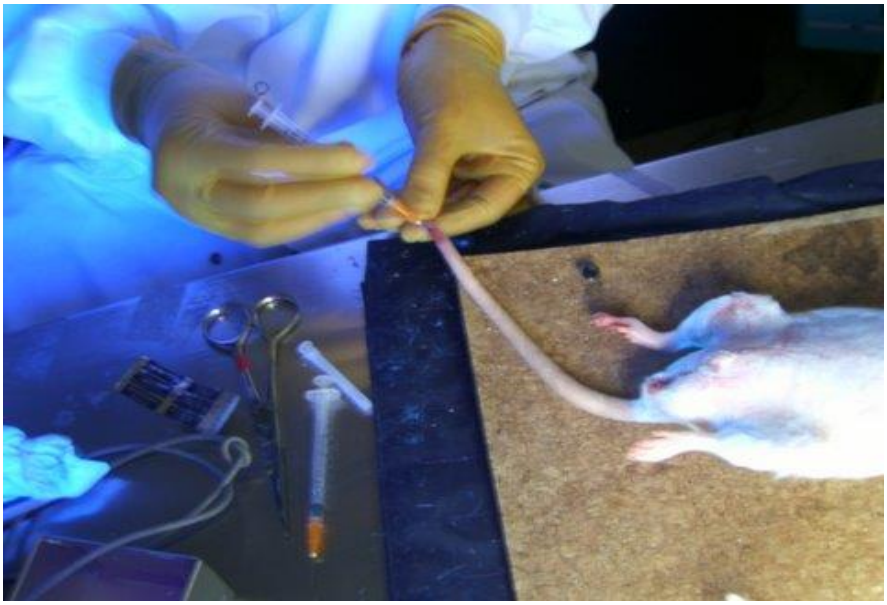

Fig.7.6 Injection of QD solution into the tail vein of the rat.

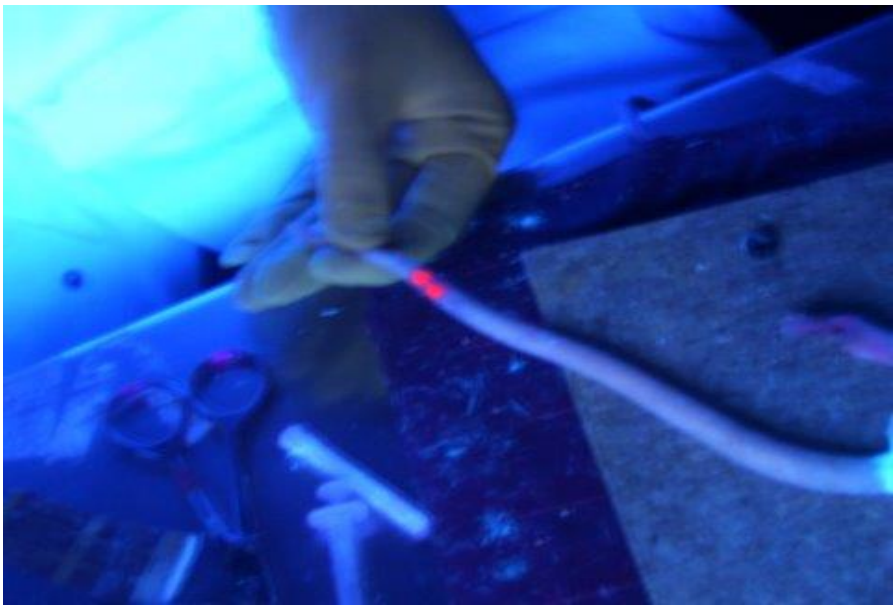

Fig.7.7 Fluorescence after injection of QDs in the lateral tail vein.

7.4 Discussion - Animal experiment performed in the SD rat demonstrated feasibility of bio-distribution studies using red emitting CdTe QDs. Distribution of QDs to inguinal node was observed 10 minutes after injecting into the interdigital web

space of hind limbs. Penetration of UV radiation using ultraviolet probe was found to be inadequate in the SD rat due to the depth of the inguinal lymph nodes and inability for the UV light to penetrate the skin to demonstrate the fluorescence without dissection. Inguinal lymph node dissection was required to identify lymph node with red fluorescence.

Injection of quantum dots into the tail vein of the rat and small bowel was found to be inconclusive. It was not possible to identify visceral distribution of the quantum dots. Further experiments using higher dose of QDs within their toxicity limit in was considered to be appropriate for bio-distribution studies.

7.5 Conclusion- Application of water soluble CdTe QDs is feasible in biodistribution studies using animal experiments. The lymph node with the QD uptake was more than likely to have been the sentinel lymph node however blue dye and radio-isotopes can be used simultaneously to assess if their activity within the sentinel node can be coordinated with the activity due to CdTe QDs. Due to low cytotoxic potential, these QDs can safely be utilized for *in vivo* studies. Due to limited depth of penetration, NIR light could be used instead of UV light for sentinel lymph node identification to detect fluorescence activity through the skin. This will allow for precise skin incision over the fluorescent lymph node for harvesting rather than formal groin dissection for its identification.

Chapter 8

Discussion

To date several methods of preparation of CdTe QDs have been described which include both organic synthesis and aqueous synthesis[14;18,21]. The high quality CdTe QDS prepared in the organic solvents cannot be utilized in the biosystems as they are hydrophobic. Several methods have been described to convert hydrophobic QDs into hydrophilic one such as ligand exchange, encapsulation into water soluble shell and arrested precipitation in water. However these processes indeed diminish their photoluminescence quantum yield (PL QY) during the transferring process.

Ying et al [24] in 2008 published a simpler approach of synthesis of luminescent cysteine–coated CdTe QDs with QY of 10% using Sodium Tellurite as the Te source. This eliminated the need for highly toxic H_2Te or highly unstable NaHTe as a Tellurium precursor for the aqueous synthesis of Thiol-capped CdTe QDs in the inert atmospheric conditions. Using thiol stabilizer Mercaptosuccinic acid (MSA) as a capping ligand and by optimizing the growth conditions, such as pH of solution and the concentration of precursor solutions, the QY could be dramatically improved up to 83% at pH 5 without any post-treatment and up to in excess of 70% at pH 6-8. CdTe QDs in this study were prepared using precursors Cadmium Chloride and Sodium Tellurite in presence of buffer solution of Mercaptosuccinic acid. The emission spectrum of quantum dots was precisely determined by the size of the QDs. The preparation of QDs with different emission spectrums could be controlled by regulating the duration of condensation and refluxation of the mixture of QD precursors. The QDs thus prepared were water soluble and stable at room temperature and could be safely be used for *in vitro* and *in vivo* experiments.

During the process of synthesis of CdTe quantum dots, in the initial phase when $NaBH_4$ powder was added to the precursor solution, this solution turned green within few seconds depending upon the pH value of the precursor solution, the

concentration of the solution and the reaction temperature. Lowering the pH value, increasing the concentration of the precursor solution or increasing the reaction temperature accelerated the formation of the CdTe QDS. During the initial stage, no photoluminescence was observed from the crude solution presumably as a result of smaller size of the QDs. Weaker luminescence was noted after prolonged boiling when the solution turned dark green in colour. With prolonging of the reflux time, the absorption spectra as well as PL emission spectra shifted to longer wavelength with increase in the size of the CdTe QDs due to quantum confinement effect. These MSA- CdTe QDs remained stable for months when stored in the refrigerator at 4ºC indicating attractive bio-labeling and bio-imaging applications.

In this experiment, Red emitting CdTe QDs stabilized in Mercaptosuccinic acid had a wide absorption spectrum with an excitonic absorption peak of 380 nm and a very narrow symmetrical emission spectrum of 630nm at spectrophotometeric analysis. They were present in the form of isolated crystals or clusters measuring 5nm to 10 nm in diameter. Their elemental localization at the cellular or sub-cellular level could be confirmed successfully using transmission Electron Microscopy supplemented by X-ray Microanalysis.

CdTe QDs were able to bind to the HT29 colon cancer cells. Minimal binding was noted after the cells were washed with phosphate buffered saline (PBS).More significant, stable and prolonged binding of QDs was noted to these colon cancer cells after bioconjugation with RGD (Lysine) and RGD (Cysteine). This is in line with reports on successful binding of QDs to cancer cells over-expressing various tumor markers such as CEA[63], Ca 125[51], PSMA[67], Her2[28,70] and others.

Elemental Cadmium and Tellurium are known to be cytotoxic to the live cells. Prior to the analysis of cytotoxicity of CdTe QDs, it was deemed necessary to assess the

minimum concentration necessary to produce cytotoxicity to the C2C12 mouse skeletal muscle cells. Elemental Cadmium was found to be toxic to these cells at a concentration of 5 µg/ml. Using Yo Pro-1 Iodide reagent and Cell titer blue reagent, elemental Tellurium was found to be cytotoxic at a concentration of 50 µg/ml. However both unconjugated and conjugated QDs were nontoxic to C2C12 mouse skeletal muscle cells at a concentration of 50 µg/ml.

Animal experiment performed in the brown rat demonstrated feasibility of bio-distribution studies using red emitting CdTe QDs with a very small dose equivalent to 10µg/ml. Distribution of QDs to inguinal node was observed 10 minutes after injecting into the interdigital web space of hind limbs. Penetration of UV radiation using ultraviolet probe was found to have been inadequate in brown rat due to the depth of the inguinal lymph nodes. Inguinal lymph node dissection was required to identify first illuminating lymph node with red fluorescence which was presumed to have been the sentinel lymph node.

Injection of QDs into the tail vein of the rat and small bowel was found to have been inconclusive. It was not possible to identify visceral distribution of the QDs. Further experiments using higher dose of QDs within their toxicity limit in nude mice was considered to be appropriate for bio-distribution studies.

The translation of QDs in *in vivo* applications has been limited not only because of questions related to possible toxicity, but also due to restricted penetration of light into the tissues under investigation[41,42].

Chapter 9

Summary and future direction

According to the office for national statistics, cancers remain third leading cause of death in England and Wales following ischaemic heart diseases and cerebrovascular diseases. Early detection of cancers is associated with >90% 5 year survival. However for majority of the patients cancer is discovered only after it has spread extensively for curative treatment to improve the life expectancy and quality of life. The conventional anatomical imaging modalities are unable to detect most cancers until they reach > 1cm in diameter. Molecular imaging, especially with QDs covalently linked to bio-recognition molecules such as peptides, antibodies, nucleic acids, or small-molecule ligands is expected to play an important role in detecting cancer early enough in the disease process that the treatment could prove successful.. Current treatment strategy involves subjecting the patients to the highly toxic compounds which are not specific to the cancer cells. As a result serious side effects are common and can be debilitating to the patients. With the help of nanotechnology it may be possible to deliver these drugs selectively to the cancer cells while avoiding excessive toxicity to the surrounding healthy cells.

QDs are semiconductor nanoparticles with structural and functional properties that are not available from discrete molecules or bulk materials. They encompass large surface areas for the attachment of multiple diagnostic (optical, magnetic or radio isotopic) and therapeutic agents. When conjugated with biomolecular affinity ligands such as antibodies, peptides or small molecules, they can be used to target malignant tumors with high affinity and specificity. Most commonly used QDs are CdSe or CdTe with a passivation shell made of ZnS which protect the core from oxidation and increases the photoluminescence quantum yield. The surface of the QD is further coated with solubilization ligand making them water soluble for their use in cell biology.

High temperature synthesis using pyrolysis of organometallic precursors has been the most frequently used method for synthesis of high quality QDs in organic solvents. However using alternative cheaper and safer Cadmium precursors, QDs with reasonable photoluminescence can be synthesized in the organic solvents. Aqueous synthesis although result in fabrication of QDs with poor size distribution and low fluorescence efficiency, it carries the advantage of being simple, less toxic and reproducible.

For efficient biodistribution of the QDs, they can be covalently conjugated to various biomolecules to specifically target the cellular organelle of interest. For a stable bioconjugation, various transmembrane proteins such as integrins can be targeted using QDs as a binding and delivery vehicle.

Despite of successful binding of QDs to cancer cells over-expressing various tumor markers such as CEA[63], Ca 125[51], PSMA[67], Her2[28,70] etc., exploitation of this technique *in vivo* has been limited due to restricted tissue penetration of light. Near infrared imaging has presented itself as a powerful diagnostic technique with a potential to serve as a minimally invasive, nonionizing method for sensitive diagnostic imaging for up to 2-3 cm depth in vivo experiments[41,42]. NIR QDs demonstrate superior optical performance with exceptional fluorescence, brightness and stability. However, the heavy metal composition and high propensity for toxicity hinder future application in clinical environments. Cancer specific application of this include- Image guided resection of cancer, real time assessment of surgical margins, intra-operative sentinel lymph node mapping, intra-operative detection of occult metastatic lesions, and identification of surgical anatomy. The implications of NIRF imaging in cancer surgery would be as follows-

1. Breast cancer- Intra-operative NIR Fluorescent imaging has a potential to replace the radioisotope (Technetium 99M sulphur colloid) and blue dye (Isosulfan blue) which has been traditionally injected around the tumour for identification of the sentinel lymph nodes. Using NIR fluorescent imaging, not only the real time sentinel lymph node mapping would be possible but by using breast cancer specific targeting molecules, adequacy of cancer resection and lymph node clearance would be ascertained.

2. Colon cancer - NIRF imaging using specific markers such as CEA, surgical resection of occult tumor extension and lymph node mapping would be possible.

3. Lung cancer- Adequacy of surgical excision, identification of occult lesions and real time imaging of lymph node drainage would be possible with NIRF imaging.

4. Prostate cancer- Besides adequate surgical clearance of the cancer, it may even be possible to directly visualize the nerves by the use of NIRF nerve targeting module.

To improve the therapeutic efficacy of chemotherapeutic agents, nanotechnology based formulations are already in use. The commonest example being Abraxane, an albumin-bound nanoparticle formulation of paclitaxel being used for metastatic breast cancer and Doxil, a long circulating liposomal formulation of doxorubicin being used in ovarian cancer. Using nanotechnology tools, drug delivery system can be developed using an array of nanoscaled polymeric, liposomal and inorganic materials. These nano drug delivery systems offer easier tissue penetration through biological and physiological barriers that are normally impermeable for larger particulate structures, due to their small size. In addition to this, they carry multifunctional capabilities of simultaneous imaging and therapeutic applications. With ongoing research in the field of nanomedicine, the same principles could be

applied to QDs. These QDs are almost always conjugated to some form of ligand for solubilization or functionalization purpose. Therefore adding tumor specific targeting ligand, cancer cells can selectively be targeted for delivering chemotherapeutic agents for maximum efficacy.

Despite of their novel biological properties, QDs can pose cytotoxic risk to the living cells due to their chemical composition and prolong half-life. Further research into methods of elimination of QDs from the biological environment after their successful application would encourage safer use of these nanoparticles in human population for oncological application.

Reference List

(1) Sullivan DC, Kelloff G. Seeing into cells. The promise of in vivo molecular imaging in oncology. EMBO Rep 2005; 6(4):292-296.

(2) Nie S, Xing Y, Kim GJ, Simons JW. Nanotechnology applications in cancer. Annu Rev Biomed Eng 2007; 9:257-288.

(3) LaRocque J, Bharali DJ, Mousa SA. Cancer detection and treatment: the role of nanomedicines. Mol Biotechnol 2009; 42(3):358-366.

(4) Ting G, Chang CH, Wang HE. Cancer nanotargeted radiopharmaceuticals for tumor imaging and therapy. Anticancer Res 2009; 29(10):4107-4118.

(5) Huo Q. A perspective on bioconjugated nanoparticles and quantum dots. Colloids Surf B Biointerfaces 2007; 59(1):1-10.

(6) Hartman KB, Wilson LJ, Rosenblum MG. Detecting and treating cancer with nanotechnology. Mol Diagn Ther 2008; 12(1):1-14.

(7) Zrazhevskiy P, Sena M, Gao X. Designing multifunctional quantum dots for bioimaging, detection, and drug delivery. Chem Soc Rev 2010; 39(11):4326-4354.

(8) So MK, Xu C, Loening AM, Gambhir SS, Rao J. Self-illuminating quantum dot conjugates for in vivo imaging. Nat Biotechnol 2006; 24(3):339-343.

(9) Obonyo O, Fisher E, Edwards M, Douroumis D. Quantum dots synthesis and biological applications as imaging and drug delivery systems. Crit Rev Biotechnol 2010.

(10) Zrazhevskiy P, Sena M, Gao X. Designing multifunctional quantum dots for bioimaging, detection, and drug delivery. Chem Soc Rev 2010.

(11) Jamieson T, Bakhshi R, Petrova D, Pocock R, Imani M, Seifalian AM. Biological applications of quantum dots. Biomaterials 2007; 28(31):4717-4732.

(12) Pinaud F, Michalet X, Bentolila LA, Tsay JM, Doose S, Li JJ et al. Advances in fluorescence imaging with quantum dot bio-probes. Biomaterials 2006; 27(9):1679-1687.

(13) Choi CL, Alivisatos AP. From artificial atoms to nanocrystal molecules: preparation and properties of more complex nanostructures. Annu Rev Phys Chem 2010; 61:369-389.

(14) Lianhua Qu ZAPaXP. Alternative Routes toward High Quality CdSe Nanocrystals. NANOLETTERS 1[6], 333-337. 2001.
Ref Type: Journal (Full)

(15) Peng ZA, Peng X. Formation of high-quality CdTe, CdSe, and CdS nanocrystals using CdO as precursor. J Am Chem Soc 2001; 123(1):183-184.

(16) Peng ZA, Peng X. Nearly monodisperse and shape-controlled CdSe nanocrystals via alternative routes: nucleation and growth. J Am Chem Soc 2002; 124(13):3343-3353.

(17) Nikolai Gaponik *DVTALR*KHEVSAKAEaHW. Thiol-Capping of CdTe Nanocrystals: An Alternative to Organometallic Synthetic Routes. J.Phys.Chem.B 106, 7177-7185. 2002. Ref Type: Journal (Full)

(18) B.O.Dabbousi JR-VFVMJRHHMROKFJaMGB. (CdSe)ZnS Core-Shell Quantum Dots: Synthesis and Characterization of a Size Series of Highly Luminescent Nanocrystallites. J.Phys.Chem.B 101[46], 9463-9475. 1997. Ref Type: Journal (Full)

(19) Mansur HS. Quantum dots and nanocomposites. Wiley Interdiscip Rev Nanomed Nanobiotechnol 2010; 2(2):113-129.

(20) Xiaogang Peng MCSAVKaPA. Epitaxial Growth of Highly Luminescent CdSe/CdS Core/Shell Nanocrystals with Photostability and Electronic Accessibility. J.Am.Chem.Soc. 119, 7019-7029. 1997. Ref Type: Journal (Full)

(21) Reiss P, Protiere M, Li L. Core/Shell semiconductor nanocrystals. Small 2009; 5(2):154-168.

(22) Frasco MF, Chaniotakis N. Bioconjugated quantum dots as fluorescent probes for bioanalytical applications. Anal Bioanal Chem 2010; 396(1):229-240.

(23) Smith AM, Duan H, Mohs AM, Nie S. Bioconjugated quantum dots for in vivo molecular and cellular imaging. Adv Drug Deliv Rev 2008; 60(11):1226-1240.

(24) Ying E, Li D, Guo S, Dong S, Wang J. Synthesis and bio-imaging application of highly luminescent mercaptosuccinic acid-coated CdTe nanocrystals. PLoS One 2008; 3(5):e2222.

(25) Bao H, Wang E, Dong S. One-pot synthesis of CdTe nanocrystals and shape control of luminescent CdTe-cystine nanocomposites. Small 2006; 2(4):476-480.

(26) Pathak S, Davidson MC, Silva GA. Characterization of the functional binding properties of antibody conjugated quantum dots. Nano Lett 2007; 7(7):1839-1845.

(27) Selvan ST, Tan TT, Yi DK, Jana NR. Functional and multifunctional nanoparticles for bioimaging and biosensing. Langmuir 2010; 26(14):11631-11641.

(28) Wu X, Liu H, Liu J, Haley KN, Treadway JA, Larson JP et al. Immunofluorescent labeling of cancer marker Her2 and other cellular targets with semiconductor quantum dots. Nat Biotechnol 2003; 21(1):41-46.

(29) A.M.Derfus WCWCSNB. Intracellular Delivery of Quantum Dots for Live Cell Labeling and Organelle Tracking. Advanced Materials 16[12], 961-966. 2004. Ref Type: Journal (Full)

(30) Fanqing Chen DG. Fluorescent CdSe/ZnS Nanocrystal-Peptide Conjugates for Long-term, Nontoxic Imaging and Nuclear Targeting in Living Cells. Nano Letters, 4[10], 1827-1832. 2004. Ref Type: Journal (Full)

(31) Courty S, Luccardini C, Bellaiche Y, Cappello G, Dahan M. Tracking individual kinesin motors in living cells using single quantum-dot imaging. Nano Lett 2006; 6(7):1491-1495.

(32) Kim BY, Jiang W, Oreopoulos J, Yip CM, Rutka JT, Chan WC. Biodegradable quantum dot nanocomposites enable live cell labeling and imaging of cytoplasmic targets. Nano Lett 2008; 8(11):3887-3892.

(33) Lovric J, Bazzi HS, Cuie Y, Fortin GR, Winnik FM, Maysinger D. Differences in subcellular distribution and toxicity of green and red emitting CdTe quantum dots. J Mol Med 2005; 83(5):377-385.

(34) Nabiev I, Mitchell S, Davies A, Williams Y, Kelleher D, Moore R et al. Nonfunctionalized nanocrystals can exploit a cell's active transport machinery delivering them to specific nuclear and cytoplasmic compartments. Nano Lett 2007; 7(11):3452-3461.

(35) Ballou B, Lagerholm BC, Ernst LA, Bruchez MP, Waggoner AS. Noninvasive imaging of quantum dots in mice. Bioconjug Chem 2004; 15(1):79-86.

(36) H.C.Fischer LLKSPWCWC. Pharmacokinetics of Nanoscale Quantum Dots: In Vivo Distribution, Sequestration, and Clearance in the Rat. Advanced Functional Materials 16[10], 1299-1305. 2006.
Ref Type: Journal (Full)

(37) Choi HS, Liu W, Misra P, Tanaka E, Zimmer JP, Itty IB et al. Renal clearance of quantum dots. Nat Biotechnol 2007; 25(10):1165-1170.

(38) Zhang LW, Yu WW, Colvin VL, Monteiro-Riviere NA. Biological interactions of quantum dot nanoparticles in skin and in human epidermal keratinocytes. Toxicol Appl Pharmacol 2008; 228(2):200-211.

(39) Schipper ML, Cheng Z, Lee SW, Bentolila LA, Iyer G, Rao J et al. microPET-based biodistribution of quantum dots in living mice. J Nucl Med 2007; 48(9):1511-1518.

(40) Yang RS, Chang LW, Wu JP, Tsai MH, Wang HJ, Kuo YC et al. Persistent tissue kinetics and redistribution of nanoparticles, quantum dot 705, in mice: ICP-MS quantitative assessment. Environ Health Perspect 2007; 115(9):1339-1343.

(41) Altinoglu EI, Adair JH. Near infrared imaging with nanoparticles. Wiley Interdiscip Rev Nanomed Nanobiotechnol 2010; 2(5):461-477.

(42) Kim S, Fisher B, Eisler HJ, Bawendi M. Type-II quantum dots: CdTe/CdSe(core/shell) and CdSe/ZnTe(core/shell) heterostructures. J Am Chem Soc 2003; 125(38):11466-11467.

(43) Hama Y, Koyama Y, Urano Y, Choyke PL, Kobayashi H. Simultaneous two-color spectral fluorescence lymphangiography with near infrared quantum dots to map two lymphatic flows from the breast and the upper extremity. Breast Cancer Res Treat 2007; 103(1):23-28.

(44) Azzazy HM, Mansour MM, Kazmierczak SC. From diagnostics to therapy: prospects of quantum dots. Clin Biochem 2007; 40(13-14):917-927.

(45) Parungo CP, Ohnishi S, Kim SW, Kim S, Laurence RG, Soltesz EG et al. Intraoperative identification of esophageal sentinel lymph nodes with near-infrared fluorescence imaging. J Thorac Cardiovasc Surg 2005; 129(4):844-850.

(46) Soltesz EG, Kim S, Laurence RG, DeGrand AM, Parungo CP, Dor DM et al. Intraoperative sentinel lymph node mapping of the lung using near-infrared fluorescent quantum dots. Ann Thorac Surg 2005; 79(1):269-277.

(47) Harrell MI, Iritani BM, Ruddell A. Tumor-induced sentinel lymph node lymphangiogenesis and increased lymph flow precede melanoma metastasis. Am J Pathol 2007; 170(2):774-786.

(48) Jain R, Dandekar P, Patravale V. Diagnostic nanocarriers for sentinel lymph node imaging. J Control Release 2009; 138(2):90-102.

(49) Kawasaki ES, Player A. Nanotechnology, nanomedicine, and the development of new, effective therapies for cancer. Nanomedicine 2005; 1(2):101-109.

(50) Larson DR, Zipfel WR, Williams RM, Clark SW, Bruchez MP, Wise FW et al. Water-soluble quantum dots for multiphoton fluorescence imaging in vivo. Science 2003; 300(5624):1434-1436.

(51) Wang HZ, Wang HY, Liang RQ, Ruan KC. Detection of tumor marker CA125 in ovarian carcinoma using quantum dots. Acta Biochim Biophys Sin (Shanghai) 2004; 36(10):681-686.

(52) Henriquez NV, van Overveld PG, Que I, Buijs JT, Bachelier R, Kaijzel EL et al. Advances in optical imaging and novel model systems for cancer metastasis research. Clin Exp Metastasis 2007; 24(8):699-705.

(53) Kaul Z, Yaguchi T, Kaul SC, Hirano T, Wadhwa R, Taira K. Mortalin imaging in normal and cancer cells with quantum dot immuno-conjugates. Cell Res 2003; 13(6):503-507.

(54) Cai W, Chen X. Preparation of peptide-conjugated quantum dots for tumor vasculature-targeted imaging. Nat Protoc 2008; 3(1):89-96.

(55) Zajac A, Song D, Qian W, Zhukov T. Protein microarrays and quantum dot probes for early cancer detection. Colloids Surf B Biointerfaces 2007; 58(2):309-314.

(56) Yezhelyev M, Yacoub R, O'Regan R. Inorganic nanoparticles for predictive oncology of breast cancer. Nanomedicine (Lond) 2009; 4(1):83-103.

(57) Clapp AR, Medintz IL, Mauro JM, Fisher BR, Bawendi MG, Mattoussi H. Fluorescence resonance energy transfer between quantum dot donors and dye-labeled protein acceptors. J Am Chem Soc 2004; 126(1):301-310.

(58) Nida DL, Rahman MS, Carlson KD, Richards-Kortum R, Follen M. Fluorescent nanocrystals for use in early cervical cancer detection. Gynecol Oncol 2005; 99(3 Suppl 1):S89-S94.

(59) Qian J, Yong KT, Roy I, Ohulchanskyy TY, Bergey EJ, Lee HH et al. Imaging pancreatic cancer using surface-functionalized quantum dots. J Phys Chem B 2007; 111(25):6969-6972.

(60) Yang D, Chen Q, Wang W, Xu S. Direct and indirect immunolabelling of HeLa cells with quantum dots. Luminescence 2008; 23(3):169-174.

(61) Li Z, Wang K, Tan W, Li J, Fu Z, Ma C et al. Immunofluorescent labeling of cancer cells with quantum dots synthesized in aqueous solution. Anal Biochem 2006; 354(2):169-174.

(62) Wang J, Yong WH, Sun Y, Vernier PT, Koeffler HP, Gundersen MA et al. Receptor-targeted quantum dots: fluorescent probes for brain tumor diagnosis. J Biomed Opt 2007; 12(4):044021.

(63) Fengqin Hu YRZZMG. Preparation of bioconjugates of CdTe nanocrystals for cancer marker detection . Nanotechnology 17[12], 2972-2977. 2006.
Ref Type: Journal (Full)

(64) Akerman ME, Chan WC, Laakkonen P, Bhatia SN, Ruoslahti E. Nanocrystal targeting in vivo. Proc Natl Acad Sci U S A 2002; 99(20):12617-12621.

(65) Knapp DW, Adams LG, DeGrand AM, Niles JD, Ramos-Vara JA, Weil AB et al. Sentinel lymph node mapping of invasive urinary bladder cancer in animal models using invisible light. Eur Urol 2007; 52(6):1700-1708.

(66) Yu X, Chen L, Li K, Li Y, Xiao S, Luo X et al. Immunofluorescence detection with quantum dot bioconjugates for hepatoma in vivo. J Biomed Opt 2007; 12(1):014008.

(67) Gao X, Cui Y, Levenson RM, Chung LW, Nie S. In vivo cancer targeting and imaging with semiconductor quantum dots. Nat Biotechnol 2004; 22(8):969-976.

(68) Estrada CR, Salanga M, Bielenberg DR, Harrell WB, Zurakowski D, Zhu X et al. Behavioral profiling of human transitional cell carcinoma ex vivo. Cancer Res 2006; 66(6):3078-3086.

(69) Diagaradjane P, Orenstein-Cardona JM, Colon-Casasnovas NE, Deorukhkar A, Shentu S, Kuno N et al. Imaging epidermal growth factor receptor expression in vivo: pharmacokinetic and biodistribution characterization of a bioconjugated quantum dot nanoprobe. Clin Cancer Res 2008; 14(3):731-741.

(70) Tada H, Higuchi H, Wanatabe TM, Ohuchi N. In vivo real-time tracking of single quantum dots conjugated with monoclonal anti-HER2 antibody in tumors of mice. Cancer Res 2007; 67(3):1138-1144.

(71) Ballou B, Ernst LA, Andreko S, Harper T, Fitzpatrick JA, Waggoner AS et al. Sentinel lymph node imaging using quantum dots in mouse tumor models. Bioconjug Chem 2007; 18(2):389-396.

(72) Qi L, Gao X. Emerging application of quantum dots for drug delivery and therapy. Expert Opin Drug Deliv 2008; 5(3):263-267.

(73) Wen Jiang BYKJTR&WCC. Advances and challenges of nanotechnology-based drug delivery systems. Expert Opin.Drug Deliv 4[6], 621-633. 2007.
Ref Type: Journal (Full)

(74) Biju V, Mundayoor S, Omkumar RV, Anas A, Ishikawa M. Bioconjugated quantum dots for cancer research: present status, prospects and remaining issues. Biotechnol Adv 2010; 28(2):199-213.

(75) Takada Y, Ye X, Simon S. The integrins. Genome Biol 2007; 8(5):215.

(76) Harris ES, McIntyre TM, Prescott SM, Zimmerman GA. The leukocyte integrins. J Biol Chem 2000; 275(31):23409-23412.

(77) Humphries JD, Byron A, Humphries MJ. Integrin ligands at a glance. J Cell Sci 2006; 119(Pt 19):3901-3903.

(78) Rao J, Dragulescu-Andrasi A, Yao H. Fluorescence imaging in vivo: recent advances. Curr Opin Biotechnol 2007; 18(1):17-25.

(79) Dunehoo AL, Anderson M, Majumdar S, Kobayashi N, Berkland C, Siahaan TJ. Cell adhesion molecules for targeted drug delivery. J Pharm Sci 2006; 95(9):1856-1872.

(80) Zhao-Yang Z, Ke-Sen X, Qing-Si H, Wei-Bo N, Jia-Yong W, Yue-Tang M et al. Signaling and regulatory mechanisms of integrin alphavbeta6 on the apoptosis of colon cancer cells. Cancer Lett 2008; 266(2):209-215.

(81) Strieth S, Eichhorn ME, Sutter A, Jonczyk A, Berghaus A, Dellian M. Antiangiogenic combination tumor therapy blocking alpha(v)-integrins and VEGF-receptor-2 increases therapeutic effects in vivo. Int J Cancer 2006; 119(2):423-431.

(82) Pang RW, Poon RT. Clinical implications of angiogenesis in cancers. Vasc Health Risk Manag 2006; 2(2):97-108.

(83) Martelli A, Rousselet E, Dycke C, Bouron A, Moulis JM. Cadmium toxicity in animal cells by interference with essential metals. Biochimie 2006; 88(11):1807-1814.

(84) Yarema MC, Curry SC. Acute tellurium toxicity from ingestion of metal-oxidizing solutions. Pediatrics 2005; 116(2):e319-e321.

(85) Walkey C, Sykes EA, Chan WC. Application of semiconductor and metal nanostructures in biology and medicine. Hematology Am Soc Hematol Educ Program 2009;701-707.

(86) Longmire M, Choyke PL, Kobayashi H. Clearance properties of nano-sized particles and molecules as imaging agents: considerations and caveats. Nanomedicine (Lond) 2008; 3(5):703-717.

(87) Hardman R. A toxicologic review of quantum dots: toxicity depends on physicochemical and environmental factors. Environ Health Perspect 2006; 114(2):165-172.

(88) Male KB, Lachance B, Hrapovic S, Sunahara G, Luong JH. Assessment of cytotoxicity of quantum dots and gold nanoparticles using cell-based impedance spectroscopy. Anal Chem 2008; 80(14):5487-5493.

(89) Chen Z, Chen H, Meng H, Xing G, Gao X, Sun B et al. Bio-distribution and metabolic paths of silica coated CdSeS quantum dots. Toxicol Appl Pharmacol 2008; 230(3):364-371.

(90) Kuo TR, Lee CF, Lin SJ, Dong CY, Chen CC, Tan HY. Studies of intracorneal distribution and cytotoxicity of quantum dots: risk assessment of eye exposure. Chem Res Toxicol 2011; 24(2):253-261.

(91) Wang L, Zhang J, Zheng Y, Yang J, Zhang Q, Zhu X. Bioeffects of CdTe quantum dots on human umbilical vein endothelial cells. J Nanosci Nanotechnol 2010; 10(12):8591-8596.

(92) Clift MJ, Varet J, Hankin SM, Brownlee B, Davidson AM, Brandenberger C et al. Quantum dot cytotoxicity in vitro: An investigation into the cytotoxic effects of a series of different surface chemistries and their core/shell materials. Nanotoxicology 2010.

(93) Hsieh MS, Shiao NH, Chan WH. Cytotoxic effects of CdSe quantum dots on maturation of mouse oocytes, fertilization, and fetal development. Int J Mol Sci 2009; 10(5):2122-2135.

(94) Rzigalinski BA, Strobl JS. Cadmium-containing nanoparticles: perspectives on pharmacology and toxicology of quantum dots. Toxicol Appl Pharmacol 2009; 238(3):280-288.

(95) Kuwada SK, Kuang J, Li X. Integrin α5/β1 Expression Mediates HER-2 Down-regulation in Colon Cancer Cells. 2005 The Journal of Biological Chemistry, 280, 19027-19035.

(96) Lee JW, Juliano RL. α5β1 Integrin Protects Intestinal Epithelial Cells from Apoptosis through a Phosphatidylinositol 3-Kinase and Protein Kinase B–dependent Pathway. Mol Biol Cell. 2000 June; 11(6): 1973–1987

(97) Varner JA, Emerson DA, Juliano RL. Integrin alpha 5 beta 1 expression negatively regulates cell growth: reversal by attachment to fibronectin.Mol Biol Cell. 1995 June; 6(6): 725–740.

(98) Schaffner F, Ray AM, Dontenwill M. Integrin α5β1, the Fibronectin Receptor, as a Pertinent Therapeutic Target in Solid Tumors. *Cancers* 2013, *5*, 27-47

Appendix

Table 1. Statistical analysis of percentage of cell survival using graded concentration of Cadmium-

P value	< 0.0001				
P value summary	****				
Are means signif. different? (P < 0.05)	Yes				
Number of groups	10				
F	45.78				
R square	0.9537				
ANOVA Table	SS	df	MS		
Treatment (between columns)	53568	9	5952		
Residual (within columns)	2600	20	130.0		
Total	56168	29			
Dunnett's Multiple Comparison Test	**Mean Diff.**	**q**	**Significant? P < 0.05?**	**Summary**	**95% CI of diff**
medium only vs 0.01	-13.73	1.474	No	ns	-41.16 to 13.70
medium only vs 0.05	-0.4567	0.04905	No	ns	-27.89 to 26.97
medium only vs 0.1	-3.337	0.3584	No	ns	-30.77 to 24.09
medium only vs 0.5	-2.897	0.3111	No	ns	-30.33 to 24.53
medium only vs 1	1.943	0.2087	No	ns	-25.49 to 29.37
medium only vs 5	40.68	4.369	Yes	**	13.25 to 68.11
medium only vs 10	87.62	9.411	Yes	***	60.19 to 115.1
medium only vs 50	91.80	9.860	Yes	***	64.37 to 119.2
medium only vs 100	92.34	9.918	Yes	***	64.91 to 119.8

Table 2. Statistical analysis of percentage of cell death using graded concentration of Cadmium-

P value	< 0.0001				
P value summary	****				
Are means signif. different? (P < 0.05)	Yes				
Number of groups	10				
F	16.33				
R square	0.8802				
ANOVA Table	SS	df	MS		
Treatment (between columns)	17.62	9	1.958		
Residual (within columns)	2.398	20	0.1199		
Total	20.02	29			
Dunnett's Multiple Comparison Test	**Mean Diff.**	**q**	**Significant? P < 0.05?**	**Summary**	**95% CI of diff**
medium only vs 0.01	-0.01400	0.04952	No	ns	-0.8470 to 0.8190
medium only vs 0.05	0.08700	0.3077	No	ns	-0.7460 to 0.9200
medium only vs 0.1	-0.04500	0.1592	No	ns	-0.8780 to 0.7880
medium only vs 0.5	-0.01967	0.06956	No	ns	-0.8527 to 0.8133
medium only vs 1	0.3804	1.345	No	ns	-0.4526 to 1.213
medium only vs 5	-0.7010	2.479	No	ns	-1.534 to 0.1320
medium only vs 10	-1.864	6.592	Yes	***	-2.697 to -1.031
medium only vs 50	-1.515	5.357	Yes	***	-2.348 to -0.6817
medium only vs 100	-1.450	5.128	Yes	***	-2.283 to -0.6167

Table 3. Statistical analysis of percentage of cell survival using graded concentration of Tellurium-

P value	< 0.0001				
P value summary	****				
Are means signif. different? (P < 0.05)	Yes				
Number of groups	10				
F	168.3				
R square	0.9870				
ANOVA Table	SS	df	MS		
Treatment (between columns)	50748	9	5639		
Residual (within columns)	670.2	20	33.51		
Total	51418	29			
Dunnett's Multiple Comparison Test	**Mean Diff.**	**q**	**Significant? P < 0.05?**	**Summary**	**95% CI of diff**
medium only vs 0.01	3.467	0.7334	No	ns	-10.46 to 17.39
medium only vs 0.05	9.333	1.975	No	ns	-4.593 to 23.26
medium only vs 0.1	17.67	3.738	Yes	**	3.741 to 31.59
medium only vs 0.5	27.00	5.712	Yes	***	13.07 to 40.93
medium only vs 1	24.67	5.219	Yes	***	10.74 to 38.59
medium only vs 5	35.86	7.586	Yes	***	21.93 to 49.78
medium only vs 10	36.89	7.805	Yes	***	22.96 to 50.82
medium only vs 50	119.7	25.33	Yes	***	105.8 to 133.6
medium only vs 100	115.9	24.53	Yes	***	102.0 to 129.9

Table 4. Statistical analysis of percentage of cell death using graded concentration of Tellurium.

Table Analyzed	Data 1				
One-way analysis of variance					
P value	< 0.0001				
P value summary	****				
Are means signif. different? (P < 0.05)	Yes				
Number of groups	10				
F	69.79				
R square	0.9691				
ANOVA Table	SS	df	MS		
Treatment (between columns)	14.90	9	1.655		
Residual (within columns)	0.4744	20	0.02372		
Total	15.37	29			
Dunnett's Multiple Comparison Test	Mean Diff.	q	Significant? P < 0.05?	Summary	95% CI of diff
medium only vs 0.01	-0.01867	0.1484	No	ns	-0.3892 to 0.3518
medium only vs 0.05	-0.0510	0.4056	No	ns	-0.4215 to 0.3195
medium only vs 0.1	-0.03100	0.2465	No	ns	-0.4015 to 0.3395
medium only vs 0.5	-0.08733	0.6945	No	ns	-0.4578 to 0.2832
medium only vs 1	-0.1467	1.166	No	ns	-0.5172 to 0.2238
medium only vs 5	-0.1727	1.373	No	ns	-0.5432 to 0.1978
medium only vs 10	-0.1923	1.529	No	ns	-0.5628 to 0.1782
medium only vs 50	-1.545	12.29	Yes	***	-1.916 to -1.174
medium only vs 100	-2.087	16.60	Yes	***	-2.458 to -1.716

Table 5. Statistical analysis of percentage of cell survival using graded concentration of CdTe Qds – Sample 1

Table Analyzed	Data 1				
One-way analysis of variance					
P value	< 0.0001				
P value summary	****				
Are means signif. different? (P < 0.05)	Yes				
Number of groups	10				
F	111.8				
R square	0.9805				
ANOVA Table	SS	df	MS		
Treatment (between columns)	16403	9	1823		
Residual (within columns)	326.1	20	16.30		
Total	16729	29			
Dunnett's Multiple Comparison Test	**Mean Diff.**	**q**	**Significant? P < 0.05?**	**Summary**	**95% CI of diff**
medium only vs QD0.01	-5.407	1.640	No	ns	-15.12 to 4.307
medium only vs QD0.05	-5.167	1.567	No	ns	-14.88 to 4.547
medium only vs QD0.1	-5.037	1.528	No	ns	-14.75 to 4.677
medium only vs QD0.5	-5.047	1.531	No	ns	-14.76 to 4.667
medium only vs QD1	-5.877	1.782	No	ns	-15.59 to 3.837
medium only vs QD5	-3.850	1.168	No	ns	-13.56 to 5.864
medium only vs QD10	5.697	1.728	No	ns	-4.017 to 15.41
medium only vs QD50	34.57	10.49	Yes	***	24.86 to 44.29
medium only vs Cadmium 50	68.55	20.79	Yes	***	58.84 to 78.26

Table 6. Statistical analysis of percentage of cell survival using graded concentration of CdTe Qds – Sample 2

Table Analyzed	Data 1				
One-way analysis of variance					
P value	< 0.0001				
P value summary	****				
Are means signif. different? (P < 0.05)	Yes				
Number of groups	10				
F	110.7				
R square	0.9708				
ANOVA Table	SS	df	MS		
Treatment (between columns)	24765	9	2752		
Residual (within columns)	745.7	30	24.86		
Total	25511	39			
Dunnett's Multiple Comparison Test	Mean Diff.	q	Significant? P < 0.05?	Summary	95% CI of diff
medium only vs 0.01	-4.973	1.410	No	ns	-15.04 to 5.095
medium only vs 0.05	-6.430	1.824	No	ns	-16.50 to 3.637
medium only vs 0.1	-14.27	4.047	Yes	**	-24.33 to -4.200
medium only vs 0.5	-5.918	1.679	No	ns	-15.98 to 4.150
medium only vs 1	-21.97	6.233	Yes	***	-32.04 to -11.91
medium only vs 5	-12.45	3.531	Yes	**	-22.52 to -2.383
medium only vs 10	0.8425	0.2390	No	ns	-9.225 to 10.91
medium only vs 50	36.44	10.34	Yes	***	26.37 to 46.51
medium only vs Cadmium 50	63.58	18.03	Yes	***	53.51 to 73.64

Table 7. Statistical analysis of percentage of cell death using graded concentration of CdTe Qds – Sample 1

Table Analyzed	Data 1				
One-way analysis of variance					
P value	< 0.0001				
P value summary	****				
Are means signif. different? (P < 0.05)	Yes				
Number of groups	10				
F	29.10				
R square	0.9291				
ANOVA Table	SS	df	MS		
Treatment (between columns)	13.86	9	1.540		
Residual (within columns)	1.058	20	0.05290		
Total	14.91	29			
Dunnett's Multiple Comparison Test	Mean Diff.	q	Significant? P < 0.05?	Summary	95% CI of diff
medium only vs 0.01	0.003667	0.01953	No	ns	-0.5496 to 0.5570
medium only vs 0.05	0.03033	0.1615	No	ns	-0.5230 to 0.5836
medium only vs 0.1	-0.04433	0.2361	No	ns	-0.5976 to 0.5090
medium only vs 0.5	-0.08233	0.4384	No	ns	-0.6356 to 0.4710
medium only vs 1	-0.1983	1.056	No	ns	-0.7516 to 0.3550
medium only vs 5	-0.05533	0.2947	No	ns	-0.6086 to 0.4980
medium only vs 10	-0.4020	2.141	No	ns	-0.9553 to 0.1513
medium only vs 50	-0.5133	2.734	No	ns	-1.067 to 0.03995
medium only vs Cadmium 50	-2.331	12.41	Yes	***	-2.884 to -1.777

Table 8. Statistical analysis of percentage of cell death using graded concentration of CdTe Qds

P value	< 0.0001				
P value summary	****				
Are means signif. different? (P < 0.05)	Yes				
Number of groups	10				
F	53.47				
R square	0.9601				
ANOVA Table	SS	df	MS		
Treatment (between columns)	6.462	9	0.7180		
Residual (within columns)	0.2686	20	0.01343		
Total	6.730	29			
Dunnett's Multiple Comparison Test	**Mean Diff.**	**q**	**Significant? P < 0.05?**	**Summary**	**95% CI of diff**
medium only vs 0.01	-0.05833	0.6165	No	ns	-0.3371 to 0.2204
medium only vs 0.05	-0.07467	0.7892	No	ns	-0.3534 to 0.2041
medium only vs 0.1	-0.06400	0.6764	No	ns	-0.3428 to 0.2148
medium only vs 0.5	-0.01400	0.1480	No	ns	-0.2928 to 0.2648
medium only vs 1	-0.2390	2.526	No	ns	-0.5178 to 0.03976
medium only vs 5	-0.08000	0.8455	No	ns	-0.3588 to 0.1988
medium only vs 10	-0.2560	2.706	No	ns	-0.5348 to 0.02276
medium only vs 50	-0.2933	3.100	Yes	*	-0.5721 to -0.01457
medium only vs Cadmium 50	-1.631	17.24	Yes	***	-1.910 to -1.352

Table 9. Statistical analysis of percentage of cell survival using graded concentration of RGD (Lysine) conjugated CdTe Qds

Table Analyzed	Data 1				
One-way analysis of variance					
P value	< 0.0001				
P value summary	****				
Are means signif. different? (P < 0.05)	Yes				
Number of groups	10				
F	43.70				
R square	0.9516				
ANOVA Table	SS	df	MS		
Treatment (between columns)	16978	9	1886		
Residual (within columns)	863.3	20	43.17		
Total	17841	29			
Dunnett's Multiple Comparison Test	**Mean Diff.**	**q**	**Significant? P < 0.05?**	**Summary**	**95% CI of diff**
medium only vs QD0.01	-5.693	1.061	No	ns	-21.50 to 10.11
medium only vs QD0.05	-12.09	2.254	No	ns	-27.90 to 3.715
medium only vs QD0.1	-12.51	2.331	No	ns	-28.31 to 3.299
medium only vs QD0.5	-11.05	2.060	No	ns	-26.86 to 4.755
medium only vs QD1	-15.35	2.862	No	ns	-31.16 to 0.4520
medium only vs QD5	-17.68	3.295	Yes	*	-33.48 to -1.871
medium only vs QD10	-25.26	4.708	Yes	**	-41.06 to -9.451
medium only vs QD50	-31.34	5.842	Yes	***	-47.15 to -15.53
medium only vs Cadmium 50	59.53	11.10	Yes	***	43.73 to 75.34

Table 10. Statistical analysis of percentage of cell survival using graded concentration of RGD (Lysine) conjugated CdTe Qds

Table Analyzed	Data 1				
One-way analysis of variance					
P value	< 0.0001				
P value summary	****				
Are means signif. different? (P < 0.05)	Yes				
Number of groups	10				
F	33.03				
R square	0.9370				
ANOVA Table	SS	df	MS		
Treatment (between columns)	17198	9	1911		
Residual (within columns)	1157	20	57.85		
Total	18355	29			
Dunnett's Multiple Comparison Test	**Mean Diff.**	**q**	**Significant? P < 0.05?**	**Summary**	**95% CI of diff**
medium only vs 0.01	3.207	0.5164	No	ns	-15.09 to 21.50
medium only vs 0.05	9.063	1.459	No	ns	-9.233 to 27.36
medium only vs 0.1	5.643	0.9087	No	ns	-12.65 to 23.94
medium only vs 0.5	16.77	2.700	No	ns	-1.530 to 35.06
medium only vs 1	4.780	0.7697	No	ns	-13.52 to 23.08
medium only vs 5	1.140	0.1836	No	ns	-17.16 to 19.44
medium only vs 10	-3.960	0.6377	No	ns	-22.26 to 14.34
medium only vs 50	-6.947	1.119	No	ns	-25.24 to 11.35
medium only vs Cadmium 50	80.31	12.93	Yes	***	62.01 to 98.60

Table 11. Statistical analysis of percentage of cell death using graded concentration of RGD (Lysine) conjugated CdTe Qds

Table Analyzed	Data 1				
One-way analysis of variance					
P value	< 0.0001				
P value summary	****				
Are means signif. different? (P < 0.05)	Yes				
Number of groups	10				
F	103.1				
R square	0.9789				
ANOVA Table	SS	df	MS		
Treatment (between columns)	7.863	9	0.8736		
Residual (within columns)	0.1695	20	0.008476		
Total	8.032	29			
Dunnett's Multiple Comparison Test	**Mean Diff.**	**q**	**Significant? P < 0.05?**	**Summary**	**95% CI of diff**
medium only vs QD0.01	-0.09267	1.233	No	ns	-0.3141 to 0.1288
medium only vs QD0.05	0.03400	0.4523	No	ns	-0.1875 to 0.2555
medium only vs QD0.1	-0.1020	1.357	No	ns	-0.3235 to 0.1195
medium only vs QD0.5	0.01900	0.2528	No	ns	-0.2025 to 0.2405
medium only vs QD1	-0.01700	0.2262	No	ns	-0.2385 to 0.2045
medium only vs QD5	-0.02133	0.2838	No	ns	-0.2428 to 0.2001
medium only vs QD10	-0.1587	2.111	No	ns	-0.3801 to 0.06281
medium only vs QD50	-0.03633	0.4833	No	ns	-0.2578 to 0.1851
medium only vs Cadmium 50	-1.738	23.12	Yes	***	-1.959 to -1.516

Table 12. Statistical analysis of percentage of cell death using graded concentration of RGD (Lysine) conjugated CdTe Qds

Table Analyzed	Data 1				
One-way analysis of variance					
P value	< 0.0001				
P value summary	****				
Are means signif. different? (P < 0.05)	Yes				
Number of groups	10				
F	103.1				
R square	0.9789				
ANOVA Table	SS	df	MS		
Treatment (between columns)	7.863	9	0.8736		
Residual (within columns)	0.1695	20	0.008476		
Total	8.032	29			
Dunnett's Multiple Comparison Test	**Mean Diff.**	**q**	**Significant? P < 0.05?**	**Summary**	**95% CI of diff**
medium only vs 0.01	-0.09267	1.233	No	ns	-0.3141 to 0.1288
medium only vs 0.05	0.03400	0.4523	No	ns	-0.1875 to 0.2555
medium only vs 0.1	-0.1020	1.357	No	ns	-0.3235 to 0.1195
medium only vs 0.5	0.01900	0.2528	No	ns	-0.2025 to 0.2405
medium only vs 1	-0.01700	0.2262	No	ns	-0.2385 to 0.2045
medium only vs 5	-0.02133	0.2838	No	ns	-0.2428 to 0.2001
medium only vs 10	-0.1587	2.111	No	ns	-0.3801 to 0.06281
medium only vs 50	-0.03633	0.4833	No	ns	-0.2578 to 0.1851
medium only vs Cadmium 50	-1.738	23.12	Yes	***	-1.959 to -1.516

Table 13. Statistical analysis of percentage of cell survival using graded concentration of RGD (Cysteine) conjugated CdTe Qds

P value	< 0.0001				
P value summary	****				
Are means signif. different? (P < 0.05)	Yes				
Number of groups	10				
F	344.1				
R square	0.9810				
Bartlett's test for equal variances					
Bartlett's statistic (corrected)	52.29				
P value	< 0.0001				
P value summary	****				
Do the variances differ signif. (P < 0.05)	Yes				
ANOVA Table	SS	df	MS		
Treatment (between columns)	45346	9	5038		
Residual (within columns)	878.6	60	14.64		
Total	46224	69			
Dunnett's Multiple Comparison Test	**Mean Diff.**	**q**	**Significant? P < 0.05?**	**Summary**	**95% CI of diff**
medium only vs 0.01	-1.727	0.8444	No	ns	-7.391 to 3.936
medium only vs 0.05	-0.5500	0.2689	No	ns	-6.213 to 5.113
medium only vs 0.1	-5.640	2.757	No	ns	-11.30 to 0.02348
medium only vs 0.5	-2.740	1.340	No	ns	-8.403 to 2.923
medium only vs 1	-4.974	2.432	No	ns	-10.64 to 0.6892
medium only vs 5	-13.52	6.609	Yes	***	-19.18 to -7.854
medium only vs 10	-12.77	6.244	Yes	***	-18.43 to -7.108
medium only vs 50	-21.79	10.65	Yes	***	-27.45 to -16.12
medium only vs Cadmium 50	74.85	36.59	Yes	***	69.19 to 80.51

Table 14. Statistical analysis of percentage of cell survival using graded concentration of RGD (Cysteine) conjugated CdTe Qds

Table Analyzed	Data 1				
One-way analysis of variance					
P value	< 0.0001				
P value summary	****				
Are means signif. different? (P < 0.05)	Yes				
Number of groups	10				
F	18.10				
R square	0.8907				
ANOVA Table	SS	df	MS		
Treatment (between columns)	17439	9	1938		
Residual (within columns)	2141	20	107.0		
Total	19579	29			
Dunnett's Multiple Comparison Test	**Mean Diff.**	**q**	**Significant? P < 0.05?**	**Summary**	**95% CI of diff**
medium only vs 0.01	-0.3033	0.03591	No	ns	-25.19 to 24.58
medium only vs 0.05	-10.40	1.231	No	ns	-35.28 to 14.49
medium only vs 0.1	-9.447	1.118	No	ns	-34.33 to 15.44
medium only vs 0.5	-15.45	1.829	No	ns	-40.34 to 9.438
medium only vs 1	-10.68	1.265	No	ns	-35.57 to 14.20
medium only vs 5	-3.697	0.4376	No	ns	-28.58 to 21.19
medium only vs 10	-18.65	2.207	No	ns	-43.53 to 6.241
medium only vs 50	-16.46	1.949	No	ns	-41.35 to 8.424
medium only vs Cadmium 50	68.25	8.080	Yes	***	43.37 to 93.14

Table 15. Statistical analysis of percentage of cell death using graded concentration of RGD (Cysteine) conjugated CdTe Qds

Table Analyzed	Data 1				
One-way analysis of variance					
P value	< 0.0001				
P value summary	****				
Are means signif. different? (P < 0.05)	Yes				
Number of groups	10				
F	83.02				
R square	0.9739				
ANOVA Table	SS	df	MS		
Treatment (between columns)	9.545	9	1.061		
Residual (within columns)	0.2555	20	0.01278		
Total	9.801	29			
Dunnett's Multiple Comparison Test	**Mean Diff.**	**q**	**Significant? P < 0.05?**	**Summary**	**95% CI of diff**
medium only vs 0.01	-0.05233	0.5671	No	ns	-0.3242 to 0.2196
medium only vs 0.05	0.05433	0.5887	No	ns	-0.2176 to 0.3262
medium only vs 0.1	-0.04500	0.4876	No	ns	-0.3169 to 0.2269
medium only vs 0.5	0.05167	0.5598	No	ns	-0.2202 to 0.3236
medium only vs 1	-0.09267	1.004	No	ns	-0.3646 to 0.1792
medium only vs 5	0.02767	0.2998	No	ns	-0.2442 to 0.2996
medium only vs 10	-0.1087	1.177	No	ns	-0.3806 to 0.1632
medium only vs 50	-0.1100	1.192	No	ns	-0.3819 to 0.1619
medium only vs Cadmium 50	-1.900	20.59	Yes	***	-2.172 to -1.628

Table 16. Statistical analysis of percentage of cell death using graded concentration of RGD (Cysteine) conjugated CdTe Qds

Table Analyzed	Data 1				
One-way analysis of variance					
P value	< 0.0001				
P value summary	****				
Are means signif. different? (P < 0.05)	Yes				
Number of groups	10				
F	45.65				
R square	0.9536				
ANOVA Table	SS	df	MS		
Treatment (between columns)	6.212	9	0.6902		
Residual (within columns)	0.3024	20	0.01512		
Total	6.514	29			
Dunnett's Multiple Comparison Test	**Mean Diff.**	**q**	**Significant? P < 0.05?**	**Summary**	**95% CI of diff**
medium only vs 0.01	-0.04833	0.4814	No	ns	-0.3441 to 0.2475
medium only vs 0.05	0.08600	0.8566	No	ns	-0.2098 to 0.3818
medium only vs 0.1	0.07553	0.7523	No	ns	-0.2203 to 0.3713
medium only vs 0.5	-0.08233	0.8201	No	ns	-0.3781 to 0.2135
medium only vs 1	-0.01533	0.1527	No	ns	-0.3111 to 0.2805
medium only vs 5	-0.02600	0.2590	No	ns	-0.3218 to 0.2698
medium only vs 10	-0.1610	1.604	No	ns	-0.4568 to 0.1348
medium only vs 50	-0.1297	1.292	No	ns	-0.4255 to 0.1661
medium only vs Cadmium 50	-1.530	15.24	Yes	***	-1.825 to -1.234

Table 17. Statistical analysis of percentage of cell survival using graded concentration of RAD conjugated CdTe Qds – Sample1.

P value	< 0.0001				
P value summary	****				
Are means signif. different? (P < 0.05)	Yes				
Number of groups	10				
F	69.50				
R square	0.9690				
ANOVA Table	SS	df	MS		
Treatment (between columns)	17617	9	1957		
Residual (within columns)	563.3	20	28.16		
Total	18180	29			
Dunnett's Multiple Comparison Test	**Mean Diff.**	**q**	**Significant? P < 0.05?**	**Summary**	**95% CI of diff**
medium only vs 0.01	-4.183	0.9654	No	ns	-16.95 to 8.583
medium only vs 0.05	-9.463	2.184	No	ns	-22.23 to 3.303
medium only vs 0.1	-6.430	1.484	No	ns	-19.20 to 6.337
medium only vs 0.5	-13.60	3.138	Yes	*	-26.36 to -0.8300
medium only vs 1	-13.46	3.106	Yes	*	-26.23 to -0.6934
medium only vs 5	-19.20	4.430	Yes	**	-31.96 to -6.430
medium only vs 10	-20.75	4.789	Yes	***	-33.52 to -7.987
medium only vs 50	-20.14	4.648	Yes	**	-32.91 to -7.373
medium only vs Cadmium 50	65.76	15.18	Yes	***	53.00 to 78.53

Table 18. Statistical analysis of percentage of cell survival using graded concentration of RAD conjugated CdTe Qds- Sample 2.

Table Analyzed	Data 1				
One-way analysis of variance					
P value	< 0.0001				
P value summary	****				
Are means signif. different? (P < 0.05)	Yes				
Number of groups	10				
F	69.50				
R square	0.9690				
ANOVA Table	SS	df	MS		
Treatment (between columns)	17617	9	1957		
Residual (within columns)	563.3	20	28.16		
Total	18180	29			
Dunnett's Multiple Comparison Test	**Mean Diff.**	**q**	**Significant? P < 0.05?**	**Summary**	**95% CI of diff**
medium only vs 0.01	-4.183	0.9654	No	ns	-16.95 to 8.583
medium only vs 0.05	-9.463	2.184	No	ns	-22.23 to 3.303
medium only vs 0.1	-6.430	1.484	No	ns	-19.20 to 6.337
medium only vs 0.5	-13.60	3.138	Yes	*	-26.36 to -0.8300
medium only vs 1	-13.46	3.106	Yes	*	-26.23 to -0.6934
medium only vs 5	-19.20	4.430	Yes	**	-31.96 to -6.430
medium only vs 10	-20.75	4.789	Yes	***	-33.52 to -7.987
medium only vs 50	-20.14	4.648	Yes	**	-32.91 to -7.373
medium only vs Cadmium 50	65.76	15.18	Yes	***	53.00 to 78.53

Table 19. Statistical analysis of percentage of cell death using graded concentration of RAD conjugated CdTe Qds

Table Analyzed	Data 1				
One-way analysis of variance					
P value	< 0.0001				
P value summary	****				
Are means signif. different? (P < 0.05)	Yes				
Number of groups	10				
F	47.42				
R square	0.9552				
ANOVA Table	SS	df	MS		
Treatment (between columns)	11.19	9	1.243		
Residual (within columns)	0.5243	20	0.02621		
Total	11.71	29			
Dunnett's Multiple Comparison Test	**Mean Diff.**	**q**	**Significant? P < 0.05?**	**Summary**	**95% CI of diff**
medium only vs 0.01	-0.1060	0.8019	No	ns	-0.4955 to 0.2835
medium only vs 0.05	0.03833	0.2900	No	ns	-0.3511 to 0.4278
medium only vs 0.1	-0.08400	0.6354	No	ns	-0.4735 to 0.3055
medium only vs 0.5	-0.08500	0.6430	No	ns	-0.4745 to 0.3045
medium only vs 1	-0.08433	0.6380	No	ns	-0.4738 to 0.3051
medium only vs 5	-0.001333	0.01009	No	ns	-0.3908 to 0.3881
medium only vs 10	-0.1470	1.112	No	ns	-0.5365 to 0.2425
medium only vs 50	-0.1610	1.218	No	ns	-0.5505 to 0.2285
medium only vs Cadmium 50	-2.095	15.85	Yes	***	-2.485 to -1.706

Table 20. Statistical analysis of percentage of cell death using graded concentration of RAD conjugated CdTe Qds

Table Analyzed	Data 1				
One-way analysis of variance					
P value	< 0.0001				
P value summary	****				
Are means signif. different? (P < 0.05)	Yes				
Number of groups	10				
F	90.78				
R square	0.9761				
ANOVA Table	SS	df	MS		
Treatment (between columns)	11.31	9	1.257		
Residual (within columns)	0.2770	20	0.01385		
Total	11.59	29			
Dunnett's Multiple Comparison Test	**Mean Diff.**	**q**	**Significant? P < 0.05?**	**Summary**	**95% CI of diff**
medium only vs 0.01	-0.09133	0.9506	No	ns	-0.3744 to 0.1918
medium only vs 0.05	-0.02133	0.2220	No	ns	-0.3044 to 0.2618
medium only vs 0.1	-0.1463	1.523	No	ns	-0.4294 to 0.1368
medium only vs 0.5	-0.2687	2.796	No	ns	-0.5518 to 0.01442
medium only vs 1	-0.1063	1.107	No	ns	-0.3894 to 0.1768
medium only vs 5	0.03867	0.4024	No	ns	-0.2444 to 0.3218
medium only vs 10	-0.1567	1.631	No	ns	-0.4398 to 0.1264
medium only vs 50	-0.1710	1.780	No	ns	-0.4541 to 0.1121
medium only vs Cadmium 50	-2.129	22.16	Yes	***	-2.412 to -1.846

Table 21. Statistical analysis of percentage of cell survival using graded concentration of polymer conjugated CdTe Qds.- Sample 1

Table Analyzed	Data 1				
One-way analysis of variance					
P value	< 0.0001				
P value summary	****				
Are means signif. different? (P < 0.05)	Yes				
Number of groups	10				
F	30.91				
R square	0.9329				
ANOVA Table	SS	df	MS		
Treatment (between columns)	20098	9	2233		
Residual (within columns)	1445	20	72.25		
Total	21543	29			
Dunnett's Multiple Comparison Test	**Mean Diff.**	**q**	**Significant? P < 0.05?**	**Summary**	**95% CI of diff**
medium only vs 0.01	-12.86	1.853	No	ns	-33.31 to 7.585
medium only vs 0.05	-21.27	3.065	Yes	*	-41.72 to -0.8248
medium only vs 0.1	-13.55	1.953	No	ns	-34.00 to 6.895
medium only vs 0.5	-20.62	2.971	Yes	*	-41.07 to -0.1681
medium only vs 1	-19.65	2.832	No	ns	-40.10 to 0.7952
medium only vs 5	-20.85	3.005	Yes	*	-41.30 to -0.4048
medium only vs 10	-19.87	2.863	No	ns	-40.32 to 0.5752
medium only vs 50	-13.82	1.991	No	ns	-34.27 to 6.629
medium only vs Cadmium 50	67.98	9.794	Yes	***	47.53 to 88.43

Table 22. Statistical analysis of percentage of cell survival using graded concentration of polymer conjugated CdTe Qds= Sample 2

Table Analyzed	Data 1				
One-way analysis of variance					
P value	< 0.0001				
P value summary	****				
Are means signif. different? (P < 0.05)	Yes				
Number of groups	10				
F	30.91				
R square	0.9329				
ANOVA Table	SS	df	MS		
Treatment (between columns)	20098	9	2233		
Residual (within columns)	1445	20	72.25		
Total	21543	29			
Dunnett's Multiple Comparison Test	**Mean Diff.**	**q**	**Significant? P < 0.05?**	**Summary**	**95% CI of diff**
medium only vs 0.01	-12.86	1.853	No	ns	-33.31 to 7.585
medium only vs 0.05	-21.27	3.065	Yes	*	-41.72 to -0.8248
medium only vs 0.1	-13.55	1.953	No	ns	-34.00 to 6.895
medium only vs 0.5	-20.62	2.971	Yes	*	-41.07 to -0.1681
medium only vs 1	-19.65	2.832	No	ns	-40.10 to 0.7952
medium only vs 5	-20.85	3.005	Yes	*	-41.30 to -0.4048
medium only vs 10	-19.87	2.863	No	ns	-40.32 to 0.5752
medium only vs 50	-13.82	1.991	No	ns	-34.27 to 6.629
medium only vs Cadmium 50	67.98	9.794	Yes	***	47.53 to 88.43

Table 23. Statistical analysis of percentage of cell death using graded concentration of polymer conjugated CdTe Qds – Sample 1

Table Analyzed	Data 1				
One-way analysis of variance					
P value	< 0.0001				
P value summary	****				
Are means signif. different? (P < 0.05)	Yes				
Number of groups	10				
F	83.92				
R square	0.9742				
ANOVA Table	SS	df	MS		
Treatment (between columns)	16.78	9	1.864		
Residual (within columns)	0.4443	20	0.02222		
Total	17.22	29			
Dunnett's Multiple Comparison Test	**Mean Diff.**	**q**	**Significant? P < 0.05?**	**Summary**	**95% CI of diff**
medium only vs 0.01	-0.05167	0.4246	No	ns	-0.4102 to 0.3069
medium only vs 0.05	0.03533	0.2903	No	ns	-0.3232 to 0.3939
medium only vs 0.1	-0.05600	0.4602	No	ns	-0.4146 to 0.3026
medium only vs 0.5	0.07100	0.5834	No	ns	-0.2876 to 0.4296
medium only vs 1	-0.001000	0.008217	No	ns	-0.3596 to 0.3576
medium only vs 5	0.06000	0.4930	No	ns	-0.2986 to 0.4186
medium only vs 10	-0.05800	0.4766	No	ns	-0.4166 to 0.3006
medium only vs 50	-0.1460	1.200	No	ns	-0.5046 to 0.2126
medium only vs Cadmium 50	-2.501	20.55	Yes	***	-2.859 to -2.142

Table 24. Statistical analysis of percentage of cell death using graded concentration of polymer conjugated CdTe Qds.- Sample 2

Table Analyzed	Data 1				
One-way analysis of variance					
P value	< 0.0001				
P value summary	****				
Are means signif. different? (P < 0.05)	Yes				
Number of groups	10				
F	58.23				
R square	0.9632				
ANOVA Table	SS	df	MS		
Treatment (between columns)	11.53	9	1.281		
Residual (within columns)	0.4399	20	0.02200		
Total	11.97	29			
Dunnett's Multiple Comparison Test	**Mean Diff.**	**q**	**Significant? P < 0.05?**	**Summary**	**95% CI of diff**
medium only vs 0.01	-0.04900	0.4046	No	ns	-0.4058 to 0.3078
medium only vs 0.05	0.03467	0.2863	No	ns	-0.3221 to 0.3915
medium only vs 0.1	-0.05900	0.4872	No	ns	-0.4158 to 0.2978
medium only vs 0.5	0.04367	0.3606	No	ns	-0.3131 to 0.4005
medium only vs 1	-0.04367	0.3606	No	ns	-0.4005 to 0.3131
medium only vs 5	0.02967	0.2450	No	ns	-0.3271 to 0.3865
medium only vs 10	-0.09733	0.8038	No	ns	-0.4541 to 0.2595
medium only vs 50	-0.1550	1.280	No	ns	-0.5118 to 0.2018
medium only vs Cadmium 50	-2.090	17.26	Yes	***	-2.446 to -1.733

Publication and presentation from the thesis

1. Conjugation of quantum dots with RGD peptides: Colon cancer cell targeting and toxicity assay. S Taribagil, SY Yang, B Ramesh, AM Seifalian and MC. Winslet

   SARS Annual Conference 2010 ,London

   poster presentation

2. Quantum Dots- Past, Present and Future? – Submitted for publication to nanomedicine. In the process of resubmission after corrections.